UNIVERSITÀ DEGLI STUDI DI MILANO

Dipartimento di Fisica

Corso di Dottorato di ricerca in Fisica, Astrofisica e Fisica Applicata

Ciclo XXIX

Hadron and Photon irradiation combined with a chemotherapy drug: an in vitro study in human cancer cells

Settore Scientifico Disciplinare FIS/07

Coordinatore: Professor Francesco RAGUSA

Supervisore: Professor Pier Francesco BORTIGNON

Co-supervisore: Professoressa Daniela BETTEGA

Tesi di Dottorato di:

Miriam LAFIANDRA

Anno Accademico 2016/2017

External Referees:

Prof. Mauro CARRARA

Prof. Lorenzo MANTI

Commission of the final examination:

Prof. Pier Francesco BORTIGNON

Prof. Rosanna NANO

Prof. Marco DURANTE

Final examination:

Date 19/07/2017

Università degli Studi di Milano, Dipartimento di Fisica, Milano, Italy

MIUR subjects:

FIS/07 - FISICA APPLICATA
(A BENI CULTURALI, AMBIENTALI, BIOLOGIA E MEDICINA)

PACS:

87.53.-j, 87.53.Jw

Keywords:

Hadron therapy, radiotherapy, combined therapies.

Dissertation presented in partial
fulfilment of the requirements
for the degree of Doctor in Science.

Once you eliminate the impossible,
whatever remains,
no matter how improbable,
must be the truth.
(Sherlock Holmes)

Contents

List of Figures

List of Tables

Introduction

Scientific Motivation

Thanks to their citotoxicity, ionizing radiations are widely used in cancer treatment (*radiotherapy*). In fact, interacting with biological tissues they can damage cancer cell genetic material preventing cell proliferation. The purpose of radiotherapy is to release a great dose of ionizing radiation inside the tumor mass, in order to inactivate its proliferative capacity and at the same time to minimize the dose to normal tissues surrounding the tumor, in order to reduce treatment's side effects. For this reason it is mandatory to find an optimal balance between the tumor local control and the risk of early and late effects that could compromise patient's life quality.

Nowadays photon beams produced by bremmstrahlung processes in Linear Accelerator (LINAC) are the kind of radiation most used in radiotherapy and for this reason photon beams are considered to be the reference radiation for radiotherapy treatment. The use of modern linear accelerator has become a more and more precise tool, capable of depositing photon dose into a well-defined volume in such a way that radiotherapy has become a very important treatment modality for many cancers. This has been possible thanks to a great improvement in technology, culminated in the state of the art Intensity Modulated Radiation Therapy (IMRT).

In recent years *hadrontherapy*, a new modality of radiotherapy that exploits charged hadrons such as protons and light ions (in particular carbon ions), has begun to spread out with the purpose of overcoming the limitation of photon therapy, leading to a better tumor local control and reducing the treatment's side effects. The advantages of this new technique are mainly linked to physical aspects, such as the modality of charged hadron interaction with matter described by the Bethe-Bloch equation. According to this equation for charged hadrons, the released dose is described by the Bragg curve, which shows a peak at the end of particle path. Thus, it is possible to deliver very high doses inside the tumor volume, sparing normal tissues surrounding it, simply by appropriately accelerating the hadrons.
Moreover, charged particles (expecially heavy ions) have a greater biological effectiveness in damaging irradiated cancer cells when compared to photons. As a matter of fact, in correspondence of the Bragg peak the density of ionizing events increases leading to a greater biological effectiveness. These properties suggest that with hadrontherapy it may be possible to achieve better cancer treatment results for deep-seated and radiore-

sistant tumors.

In order to obtain better tumor local control and to reduce metastasis risk, nowadays combined therapies are under investigation with widely increasing interest for the treatment of particularly resistant tumors, exploiting chemotherapy agents and radiation used in conjunction. In fact, it is known that some drugs have radio-sensitizing effects, for example stopping cells in the most radio-sensitive phase of their cycle or inhibiting the repair mechanisms of DNA (DeoxyriboNucleic Acid), amplifying the radiation anti-proliferative effect. Many studies with different kind of chemical agents used in combination with photon beams have been performed for different cancers, but at the moment very few data about the use of chemical agents combined with hadrons are available.

Thesis overview

The present project is a part of the RDH[1] / IRPT[2] project, sponsored by the Istituto Nazionale di Fisica Nucleare.

The purpose of the study described in this Thesis is the investigation of the interaction of charged hadrons (protons and carbon ions) and a new-generation chemotherapy agent, named Epothilone B, in different human cancer cells cultured *in vitro*. Since photon beams are the reference radiation in radiotherapy, a comparison of the obtained results with those of similar experiments on the interaction of Epothilone B with photon beams has been done.

Different biological end-points have been evaluated in irradiated human cancer cells pre-treated or not with Epothilone B. In particular, clonogenic survival, cell growth and invasive capacity have been investigated. To compare hadrons effectiveness with respect to photons, the RBE (Relative Biological Effectiveness) has been calculated for protons and carbon ions, starting from the experimental obtained results.
In order to evaluate the potential advantages of such a combined therapy, the interaction between radiation and drug has been studied. In particular, it is crucial to understand whether the interaction mechanism between the two cytotoxic agents is additive or synergic (resulting in a greater effectiveness in respect with the sum of the single radiotherapy and chemotherapy). For this reason, an analysis based on different definition of additivity between citotoxic agents has been performed.
Experiments with hadron and photon beams have been performed at the Centro Nazionale di Adroterapia Oncologica (CNAO) in Pavia and at the Istituto Nazionale dei Tumori in Milano (IRCCS foundation), respectively.

The present thesis consists of three parts, for a total of seven chapters. In the first part, the main concepts of Radio-chemotherapy will be introduced. The second part is devoted to the description of the experimental procedure and of the data analysis. In the third part the obtained results will be presented and discussed.
The first chapter will introduce the main concept of Radiobiology for Radiation Therapy, focusing on those aspect that are crucial for the presented study. In the following chap-

[1] Research and Development in Hadrontherapy
[2] Innovation in Radio and Particle Therapy

ter the fundamental of radiotherapy will be discussed and the main differences between conventional radiotherapy and hadron therapy will be presented. In Chapter 3 the rationale of combining radio- and chemotherapy will be introduced and the main properties of Epothilone B (the chemotherapy drug used in this study) will be presented. Chapter 4 will be devoted to the description of preliminary measurements necessary to characterize the biological system and the chemotherapy drug. In Chapter 5 the experimental setup and procedure will be described, while Chapter 6 and 7 will be devoted to the description of the data analysis and to the discussion of the experimental results, respectively.

CHAPTER 1

Radiobiology for Radiation Therapy

Giving a complete definition of Radiobiology is quite hard, considering that it is a very multidisciplinary science exploiting physical, chemical and biological aspects. In a very general way, Radiobiology can be defined as a science investigating the interaction of ionizing radiations with living organism (cells, tissues, plants, animals and human beings) through excitation and ionization processes. Due to its social implication, Radiobiology has been spreading out since the last century, in parallel with the discoveries in the field of Nuclear Physics. The first radiobiological observations rapidly followed the discovery of X-rays: tumor induction, skin reactions, damages of intestinal epithelium and so on have been qualitatively described since 1902.

X-rays have been gradually introduced in diagnostic and radiation started to be applied in cancer therapy, due to their lethal effect. In 1906 Bergonié and Tribondeau formulated a law, still substantially valid, according to which radiations result more effective in highly-proliferating tissues. Moreover, they definitely confirmed the cancerous action of radiation on normal tissues and they started to discuss the role of fractionated irradiation in radiotherapy treatments.

In the Thirties, new hypothesis concerning biological radiation effects through "indirect radiation action" begun to spread out, stimulated by the new findings on water radiochemistry: radiation-water reaction products (radicals, ions, molecular products) can diffuse in materials irradiated in the aqueous phase and modify molecules. The rising of these new theories, as well as the progress of biochemistry, gave a big contribution on Radiobiology development.

Since 1945 it was registered a huge increase in radiobiological literature, justified by the explosion of nuclear weapons in Japan, by a long series of nuclear tests during the Fifties and by the diffusion of nuclear power plants. Starting from this years, *in vitro* and molecular radiobiology hugely spread out in parallel with *in vivo* radiobiology studies on little animals.
Many effects such as the Oxygen Effect or the role of chemical radioprotector begun to be systematically studied. Research on molecular DNA repair mechanism, chromosomes' damages and comparison between the effectiveness of different types of radiation started in this years.

Nowadays Radiobiology have drastically spread out and is involving more and more physical, genetical, chemical, immunological and biological aspects. Various biological end-point are being studied both *in vitro* and *in vivo* for many different applications:

improvements in radiation therapy, in nuclear medicine and diagnostic as well as studies on appropriate shielding for interplanetary mission and so on.

In the field of Radiotherapy, Radiobiology is giving an increasing contribution, identifying more and more precisely the mechanisms at the basis of the tumor and normal tissue response to irradiation.
Thanks to *in vitro* radiobiology studies, it has been possible to quantitatively determine dose-effect dependencies. In particular, the surviving fraction of irradiated cells has been studied as a function of dose, and models to describe cell response to irradiation have been introduced (i.e. the "linear-quadratic model"). Quantities such as The Oxygen Enhancement Ratio have been introduced to better quantify cell response to irradiation in different condition, for example in the case of hypoxic tissues.
Since for many years radiation therapy exploited photon irradiation, photon beams are considered to be the reference radiation in radiotherapy. Nowadays another kind of therapy, named hadrontherapy, which takes advantage of charged particles energy deposition in biological tissues is spreading out for cancer treatment. Radiobiology is giving an important contribution in the development of this kind of therapy, comparing biological effects of charged particles to that of photons and identifying quantities such as the Relative Biological Effectiveness.
Moreover, bio-molecular and genetic studies are being performed to better understand the mechanism that regulate healthy and cancer cells response to irradiation.

The present study is in the field of *in vitro* radiobiological studies on radiotherapy (in particular hadrontherapy) combined with chemical agents. As a matter of fact, the clinical interest in the so-called combined therapies that exploit different citotoxic agents such as radiation and chemotherapy drug is recently rising, with the aim of obtaining better and better results in cancer treatment. From this point of view, Radiobiology can give an important contribution in the study of the response of cancer cells treated with drugs and irradiated, analyzing different end-points and quantitatively identifying the interaction mechanism between radiation and chemical agents.
The main goal of this study is to understand whether the interaction between charged particle beams used in hadrontherapy (proton and carbon ion beams) and the chemotherapy agent Epothilone B is additive or synergic and to analyze different end-points (i.e. clonogenic survival, invasive capability and cell growth) after cell exposure to radiation and Epothilone B.
Other important aspects of this work are the determination of charged particle Relative Biological Effectiveness and the comparison of results obtained with charged particles with those obtained with photons, that, as mentioned before, are the reference radiation in Radiotherapy.

In this Chapter the main physical quantities and principles of *in vitro* Radiobiology will be introduced, focusing on the aspects that are more important for the present study, such as the biological effectiveness of different radiation types and the effects of radiation at cellular level.
In particular the main differences in cell response to photons or charged particle irradiation will be described.

1.1 Absorbed Dose and Linear Energy Transfer

The fundamental physical quantities in Radiobiology are the Adsorbed Dose and the Linear Energy Transfer.

The Adsorbed Dose was introduced by the International Commission of Radiation Units and Measurements in 1971 (ICRU, 1971), in order to describe the effects of energy losses by ionizing radiation in the material.
It is a non-stochastic quantity, defined as the ratio between the mean energy dE deposited by ionizing radiation, and the unit of mass, dm:

$$D = \frac{dE}{dm} \tag{1.1}$$

The energy dE is the difference between all the energy entering the considered volume and the energy leaving the volume, taking into account any mass-energy conversion within the volume. Energy deposition occurs in a stochastic way; thus, this definition is meaningful only if the elementary mass dm is great enough to guarantee a statistically relevant number of energy releases. In the International System, the unit used to express the dose is the Gray (Gy): $1Gy = 1Jkg^{-1}$.
The adsorbed dose is a crucial quantity in Radiobiology, because it describes in a macroscopic way the energy released by ionizing radiation interacting with matter, but it is not enough to completely describe and predict the biological effects: other parameters are needed, such as the *Linear Energy Transfer*, the *Relative Biological Effectiveness* and the *Oxygen Enhancement Ratio*. These parameters will be discussed more in detail in the next sections.

The biological effectiveness dramatically depends on radiation-matter interaction modes. For electromagnetic radiation ionizations are uniformly distributed, while for particles they are localized in proximity of the particle's track. For this reason it is important to introduce a quantity that takes into account the energy locally released by radiation: the Linear Energy Transfer (LET). It is defined as the average energy deposited per unit length of radiation track in the crossed medium:

$$LET = \frac{dE}{dx} \tag{1.2}$$

In order to quantify the energy locally transferred in the medium along the track, an energy threshold $\triangle$ is introduced: it corresponds to the range of secondary electrons over which the energy release is no more considered to be local. If $\triangle$ is large enough to consider every energy deposition to be local, the Linear Energy Transfer coincides with the Stopping Power.
High-LET radiations release great energy amount in a short path, causing complex damages to every structure near the particle track. For this reason, high-LET radiation biological damages are poorly repaired in a correct way. In figure 1.1 a comparison between the energy depositions in a typical cellular volume for low and high-LET ionizing radiations is shown. In panel a) it is possible to see that the spatial dose distribution of X-rays is highly uniform; for this reason low LET radiations are called sparsely ionizing radiations. In the other panels the spatial dose distribution for carbon ions (high-LET radiation) at 1 MeV/u, 15 MeV/u, 200 MeV/u is reported. In this case the local dose shows sharp peaks due to the high-LET along the track, and, as the energy increases,

a background of low dose. The latter contribution is due to low-LET δ rays. high-LET radiations are called densely ionizing radiations.
Due to their large Stopping Power, heavy ions, such as carbon ions, are classified as high-LET radiation, whereas protons and photons are typically considered to be low-LET radiations.
In table 1.1, different radiations' LET values in water are reported. Since secondary

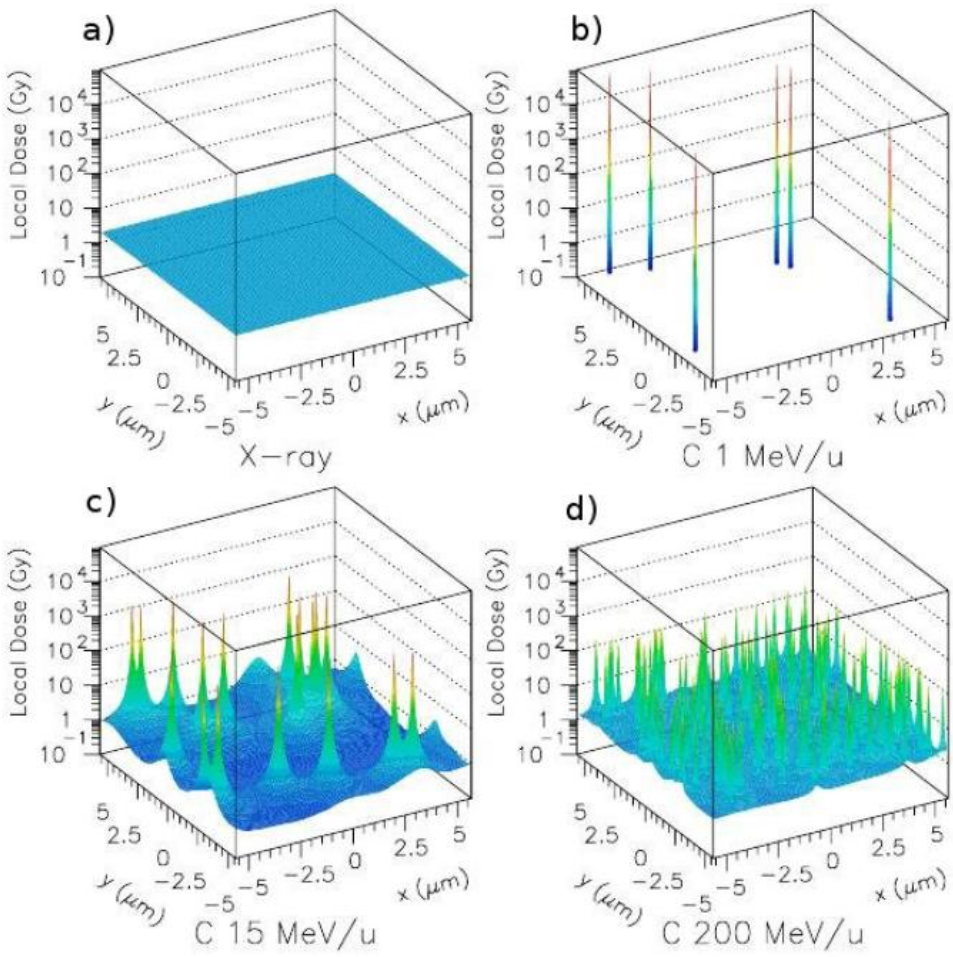

Figure 1.1: Simulations of microscopic dose distribution by X-rays (a) and carbon ions at different energies (b,c,d) (Scholz, 2003).The average macroscopic dose is 2 Gy in all the cases.

particles have different charge and velocity, they have different LET values; for this reason an average LET is calculated and, despite not fully describing energy releases at a microscopic level, it is used to characterize radiation quality.
Moreover, when dealing with thick targets, it is necessary to consider that the LET changes with depth due to the beam hardening.
Dose and LET concepts do not permit a precise prediction of the energy deposited in a microscopic site, for this reason microdosimetry affirmed itself. The two main physical quantities in microdosimetry are the *specific energy* and the *lineal energy*. Microdosimet-

Low-LET Radiation	LET [keV/μm]
γ-rays (^{60}Co)	0.3
X-rays (250 kV)	2
X-rays (3 MV)	0.3
protons (200 MeV)	0.4
High-LET Radiation	LET [keV/μm]
Neutrons (14 MeV)	2.3
α-particles (5 MeV)	95
Carbon Ions (10-250 MeV/u)	15-170
Heavier Ions	100-2000

Table 1.1: LET values in water for different types of radiation. LET=10keV/μm separate high-LET from low LET. Data taken from (Podgorsak, 2010).

ric quantities are required when dealing with volumes small enough that the relative fluctuations of energy deposition are not negligible. Relative fluctuations are larger for small volumes and small doses. (Kellerer, 1984)
The specific energy z is the random variable corresponding to the absorbed dose. In order to define the dose starting from the specific energy, it is useful to consider its distribution function $F(z)$, whose derivative with respect to z represents the probability density $f(z)$. The absorbed dose is then equal to the mean specific energy:

$$D = \bar{z} = \int_0^\infty z f(z) dz$$

The lineal energy y is the random variable corresponding to the LET and it is defined as the ratio between the imparted energy and the mean chord lenght. This quantity is related to energy increments produced by single energy deposition events.

1.2 Physical and Chemical effect of ionizing radiation in biological systems

Ionizing radiation can be divided in two groups: directly and indirectly ionizing radiations.
Directly ionizing radiations deposit energy by Coulomb interaction with molecules, directly exciting and ionizing them. This kind of interaction is typical of charged particles and its typical time scale is 10^{-16} s.
Indirectly ionizing radiations deposit energy through a two-step process: interacting with biological matter, they produce secondary electrons that can excite and ionize molecules inside the cell. These processes are typical of photon interaction with matter and they take longer time.

To describe more in detail the biological effect of radiation, we can identify three main phases that characterize the interaction of ionizing radiation with biological system.
In the Physical phase, radiation ionizes molecules inside the cell. The typical time scale of this phase varies between 10^{-16} s and 10^{-12} s, depending on the kind of radiation (directly or indirectly ionizing).

The following phase, in which the ionized molecules chemically react causing free-radical formation, is called chemical phase. Free-radicals are molecules with unpaired electrons and have high probability to interact with cellular targets (i.e. DNA), modifying their structure and damaging them. This phase takes from $10^{-12}s$ to $10^{-6}s$.
When a charged particle directly ionizes a biologically important molecule inside the cell (i.e. DNA), we speak about "direct action" of radiation. This process can be schematically summarized:

$$RH \rightarrow RH + e^- \rightarrow R^0 + H^+ + e^-$$

When particles ionize, for instance, water molecules inside the cell, the radiation action is "indirect". Most of the damages induced by low-LET radiation (such as photons) are due to the indirect action, while for high-LET radiation like carbon ions the contribute of the indirect action to the damages is quite negligible.
In the case of indirect action the chemical phase is more complex, and can be summarized in different steps:
- after the ionization of a water molecule, the free electron produced can be captured by another molecule. In this way the molecules H_2O^+ and H_2O^- are produced. These molecules are very unstable and they dissociate in $10^{-10}s$ producing H^0, OH^-, H^+ and OH^0. Other reactions can occur, producing, in particular, hydrated electrons; this electrons are shielded by a water molecule and their life is longer than that of free electrons.
- All these reactions products can diffuse, recombine or react with complex and biologically important molecules, altering their structures:

$$RH + OH^0 \rightarrow R^0 + H_2O$$
$$RH + H^0 \rightarrow R^0 + H_2$$

The radical R^0 is produced both in the case of direct and indirect action. It can alter the complex structure it belongs to (for example a chromosome), modifying or inhibiting its functions. When Oxygen is present, the radical R^0 reacts with it, becoming a peroxide. The peroxide radical is stable, thus the damage cannot be spontaneously repaired

by recombination with positive ions: the damage is thus fixed.
The biological phase is made up of all the processes that occur after the damages at the main biological targets. The fixed damages can be repaired through enzymatic processes, such as the homologous recombination and the nonhomologous end-joining. The efficiency of this repair pathways dramatically depend on the complexity of the damages. If the repair is successful, no biological damage occur and the cell can undergo its life-cycle without any problem; otherwise cell death, genetic or cancer effects can take place.

1.2.1 DNA damages

The most critical macromolecule inside the cell is the DNA, contained in the cell nucleus. There are some evidences that DNA is the most important structure in the cell: for simple organisms it has been possible to find a quantitative relation between biological functions and DNA damages. In more complex biological systems it has been observed that the loss of some biological functions can be directly linked to DNA damages.
The typical DNA structure is a double-stranded helix consisting on two long polymers made up of monomers called nucleotides, each of them constituted by a phosphoric acid molecule, a molecule of deoxyribose and an organic nitrogenous base (Adenine, Thymine, Guanine or Cytosine). The two strands are coupled thanks to the complementarity between nitrogenous bases and their typical distance is of few nanometers.
Nucleotides are arranged in a highly specific sequence that encodes all the genetic information necessary for the development and correct functioning of living organisms. Since the genome is contained in a single copy within the cell, it is crucial to preserve this sequence, to prevent and eventually repair DNA damages.
DNA lesions can occur due to different agents, such as ionizing radiations. For the

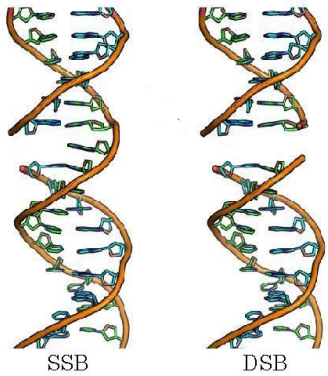

Figure 1.2: Single-Strands Breaks (SSB) and Double-Strand Breaks (DSB) in DNA double-helix. (http://www.bioquicknews.com/node/2696).

present study two kinds of lesions are particularly relevant: Single and Double Strand Breaks, schematically described in figure 1.2.

Single-Strand Breaks: Only one of the two DNA strands is damaged. This damage can be easily repaired by the cell, thanks to the undamaged strand that can be used as a template to reconstruct the damaged one.

Double-Strand Breaks: both the strands are damaged. If the lesions are far enough from each other, they can be repaired as single strand breaks, otherwise more complex repair mechanisms are needed, with lower efficiency. If the lesion is uncorrectly repaired cell death or chromosome aberrations (leading to carcinogenesis) can occur. Multiple lesions, formed in few helical turns of the DNA molecule are considered **clustered damage**, very complex lesions, sometimes difficult to be repaired. The DSB distribution is dramatically affected by the radiation type and LET. In figure 1.3 a comparison between the expected DSB distributions after different LET irradiation is reported.

After DNA damages occurring, cells can undergo different fates; if lesions are not lethal,

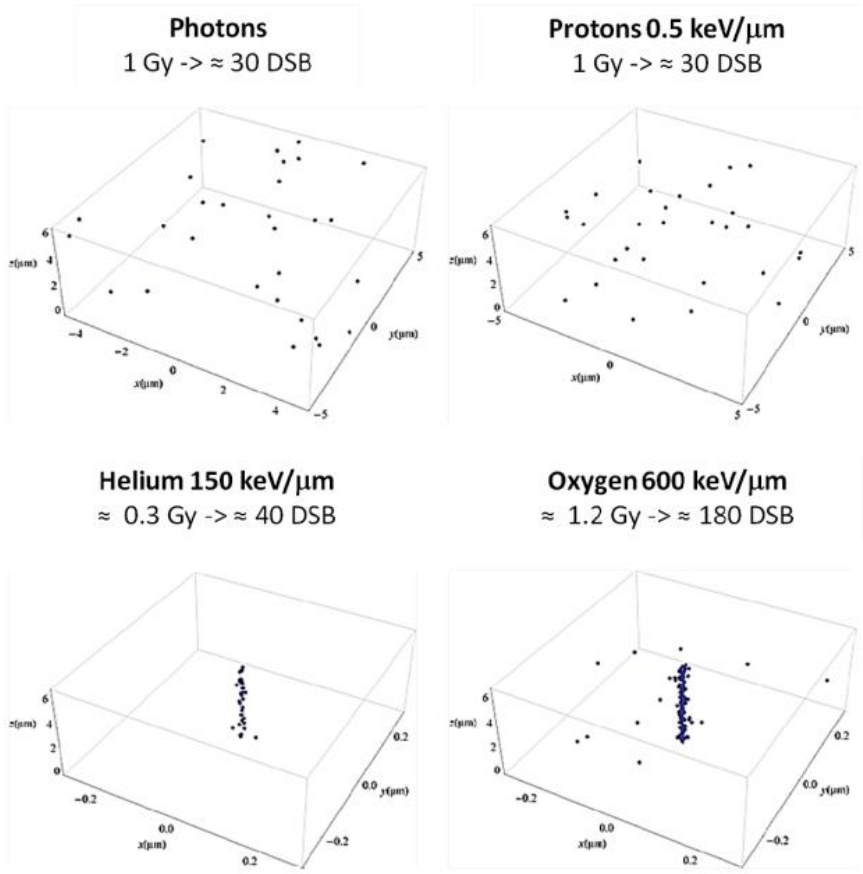

Figure 1.3: Simulated patterns of DSB distribution after different LET irradiation in a cell nucleus (Tommasino and Durante, 2015).

they can report no consequences after irradiation or they can suffer a division delay; otherwise when lethal lesion occurs cells can die via *apoptosis* (they die before division or just afterwards by fragmentation into smaller bodies) or undergo a *reproductive failure* (cells die attempting the first or the subsequent divisions, definitively loosing their clonogenic ability).

1.2.2 Cell damages: clonogenic death

One of the main biological effects in radiotherapy is the reproductive death of irradiated cells. This is one of the most common end-point studied in Radiobiology: the clonogenic survival of a single cell is defined as its ability to give rise to a colony of "daughter" cells.
It often happens that after being damaged, a single cell is able to divide two or three times before definitely loosing its clonogenic capacity without further dividing; for this reason, conventionally a cell is considered to have survived from a clonogenic point of view when it produces a colony made up of at least 50 cells.

In order to evaluate clonogenic survival as a function of radiation dose, clonogenic assays can be performed measuring the plating efficiency, as it will be described in Chapter 5.

Usually, the relation between the surviving fraction of an irradiated population and the radiation dose is plotted as shown in figure 1.4: the surviving fraction is reported on a logarithmic scale on the ordinate, while dose is plotted on a linear scale on the abscissa. The shape of the curve depends not only on the kind of irradiated cells, but also on the type of radiation. In particular, densely ionizing radiations give rise to a cell survival curve that exponentially depends to radiation dose. For sparsely ionizing radiations, on the contrary, the curve shows a "shoulder", that typically is related to the DNA repair capacity. In fact, considering that High-LET radiations cause more complex and difficultly repairable damages, this shoulder does not appear in high-LET radiation survival curves. Moreover in very radiosensitive cells, lacking efficient repair mechanisms, the quadratic term is usually small.

At the moment, the most accredited model used to parametrize the dose-survival curve of irradiated cells is the Linear Quadratic (LQ) Model. This model conjectures that the lethal lesions are the double strand breaks that can be caused by a single radiation hit (linearly depending from dose) and by the interaction of two radiation hits (quadratically depending from dose). Thus, the frequency f of lethal lesions can be expressed as a function of dose:

$$f(D) = \alpha D + \beta D^2 \tag{1.3}$$

In the hypothesis of a random frequency of lethal lesions, the surviving fraction $S(D)$, representing the fraction of cells carrying no lethal damages, can be expressed according to the Poisson distribution, obtaining:

$$S(D) = e^{-\alpha D - \beta D^2} \tag{1.4}$$

For high-LET radiations, the first kind of damages is more probable, so that the β parameter is usually negligible in respect with α. Otherwise, for low-LET radiations, the lethal damage can be caused by the interaction of sub-lethal lesions due to different radiation hits. For this reason the parameter β is not negligible anymore and dose-survival curves show the typical shoulder (dominant especially for low doses) reported in figure 1.4.

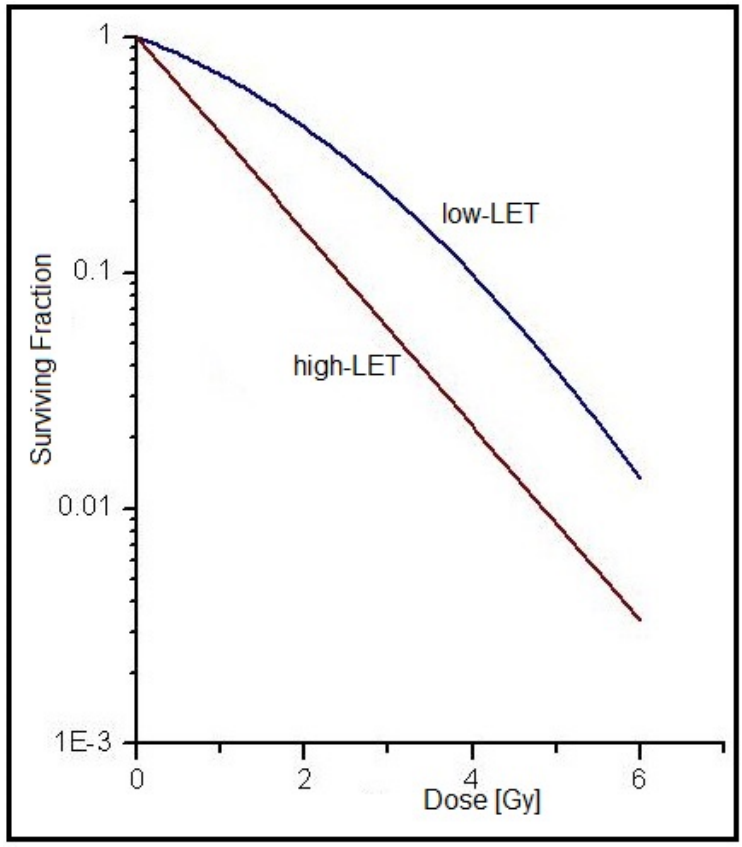

Figure 1.4: Dose-Survival curves for low-LET (blue) and high-LET (red) radiation.

1.3 Relative Biological Effectiveness

Nowadays charged particle therapy (in particular with protons) is a consolidate alternative to photon radiotherapy. When dealing with different irradiation modalities, it is necessary to consider the potentially different biological effectiveness of different treatment planning. As a matter of fact, charged particles are characterized by energy releases that are substantially different from the photon ones, as mentioned before. The increased LET values of charged particles at the end of their track in respect with photons, usually reflects in a grater biological effectiveness in cell killing. By the fact, as mentioned in the previous sections, high-LET (densely ionizing) radiations typically induce a greater frequency of unrepairable damages. In order to quantify this greater effectiveness, the *Relative Biological Effectiveness* (RBE) is introduced.

RBE is defined as the ratio between photon and charged particles dose resulting in the same level of a given biological effect (i.e. the same surviving fraction).
In figure 1.5 RBE is reported as a function of LET for different particles in V79 cells. It is possible to notice that RBE increases with LET, reaching a maximum at LET values equal to $100 - 150$ keV/μm; after this maximum, RBE decreases. This behavior can be explained considering that DNA damages are more effective when the distance between

two consecutive energy deposition is of the order of few nanometers (the distance between the two DNA strands). When the radiation is sparsely ionizing, DNA repair is more efficient, while when the ionization density is very high, *overkilling* can occour: apart of the energy released inside the cel nucleus does not have a role in DNA breaks and at the same time the number of cells crossed by radiation decreases.
RBE depends not only by radiation LET and particle type, but also on multiple physical

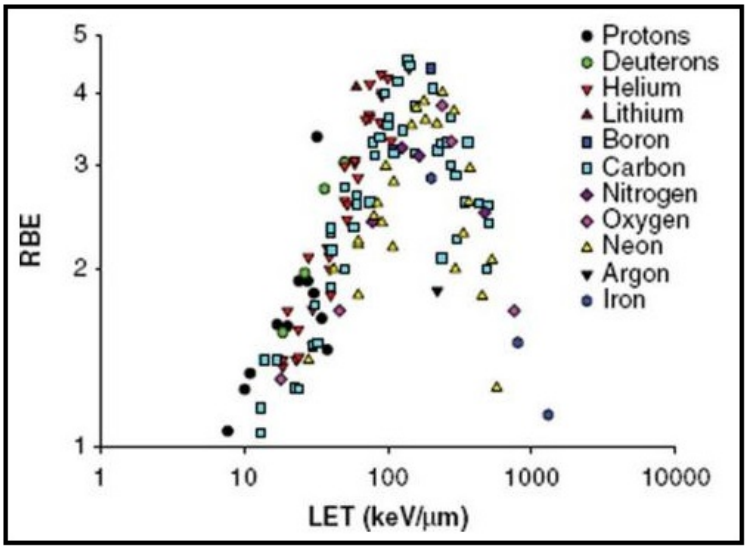

Figure 1.5: RBE as a function of LET for different particles in V79 cells (Sorensen et al., 2011).

and biological factors, such as cell types, beam characteristics, the cycle phase in which cells are irradiated and so on. Even the biological end points studied differently modulate RBE values. Despite RBE is nowadays widely use in clinics to define and compare treatment planning, it is still an issue that needs further investigation, due to its complex dependence on all the mentioned factors.

In hadron therapy the dose is prescribed in Gy(RBE), following the prescription of the International Commission on Radiation Units and Measurements ((ICRU, 2007)): for example, when using a proton RBE of 1.1, a prescription dose of 2 Gy(RBE) in proton therapy corresponds to a physical dose of 1.8 Gy.
Very important phenomena that can modulate charged particles RBE are the target and projectile fragmentation, as well as range uncertainties.

1.4 Cell cycle effects

The *cell proliferation cycle* is made up of two well-defined periods: the synthesis (S) of DNA, in which the genome is duplicated in order to guarantee that each of the two daughter cells preserve all the necessary genetic information, and the cell division, named mitosis (M). These periods are separated by two gaps: G1 and G2. In the G1 phase the DNA has not yet been duplicated, while the G2 gap separates the S and the M phases. After the mitosis, cytodieresis occurs.

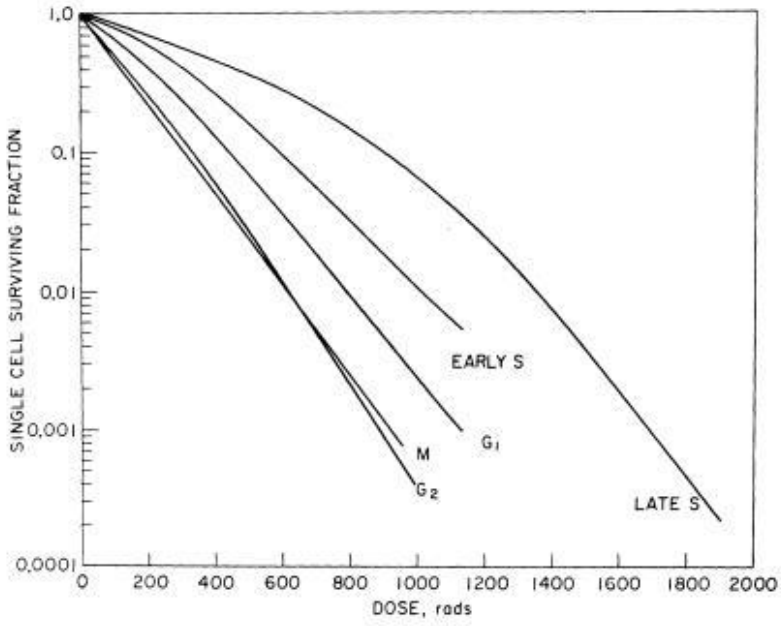

Figure 1.6: Dose-survival curves of V79 cells irradiated in different phases of their cycle (Sinclair and Morton, 1966). Cells irradiated in the G2-M phase are more radiosensitive.

From the comparison between dose-survival curves of synchronized cells irradiated in different phases of their cycle reported in figure 1.6, it is possible to notice that their radiosensitivity is very different in different phases. Generally, cells are most most radiosensitive in the G2-M phases. By the fact, during this phase the genetic material is in duplication and the chromatin is gathered in the chromosomes so that the probability of DNA breaks induced by radiation increases. Moreover it is well-known how in this cycle phase, DNA repair pathways are less effective than in the other phases.

This dependence of radiosensitivity from the cell cycle phase, justify the concomitant use of radiation and drugs able to modify the cell cycle and eventually stop cells in the G2-M phase, or able to inhibit DNA repair, as we did in the present study.

1.5 Oxygen Enhancement Ratio

As mentioned in section 1.2, the presence of Oxygen in irradiated tissues can modify the effect of radiation fixing DNA damages that consequently cannot be spontaneously repaired by free-ions recombination. In order to quantify this effect, the *Oxygen Enhancement Ratio* (OER) has been introduced. It is defined as the ratio between the doses necessary to produce the same level of a certain biological effect in hypoxic or normoxic conditions:

$$OER = \frac{D_{hypoxic}}{D_{normoxic}}$$

In scarcely vascularized tumor tissues, the content of Oxygen is generally low, contributing to tumor radioresistance.

Looking at the graph reported in figure 1.7, it is possible to notice that dealing with low-LET radiations (LET $< 10keV/\mu m$) the OER vary between 2 and 3, while for high-LET radiation it is normally lower. As a matter of fact, for low LET radiation biological effects are mainly due to free radicals and to the fixing of the damage made possible by the presence of Oxygen. In the case of high-LET radiation, the direct breaking of DNA molecules prevails.

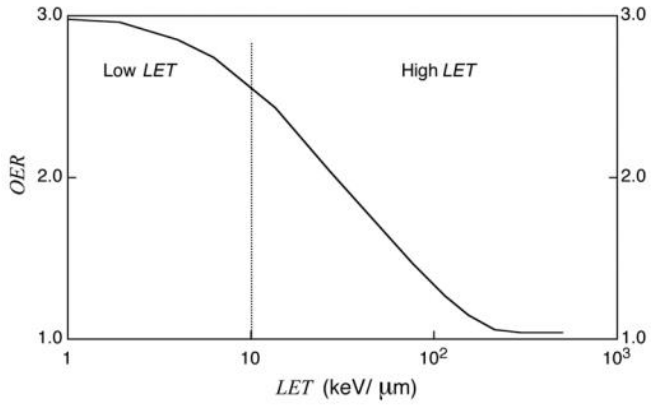

Figure 1.7: OER against LET. The vertical line conventionally separates the low LET region (LET $< 10keV/\mu m$) from the high-LET region (LET $> 10keV/\mu m$) (Podgorsak, 2005).

1.6 Dose fractionation effects

Cell response to irradiation can be modulated also by dose fractionation. In fact, delivering the same radiation dose in more than a single fraction could produce less cell killing because sublethal damage repair and cells repopulation occur between a fraction and the subsequent. The former is prevalent for late-reacting tissues and the latter for early-reacting ones (Podgorsak, 2005).

From one hand, dose fractionation results in a better therapeutic ratio; anyway, from the other hand, in a fractionated treatment it is necessary to reach a grater total dose than in a single section, in order to achieve a desired level of biological damage to the tumor. The rationale of fractionation can be schematically explained taking into account two aspects (Podgorsak, 2005): as mentioned before, dose fractioning spares normal tissues thanks to repair of sub-lethal damages and cells repopulation and fractionation can increase tumor damage by reoxygenation and redistribution of tumor cells.

It has been noticed that dose fractionation effects are significantly reduced in high-LET radiation exposure. This fact can be explained considering that this radiations mainly induce directly lethal lesions, so that sub-lethal lesions interaction became negligible.

CHAPTER 2

Fundamentals of Radiotherapy

The main purpose of Radiotherapy is to obtain an optimal tumor local control, avoiding as much as possible any kind of possible side-effect.
As the conformity of the irradiation to the tumoral volume increases, the probability of curing the tumor avoiding side-effects becomes greater. For this reason any irradiation technique which allows a great radiation dose in tumoral tissues is advantageous; in fact, it is possible to reduce the dose absorbed by healthy tissues, avoiding several complications and maintaining high the dose to the tumor, or, viceversa, it would be possible to increase the dose to the tumor and achieve a better local control with a dose to healthy tissues comparable to the one delivered in conventional therapies.
The use of hadrons in radiotherapy was first suggested by Wilson in 1946. The main idea was to exploit the physical selectivity of proton and light ion beams in order to irradiate tumors closed to organ at risk that otherwise would be irradiated. Moreover, when compared to protons, light ions, such as carbon ions ($^{12}C^{6+}$), have the advantage of a greater ionization density at the end of their range, leading to a greater biological effectiveness (Amaldi, 1999). This property is valuable in the treatment of radio-resistant tumors. Nowadays, apart from proton beams that are quite diffused, carbon ions are the light ions most used in hadron therapy. This is due to the fact that, with increasing atomic number Z, the biological effectiveness increases, but the projectile fragmentation became less and less negligible, leading to dosimetrical issues. As a matter of fact, carbon ion beams seem to be a good compromise between the high biological effectiveness and the complications arising from the projectile fragmentation.

In the following sections the main physical differences between conventional radiotherapy and handrontherapy will be discussed more in detail.

2.1 Conventional radiotherapy

Conventional radiotherapy exploits photon beams produced using electron linear accelerators (LINAC). This accelerators produce a continuous photon spectrum by bremsstrahlung processes, slowing down a monochromatic electron beam in a target made up of an heavy material, such as Tungsten. As showed in figure 2.1, photon beams are characterized by an exponential absorption, after a maximum, reached after very few centimeters, depending on the photon's maximum energy. This depth is called *"build-up"* and corresponds to the maximum range of secondary electrons produced by the primary photons interacting with the most superficial layers of the irradiated material. In the ionizing energy region, photons interact with matter by three different processes, each of them

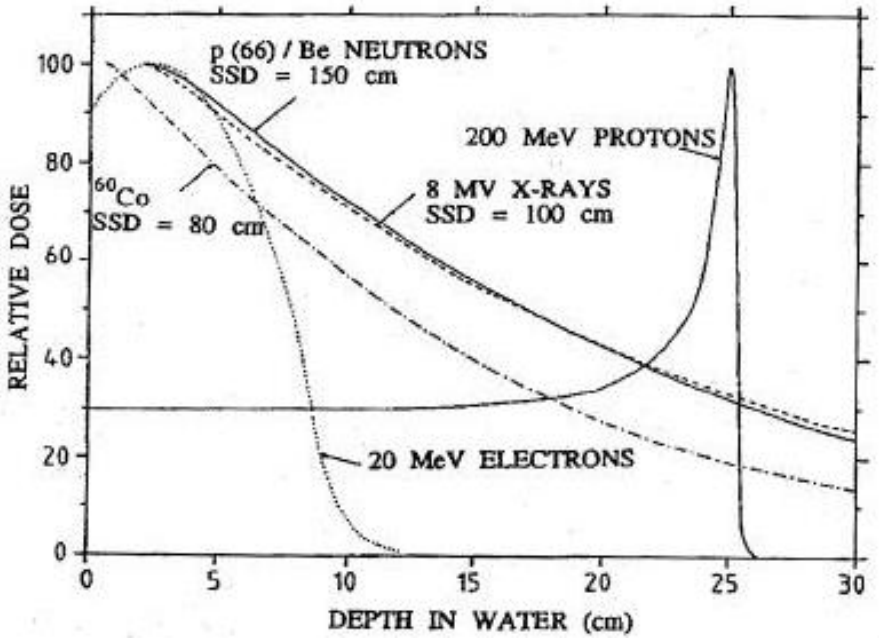

Figure 2.1: Depth-dose curves in water for 20MeV electrons, photons from a Cobalt source and 8MV LINAC, neutrons and 200 MeV protons (Amaldi, 1999).

dominant in a given energy range: photoelectric effect, Compton effect and pair production.

In figure 2.2 photoelectric effect, Compton effect and pair production cross sections are reported in function of the primary photon energy. In the typical energy range of photon-radiotherapy, the Compton effect is the dominant one.
In the Compton scattering, a photon interacts with an electron of the absorbing material and is deflected at an angle ϑ. It transfers a portion of its energy to the recoil electron. Since all scattering angles are possible, the energy transferred to the electron ranges from zero to a great portion of the incident photon energy.
The energy of the scattered photon is given by ((Knoll, 2000)):

$$h\nu' = \frac{h\nu}{1 + \dfrac{h\nu}{m_0c^2(1 - cos\vartheta)}} \tag{2.1}$$

The angular distribution of scattered photons is described by the *Klein-Nishina formula*:

$$\frac{d\sigma}{d\Omega} = Zr_0^2 \left(\frac{1}{1 + \alpha(1 - cos\vartheta)}\right)^2 \left(\frac{(1 + cos^2\vartheta)}{2}\right) \left(1 + \frac{\alpha^2(1 - cos\vartheta)^2}{(1 + cos^2\vartheta)\,[1 + \alpha(1 - cos\vartheta)]}\right) \tag{2.2}$$

where $\dfrac{d\sigma}{d\Omega}$ is the differential scattering cross section, Z is the atomic namber of the ab-

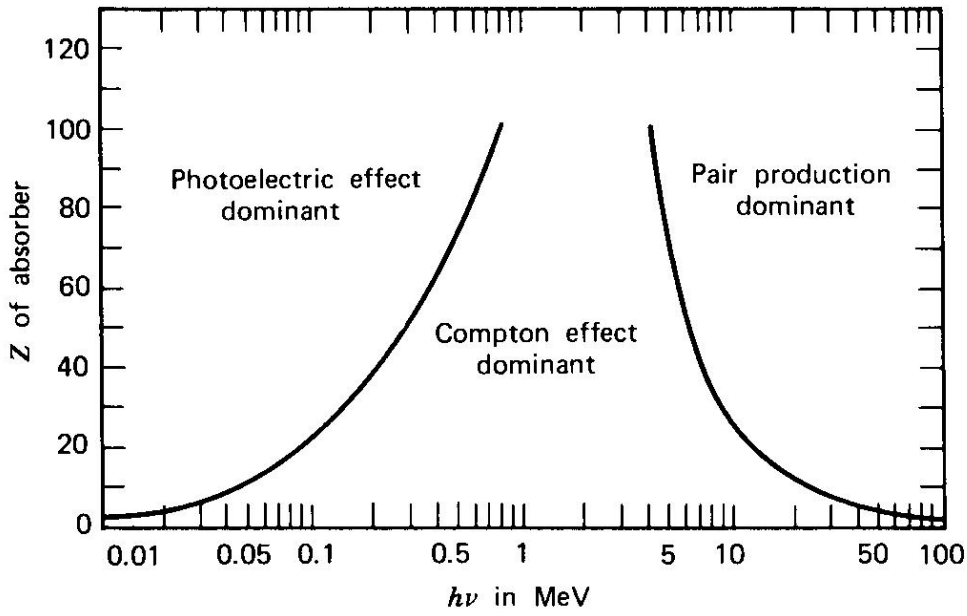

Figure 2.2: Photoelectric process, Compton effect and pair production cross sections as a function of incident photon energy. (Knoll, 2000).

sorber material, r_0 is the classical electron radious and $\alpha = \dfrac{h\nu}{m_0 c^2}$ is the fine structure constant.
The angular distribution for different energies is reported in a polar plot in figure 2.3. It is possible to notice that, for the photon energy range typically used in radiotherapy, photons are scattered mostly in the forward direction.

In photoelectric process, a photon of energy $h\nu$ interact with an absorber atom. As a result of this interaction, the photon completely disappears and a photo-electron is ejected by the atom with an energy $E = h\nu - E_b$, where E_b is the electron binding energy Knoll (2000).
As a consequence of the electron emission, the interaction gives origin to an ionized absorber atom, with a vacancy in one of the bound shells. This vacancy is filled capturing a free electron or rearranging electrons from other shells, producing characteristic X-rays or Auger electrons.

The pair production process is possible if the photon energy exceeds twice the electron energy rest-mass (1.02 MeV). In the interaction with the Coulomb field of a nucleus, the photon disappears and origins an electron-positron pair, the energy exceding 1.02 MeV is converted in the kinetic energy of the electron and the positron. As we can see from figure 2.2, this process is dominant for high energy value of the incoming photon.

Despite the exponential decay of the absorbed dose with depth shown in figure 2.1, photon beams can be used even to irradiate deep-seated tumors: this can be done using multiple beams entry ports. To apply this irradiation techniques it is necessary that

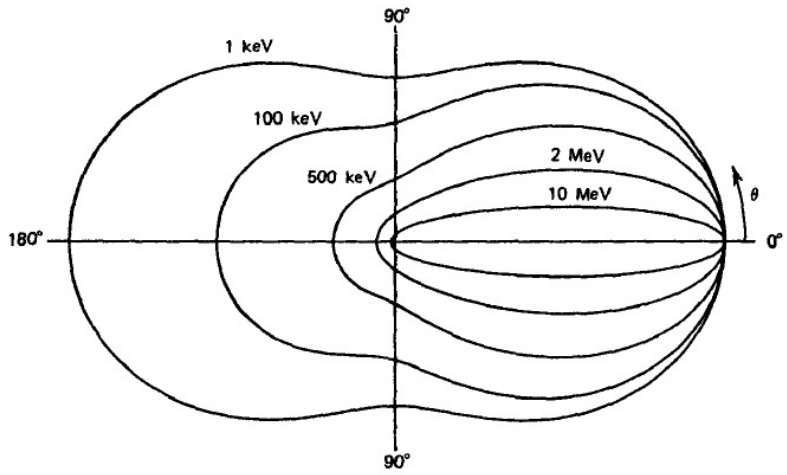

Figure 2.3: Number of photons (incident from the left, energy indicated in the plot) scattered at angle ϑ (Knoll, 2000).

the accelerating structure has the capability to rotate around an horizontal axis (Amaldi, 1999). The state of art in photon beam radiotherapy is represented by the *conformed Intensity Modulated RadioTherapy* (IMRT), in which tens of non-complanar photon beams are exploited and their intensity is varied across the irradiation field thanks to variable collimators and personalized absorbers, in order to achieve a better and better tumor local control. Also electron beams produced by LINAC can be used for the treatment of superficial tumors; in fact, as it can be seen in figure 2.1, their dose-profile is characterized by a maximum range (that depends on the initial beam's energy), followed by a low tail due to bremsstrahlung photons.

2.2 Hadrontherapy

The word "hadrontherapy" refers to different oncological radiotherapy techniques that exploits non-elementary particles made of quarks, such as protons, light nuclei and neutrons. Nowadays the use of neutron in cancer treatment is becoming less and less important, while the use of charged hadrons is spreading out: protons and carbon ions are the most utilized charged particles in radiotherapy treatments.

As shown in figure 2.1, the depth-dose curve of protons is completely different from that of photons and neutrons; in fact charged hadrons loose their energy interacting with matter in a very different way from other particles: they are characterized by little lateral scattering when penetrating matter and they release the maximum energy at the end of their track, this permits to release high doses even in deep-seated tumor and to spare organs at risk (OAR) in the proximity to the distal part of the tumor volume. In figure 2.4 a comparison between treatment plannings with conventional X-rays and with protons is displayed: thanks to their finite range, protons spare the OAR anterior to the vertebral column.
The enhanced selectivity of charged hadron beams, compared to photon beams, allows

to obtain the same tumor control probability and a smaller normal tissue complication probability, or viceversa a better tumor control and the same level of normal tissue complications.

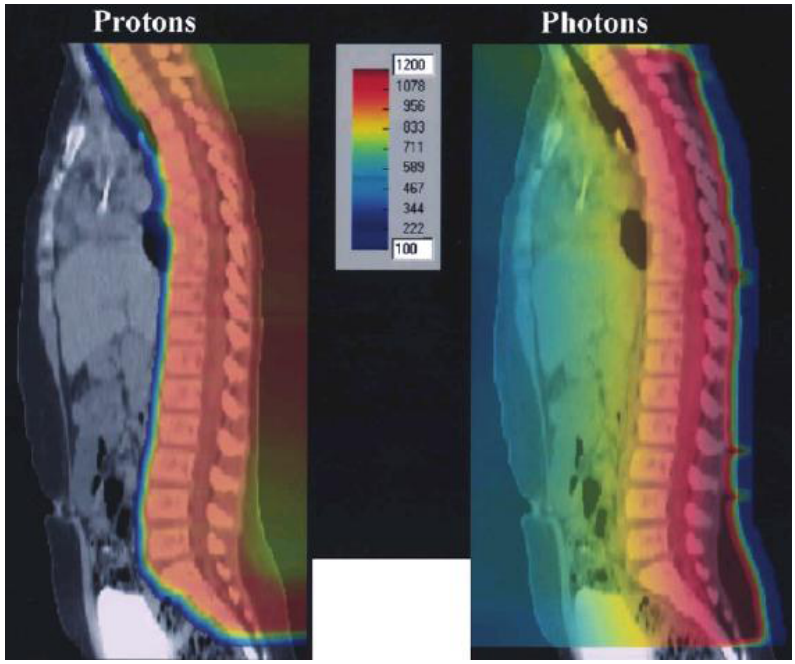

Figure 2.4: Dose calculation in a treatment planning for a patient with medulloblastoma. Right side: irradiation with posterior 4 MV LINAC photon beam. Left side: irradiation with posterior proton beam (Suit et al., 2003).

Energy losses for charged hadrons are described by the Bethe-Bloch equation (Bethe, 1930; Bloch, 1933), that will be discussed in the next section.

2.2.1 Bethe-Bloch equation

We consider a charged particle, i.e. a proton or a light nucleus, with charge ze and velocity v passing through a material with atomic number Z and we neglect the interaction between the moving particle and the nuclei of this material. Thus the dominant mechanism for energy loss is the excitation or ionization of the crossed material. We consider the interaction of a fast particle with an electron initially at rest at a distance b (called *impact parameter*) from the track particle. The essential physics of the energy loss process can be firstly described using a classical approach (by way of example, see Cottingham and Greenwood (2001)).

The equation of motion for the fast particle is

$$\frac{d\mathbf{p}}{dt} = ze\mathbf{E},$$

where **p** and **E** are the fast particle momentum and the electric field of the rest electron, respectively. The magnetic field due to the rest electron is considered to be negligible. The particle acquires a momentum

$$\Delta \mathbf{p} = \int ze \cdot \mathbf{E} dt$$

Its longitudinal component $\Delta p_{\parallel}$ cancels for symmetry, while the transverse component $\Delta p_{\perp}$ (which is the same both in the laboratory and in the particle frame) is given by

$$\Delta p_{\perp} = p_T = \int ze \cdot E_{\perp} dt = \frac{ze}{v} \int E_{\perp} dx$$

if we approximate the particle motion by $x = vt$. This integral can be evaluated applying the Gauss theorem to a cylindrical surface with radius b and infinite length, around the particle track.

$$p_T = -\left(\frac{ze^2}{4\pi\epsilon_0}\right)\frac{2}{bv} \tag{2.3}$$

Since momentum is conserved, the rest electron acquires a momentum $-p_T$ and, in a non-relativistic approximation, it gains the energy ΔE, lost by the fast particle.

$$\Delta E = -\frac{p_T^2}{2m_e} = -2\left(\frac{ze^2}{4\pi\epsilon_0}\right)^2 \frac{1}{b^2 v^2 m_e} \tag{2.4}$$

where m_e is the electron rest mass. When the fast particle moves throught a distance dx in the material it passes a number of electron with impact parameter between b and $b+db$ given by

$$Z\frac{\rho}{A}(2\pi b db dx)$$

where Z, ρ and A are respectively the atominc number, the mass density and the mass number of the material.

Thus, the energy lost interacting with these electrons is given by

$$d^2E = -4\pi\left(\frac{ze^2}{4\pi\epsilon_0}\right)^2 Z\frac{\rho}{A}\frac{db}{bm_e v^2}dx.$$

Integrating this expression over all the impact parameter between b_{min} and b_{max} we obtain the *stopping power*:

$$-\frac{dE}{dx} = 4\pi\left(\frac{ze^2}{4\pi\epsilon_0}\right)^2 \frac{\rho Z}{Am_e}\frac{1}{v^2} log\left(\frac{b_{max}}{b_{min}}\right) \tag{2.5}$$

b_{max} and b_{min} can be estimated with the following consideration (Cottingham and Greenwood, 2001):

- due to the Heisemberg indetermination principle, the minimum size of a wave packet is $\frac{\hbar}{p} = \frac{\hbar}{\gamma m v}$. The dimensions of a wave-packet must be less than the impact parameter b in order to apply the classical approach with good approximation. In the centre of momentum frame, the uncertainty in the position of the two particles is the same, thus, considering that the fast particle is much more massive than the electron, in the centre of momentum frame it can be considered to be at rest while the electron moves with velocity near to v and momentum $p \approx \gamma m_e v$. As a consequence,
  $b_{min} \approx \frac{\hbar}{\gamma m_e v}$.

- at large impact parameter, the energy transfer is small so that it is necessary to take into account the fact that electrons are bound in atoms and that there is a minimum ionization energy I. For the indetermination principle, the energy E of a particle can be known with an uncertainty $\Delta E = \frac{\hbar}{\tau_c}$, where $\tau_c \approx \frac{b}{\gamma v}$ is the collision time. For this reason
  $b_{max} \approx \frac{\hbar \gamma v}{I}$.

The equation 2.5 can be so re-written

$$-\frac{dE}{dx} = 4\pi \left(\frac{e^2}{4\pi\epsilon_0 c}\right)^2 \left(\frac{z}{\beta}\right)^2 \rho \frac{Z}{m_e A} log\left(\frac{\gamma m_e c^2 \beta^2}{I}\right) \tag{2.6}$$

Equation 2.6 is known as *Bohr formula* and describes the energy loss of a charged particle heavier than an electron moving through matter.

A calculation of the ionizing energy losses that takes into account relativistic and density effects has been performed by Bethe and Bloch, leading to the following equation for the stopping power:

$$-\frac{dE}{dx} = 4\pi \left(\frac{e^2}{4\pi\epsilon_0}\right)^2 \left(\frac{z}{c\beta}\right)^2 \rho \frac{Z}{m_e A} \left(log\left(\frac{\gamma m_e c^2 \beta^2}{I}\right) - \beta^2 - \frac{\delta(\beta\gamma)}{2}\right) \tag{2.7}$$

The term $\delta(\beta\gamma)$ takes into account density effect that inhibits the logaritmical growth on energy losses at large γ: atoms' polarization shields the electric field from electrons that are far from the particle tracks. Thus, collision with this electrons have a lower contribution to energy loss.

In figure 2.5, it is shown the energy loss (Bethe-Bloch equation 2.7) as a function of $\beta\gamma$ for different materials.

It is possible to distinguish three main region:

- a first region, at low β values, where the energy loss is proportional to $\frac{1}{\beta^2}$: thus, as the particle slow down the energy loss increases.

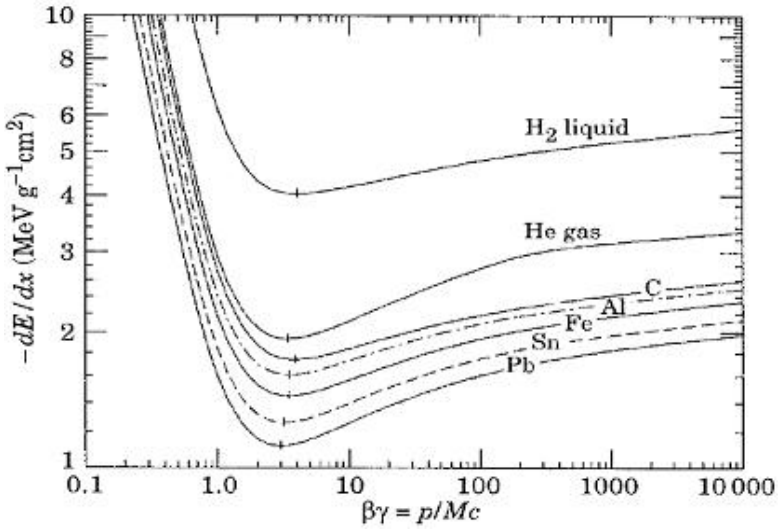

Figure 2.5: Ionizing energy loss as a function of $\beta\gamma$ for Hidrogen, Helium, Carbon, Aluminum, Iron, Tin and Lead
(http://mxp.physics.umn.edu).

- A minimum, whose position is very weakly dependent on the material in which the particles move. Particles with $\beta\gamma$ values proximum to the minimum are called MIP (*Minimum Ionizing Particles*) and the energy loss is about $1 \div 2 MeV gr^{-1} cm^2$
- a *relativistic rise*: the energy loss grows logarithmichally. As previously mentioned, this rise is limited by the density effect in such a way that at large $\beta\gamma$ the energy loss became constant.

When entering the human body, charged particles used in hadrontherapy are characterised by $\beta\gamma$ values in the first region, so that for this particles the energy loss is proportional to the square of their charge and to the inverse of the square of their velocity:

$$-\frac{dE}{dx} \propto \left(\frac{ze}{\beta^2}\right)^2 \tag{2.8}$$

2.2.2 Bragg curve and its applications in hadrontherapy

In figure 2.6 it is reported the Bragg curve, that represents the number of ionization of charged particles with low β values as a function of the penetration depth for a single particle an for a parallel beam.

As we know from equation 2.7, for this particles the main contribution to energy losses is given by $z^2\beta^{-2}$ and depends on the medium in which particles travel: when the particles slow down they loose more energy and ionize more. In fact, as we can see in figure 2.6, there is a sharp peak at the end of the particle track, named *Bragg peak*. After reaching this maximum the number of ionization dramatically decrease. This *inverse region* is due to electronic capture processes that occure at very low velocity of the

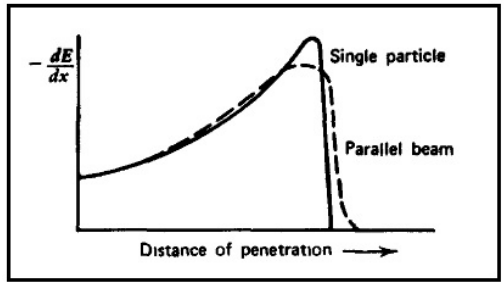

Figure 2.6: Bragg curve for charged particles heavier than electrons (the solid line represents the Bragg curve of a single particle, the dashed one represents the Bragg curve of a parallel beam) (Knoll, 2000).

incident particle and that neutralize it.
For a given particle beam, the depth of the Bragg peak depends on the particle initial energy and its width on the beam's energy spread.
When compared to protons, carbon ions are chatacterized by a more sharp Bragg peak, this is because they are heavier so that they have less straggling. Moreover, due to their higher atomic number Z, as we can see from equation 2.7, at the end of their track (in the Bragg peak region) they are more ionizing than protons: this implies a greater biological effectiveness of carbon ions in damaging the irradiated cells.
In table 2.1 the the widths (in terms of FWHM) and the depths of protons and carbon ions Bragg peaks in water are reported corresponding to the minimum and the maximum energies achievable for this particles with the CNAO syncrotron (Mirandola et al., 2015).

Particle	Energy	Bragg peak width [mm]	Bragg peak depth[mm]
p	62.73 MeV	2.8	30
C-12	115.23 MeV/u	0.9	30
p	228.57 MeV	26.1	320
C-12	398.84 MeV/u	9.3	270

Table 2.1: Widths and depths of the Bragg peaks in water for both available particles species for the minimum and the maximum achievable energies at CNAO (Mirandola et al., 2015).

Hadrontherapy exploit this property of charged particles by selecting particles' initial energy in order to irradiate the tumor in a very conformed way, giving a very low dose at the entrance of the body and to the tissues surrounding the tumor. In order to irradiate uniformly the whole longitudinal depth of the tumor, the beam energy is varied during the irradiation in a controlled way, so that it is possible to superimpose many narrow Bragg peaks and to obtain a *Spread Out Bragg Peak* (SOBP) as the envelope of all this peaks (figure 2.7).

The beam energy can be varied in two ways (Amaldi, 1999)

- *passive modulation*: a tissue-equivalent absorbing material of variable thickness is interposed in the beam path. This is the most diffused kind of beam modulation in hadrontherapy.
- *active modulation*: the beam energy is changed actively during the irradiation. This modulation is easily feasible in synchrotrons, but it is more difficult with other accelerators such as cyclotrons. At the Centro Nazionale di Adroterapia Oncologica

(CNAO,Pavia), where the presented study has been performed, they use this kind of beam modulation to obtain the SOBP.

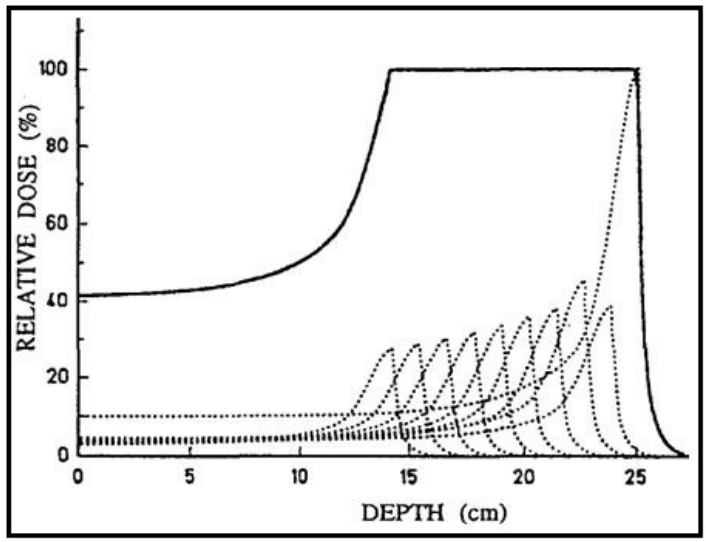

Figure 2.7: proton Spread Out Bragg Peak (SOBP), obtained as the envelope of many Bragg peaks.

The delivered dose has to be conformed to the tumor shape and size even in the transverse direction. In the past, this was done with *passive spreading systems*, through which hadrons were diffused by a scatterer and their energy was adapted to the tumors using appropriate absorbers: the transverse form of the irradiation field was defined by collimators.
More recently rotating gantries and a new *active spreading systems* have been introduced. With active systems the target volume is suddivided in thousands of voxels , each of them being irradiated at successive steps, by sending the proton beam with a section of very few millimiters in the opportune direction. (Amaldi, 1999).

2.2.3 Residual range

The *range* of a fast particle is defined as the mean distance it travels before stopping.
In figure 2.8 it is shown the ratio between the intensity of a particle beam and its initial intensity as a function of the penetration depth: from this graph, it is possible to identify the mean range (R_m), defined as the depth in the absorbed material necessary to stop half of the particles. In this picture it is also shown the extrapolated range (R_e).

For a particle of initial kinetic energy E_0 it can be evaluated from 2.7:

$$R(E_0) = \int_{E_0}^{0} \left(\frac{dE}{dx}\right)^{-1} dE$$

The integral can be performed numerically for different particles and different materials.

Statistical fluctuations on $\frac{dE}{dx}$ give rise to range statistical fluctuations (*straggling*).
Range uncertainties introduce practical limitation in clinical treatments. In fact the actual

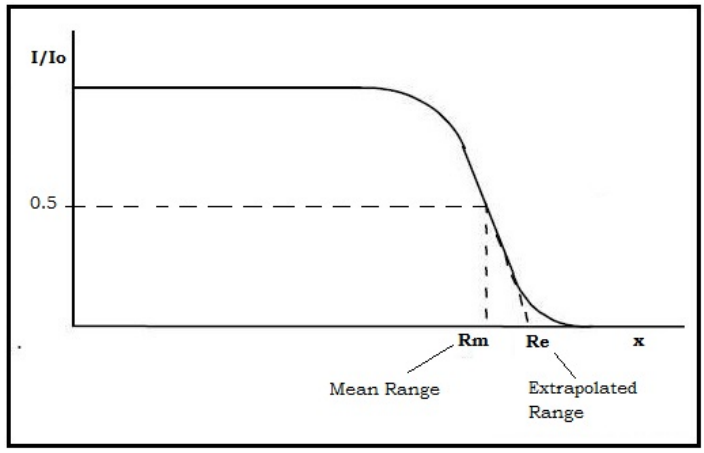

Figure 2.8: Mean range and extrapolated range.

Bragg peak position is known with an uncertainty that can be of the order of 3% (Moyers et al., 2001) of the estimated range. This can implicate risks of serious side effects for tissues near to the distal end of the Bragg Peak, where the dose gradient is very sharp: in particular this risk is very serious when an organ which sparing is mandatory is located at the end of the SOBP.
In order to minimize the risks related to physical range uncertainties, safety margins are defined in the treatment planning and single fields in the direction of organs at risk are avoided using multiple fields. From the other hand, multiple fields increase the fraction of normal tissues being irradiated.
Even biological uncertainties have to be take into account, because they can give rise to "biological range extension" (Carabe et al., 2012). As a matter of fact, at the distal end of the Bragg Peak, dose drastically decreases and in parallel the LET increases; as a consequence, RBE significantly increases and a greater biological dose is given to the healthy tissues beyond the tumor. This fact results in greater uncertainties.

CHAPTER 3

Combined treatments: radio-chemotherapy

In the recent years, combined treatments are widely spreading-out in oncological field and combined therapies that exploit radiation and chemotherapy drugs are being investigated.
The idea of combining radio- and chemotherapy dates back to the early Seventies. In 1979 Steel and Peckham (1979), focusing on *in vitro* cytotoxicity, proposed an approach based on the concept of "additivity envelope" in order to find a mathematical way to determine whether cell killing in combined treatments is greater than additive, enhancing the effectiveness of the single chemo- and radiotherapy treatments.
More recently, Bentzen et al. (2007) adapted Steel and Peckham framework, proposing diverse mechanisms in which the combination of radiation and drug can act. These mechanisms will be described in the next section.
Luttjeboer et al. (2010) proposed a strategy for the analysis of *in vitro* radiation-drug interaction. In the present study, we applied this method to determine if the interaction between charged hadrons or photons and the chemotherapy drug Epothilone B is simply additive or synergic. The Luttjeboer's method and its application in our study will be described in Chapter 5.

3.1 Framework for radiation-drug combination

In this section the Bentzen et al. (2007) framework for radiation-drug combination is summarized. According to this framework, five mechanisms are proposed to motivate the combination of radio- and chemotherapy: *cytotoxic enhancement, spatial cooperation, biological cooperation, temporal modulation* and *normal tissue protection*, schematically described in figure 3.1.

3.1.1 Cytotoxic enhancement

This mechanism of interaction between radiation and drug is the rationale of the study presented in this thesis: exploiting drugs able to modify the response of cancer cells to irradiation, for example inhibiting DNA repair, can lead to an enhancement in cell killing, resulting in better tumor local control.
It is important to underline that in order to exploit this mechanism, the drug must be administered during or just before irradiation. For this reason, radio- and chemotherapy should be administrated concomitantly. The main goal of this kind of radiation-drug combination is a better locoregional control of the disease.

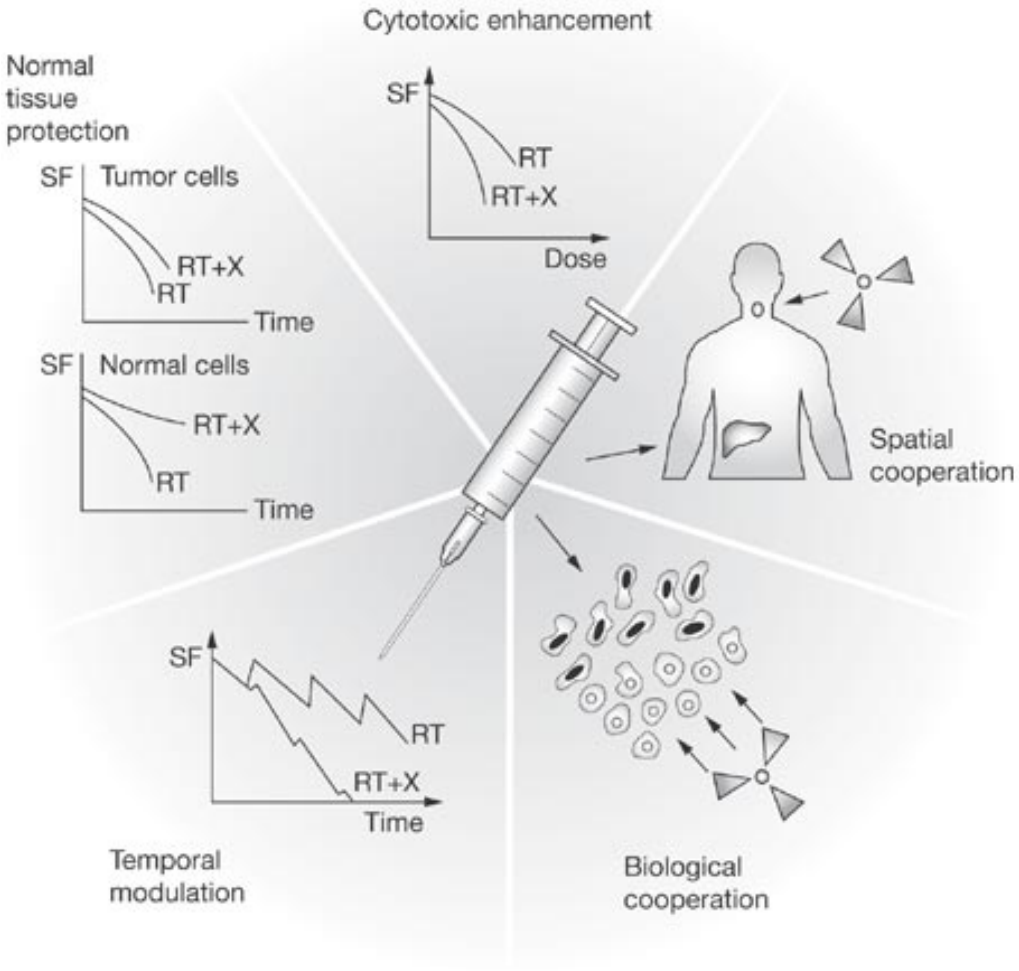

Figure 3.1: Diagram describing the five different mechanism in which radiation and drug can act in combined cancer treatments: spatial cooperation, cytotoxic enhancement, normal tissue protection, temporal modulation and biological cooperation.(Bentzen et al., 2007).

3.1.2 Spatial cooperation

Since radiotherapy is a locoregional treatment, there is a strong rationale for combining it with agents that act systemically, such as chemotherapy drugs.
In this case, radiation and drug act independently and an interaction at cellular level between these two agents is not required. For this reason, in cancer treatments exploiting spatial cooperation, chemotherapy and radiotherapy are usually administrated in sequence, in order to obtain tumor control both locally and in distant sites.

3.1.3 Protection of normal tissue

The use of drugs that can modulate the response of normal tissue to irradiation, making them more radioresistant, could permit to enhance the radiation dose given to the tumor, or to avoid treatment side effects.
Several drugs, such as free-radical scavengers, have been proposed as radioprotectors for normal tissues. Depending on their action, these drugs can be administrated during, before or after the radiotherapy treatment.

3.1.4 Temporal modulation

As mentioned in Chapter 1, the rationale in fractionated radiotherapy is given by DNA repair mechanisms, reoxygenation, redistribution from more to less resistant phases of cell-cycle and reoxygenation of irradiated tissues. Thus, it is possible to combine irradiation with the use of drugs that act on one or more of these mechanisms. Since these mechanisms act at different time in normal and tumoral tissues, when combining radiation and drug it is possible to optimize tumor control, changing the dose-distribution over time, varying the time interval between each fraction, the dose per fraction and the total duration of the radiotherapy treatment.
Even in this case, the main clinical end-point is the locoregional control of the disease.

3.1.5 Biological cooperation

In biological cooperation, radiation and drug target different cells populations. For example, it is possible to complement radiation effects, administrating drugs that act specifically on hypoxic tumor cells.
Even in this case the main goal is to obtain a better locoregional control of the tumor and radio- chemotherapy should be administrated sequentially or concomitantly.

3.2 Combined treatment: radiation and Epothilone B

In concurrent chemoradiotherapy treatments, particular attention is given to Microtubule Stabilizing Agents (MSAs), that are drugs interfering with the mitotic spindle, such as the Taxanes. These drugs are able to promote the stabilization of the mitotic spindle, leading to an accumulation of cells in the G2/M phase of the cell cycle, known to be the most radiosensitive one, as described in Chapter 1. As a consequence of this arrest in cell cycle progression, cell proliferation inhibition and cell death via apoptosis and necrosis

can occur. Some Taxanes, such as Placitaxel, are used not only in chemotherapy treatments, but also as radiosensitizers in combination with radiation. Anyway, the clinical use of Taxanes is limited for example by multidrug resistance.
In recent years, a great deal of attention has been focused on a new class of MSAs: the Epothilones. Epothilones act similarly to Taxanes, but they are effective at lower concentrations (sub-nanomolar) and they are more water soluble, thus avoiding the use of toxic excipients and inducing fewer side effects (Altmann et al., 2000).
In the present study, we have evaluated the combination of radiation and Epothilone B (EPO906, Patupilone), a metabolite of bacterial origin that has been studied both in vitro and in vivo even in combination with photon beams (by way of example see Kim et al. (2003); Hofstetter et al. (2005); Baumgart et al. (2012a); Roher Bley et al. (2009)). It has been used in clinical trials as a chemotherapy drug even for the treatment of glioblastomas (Oehler et al., 2012), and it has also been combined with photon radiotherapy for the treatment of brain malignancies (Fogh et al., 2010), with encouraging results.
In the next paragraphs, some of the Epothilone B effects reported in literature will be introduced, with particular emphasis on those effects motivating its use in combination with radiation.

3.2.1 Epothilone B effects on cell cycle distribution

Epothilone B target tubulin, a globular protein present in cell cytoplasm that is the fundamental unit of cytoskeleton's microtubules. In particular, acting on β-tubulin, Epothilone B is able to interfere with the mitotic spindle formation, causing cell-cycle arrest in the G2/M phase, altering the normal cell cycle distribution.
Baumgart et al. (2012b) analyzed the effect of Epothilone B at different concentrations on cell cycle progression of FaDu and A549 cells using flow cytometry. They treated cells for 24 hours with Epothilone B at concentrations from 0.1 nM to 10 nM, which is known to be the maximum concentration tolerate in patient's plasma. In figure 3.2 the results of this analysis are shown. It is possible to notice a concentration-dependent accumulation in the G2/M phase, while the G0/G1 peak gradually reduces. This accumulation in the most radiosensitive phase of cell cycle is one of the rationale for using Epothilone B in conjunction with radiation.
Moreover a sub-G1 peak and an hyperdiploid population became more evident when Epothilone B concentration increase. This aspect will be investigated more in detail in the next paragraph. According to the study of Baumgart et al. (2012b), treatment at concentration lower than 0.25 nM resulted in minor difference in cell cycle. Despite this fact, radiosensitizing effects induced by Epothilone B in cells irradiate with photon beams have been reported in literature (Baumgart et al., 2012a; Roher Bley et al., 2013, 2009; Hofstetter et al., 2005)even at lower concentrations. This aspect will be discussed more in details in the next Chapter.

3.2.2 Epothilone B-induced cell death mechanism and other effects

As reported by Baumgart et al. (2015) and by Kim et al. (2003), the cytotoxic activity of Epothilone B induces cell death via apoptosis. The hypodiploid population in the sub-G1 peak can be seen as an hallmark of apoptosis.
Apoptosis consists in a "programmed" cell death. Some of the morphological changing typical of apoptosis are, for instance, nuclear fragmentation, cell shrinkage and chro-

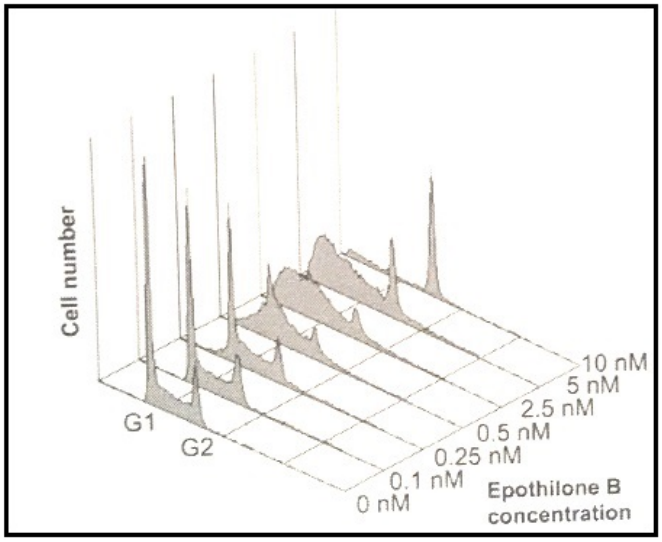

Figure 3.2: Histograms of cell cycle distribution of FaDu cells after an incubation of 24 hours with different Epothilone B concentrations. (Baumgart et al., 2012b).

matin condensation. It is a cell-death mechanism highly regulated through enzymatic processes that occur for example when cell's DNA is irreparably damaged.

Baumgart et al. (2015) observed the production of hyperdiploid cells after the G2/M cell cycle block and the presence of multinucleated cells. These events can be interpreted as indication of mitotic catastrophe. Mitotic catastrophe consist in a sequence of events caused by an inappropriate cell's entry in mitosis, it is unrelated to apoptosis, and often observed in cells missing correctly functioning apoptosis pathways. Moreover this kind of cell death is typically observed after the treatment with chemicals targeting the mitotic-spindle formation, such as Epothilone B, or after irradiation.

Epothilone B has also been demonstrated to be able to cross the blood-brain barrier and to retain in brain tissue in rats, mice and dogs (O'Reilly et al., 2008); this property makes it a very promising chemotherapy agent for the treatment of brain malignancies.

It has even shown antivascular and antiangiogenic effects (Stalder et al., 2005; Ferretti et al., 2011; Bocci et al., 2002) and the ability to effectively inhibit cells' migration at non-cytotoxic concentration (Pagano et al., 2012; Furmanova-Hollenstein et al., 2013).

3.2.3 Epothilone B effects on DNA-repair capacity

Through γH2AX foci assays, Baumgart et al. (2012a) found a tendency that Epothilone B increases the number of double strand breaks after photon irradiation, even at low concentration (1 nM), suggesting a reduction in DNA damage capacity. In fact, when a double strand break occurs, the H2AX histone is phosphorilated (γH2AX) as an incipit of DNA repair pathway. When this repair is inhibited, the number of γH2AX remains high, as shown in figure 3.3. Thanks to this repair's inhibition, radiation effectiveness

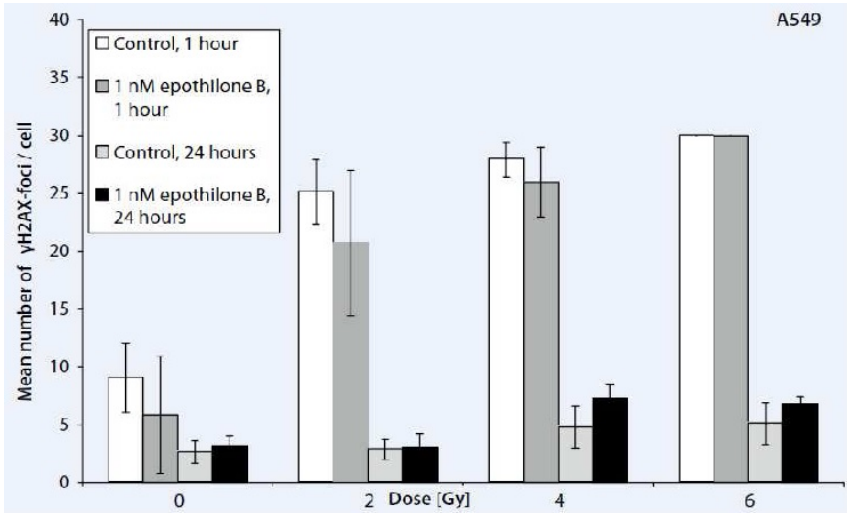

Figure 3.3: Mean number of γH2AX foci per cell (after 1h and 24h of repair time) with and without Epothilone B (A549 cells) (Baumgart et al., 2012a). The presence of this histone can be related to the presence of Double Strand Breaks.

in damaging DNA can be increased using Epothilone B concomitantly to irradiation, exploiting the cytotoxic enhancement.

Thanks to the properties described in the previous sections, Epothilone B is suitable not only to be used as a chemotherapy drug, but also in combination with radiation, enhancing its effects.

CHAPTER 4

Preliminary measurements: cell lines and Epothilone B characterization

In this chapter the characterization of the biological systems studied will be introduced. In particular the main properties of the cell-lines investigated will be presented. Moreover the preliminary measurements performed to characterize Epothilone B will be described.

4.1 Biological system

In experiments devoted to the study of radiation effect at cell level, the main advantage of *in vitro* biological systems, with respect to *in vivo* experiments, is the fact that they ensure a better reproducibility and avoids many issues related to more complex organisms.
In order to study the effects of the combination irradiation - Epothilone B, three different estabilished cell lines have been used: A549, U251MG and DAOY.
Established cells derives from primary cell cultures. They are not part of the organized tissues they belong to, but they can maintain their functionality and can indefinitely reproduce, under suitable culture conditions.
We have chosen these three cell lines because they derives from cancers that can potentially benefit of a chemo-radiotherapy treatment for different reasons.

A549 . This cell line is derived from human lung adenocarcinoma, a kind of non-small cell lung cancer (NSCLC) that affects the epithelial cell of the bronchial tube and it is a very common lung neoplasia in non-smokers. It can benefit of combined chemo-radiotherapy with hadrons because it is quite resistant to conventional radiotherapy and because lungs are very close to organ-at-risk such as the spinal cord and the esophagus.

U251MG . This cell line is derived from human glioblastoma multiforme (GBM). GBM is the most frequent primary tumor of the central nervous system. It is particularly aggressive, highly angiogenic and typically it is associated with a very poor prognosis. One of the main biological features of GBM is the local invasion of the surrounding brain tissue. Such an invasive behaviour is the main obstacle to an effective treatment of this tumor (Pagano et al., 2012). Currently, the standard treatment for glioblastoma combines chemotherapy, radiotherapy and surgical resection. Typically after surgical resection, radiotherapy is combined to the use of TMZ, a DNA-binding agent (Stupp et al., 2009; Mirmanoff et al., 2006). Thus, it can

be interesting to study the effect of irradiation combined to another chemotherapy agent such as Epothilone B.

DAOY . This cell line is derived from human pediatric medulloblastoma. It is a tumor of the posterior cerebral fossa and it is the most common brain tumor in children. This cell line is a very radiosensitive one, in fact it is derived from a pediatric patient tissue. Despite being very radiosensitive, this kind of tumor can benefit from a combined treatment with hadrons (especially protons) due to patient's youth and their significantly long life expectation. In fact, a very conformed therapy such as protontherapy might reduce the probability of secondary cancers induced by irradiation. Due to the great radiosensitivity of this kind of tumor, an irradiation with high-LET radiation seems not necessary and, since carbon ion irradiation late effects are still debated, at the moment proton beams are considered very suitable for the treatment of pediatric tumors. For this reason, in this thesis, only photon and proton irradiation have been studied for DAOY cells.

All cell lines were supplied by the ICLC (Interlab Cell Line Collection, Genova, Italy), and they were stored at -191^oC in liquid nitrogen, in a solution containing 40% of medium, 50% of fetal bovine serum and 10% of dimethyl sulfoxide (DMSO), a cryoprotective agent. After thawing, cells were maintained at 37^oC in humidified atmosphere containing 5% CO_2 in air as exponentially growing cultures in opportune mediums. A549 cells were cultured in Dulbecco Modified Eagles Medium (DMEM, Sigma-Aldrich), while U251MG and DAOY were cultured in Eagles Minimum Essential Medium (EMEM), both supplemented with 10% fetal bovine serum (FBS, Sigma-Aldrich) and Gentamicin (50 $\mu g/ml$) (Sigma-Aldrich).

4.2 Cell lines characterization

All the cell lines have been preliminary tested in term of plating efficiency and doubling time.

4.2.1 Plating efficiency

The plating efficiency (PE) have been measured as the ratio between the number n_0 of cells seeded into a flask T25 and the number of colony-forming cells (giving rise to a colony made up of at least fifty cells), n.

$$PE = \frac{n}{n_0}.$$

In our experimental conditions, the measured PE for each cell line is reported in table 4.1.

Cell growth

In order to evaluate cell growth parameters, cells were seeded in flasks T25, let grow for five days and counted at different time. The ratios $\frac{n(t)}{n0}$ have been measured as a function of time, in order to obtain growth curves.

cell line	PE
A549	80%
U251MG	85%
DAOY	60%

Table 4.1: Plating Efficiency (PE) values for A549, U251MG and DAOY cells.

In figure 4.1 the ratio $\frac{n(t)}{n0}$ of A549 cells is reported as a function of time, as an exam-

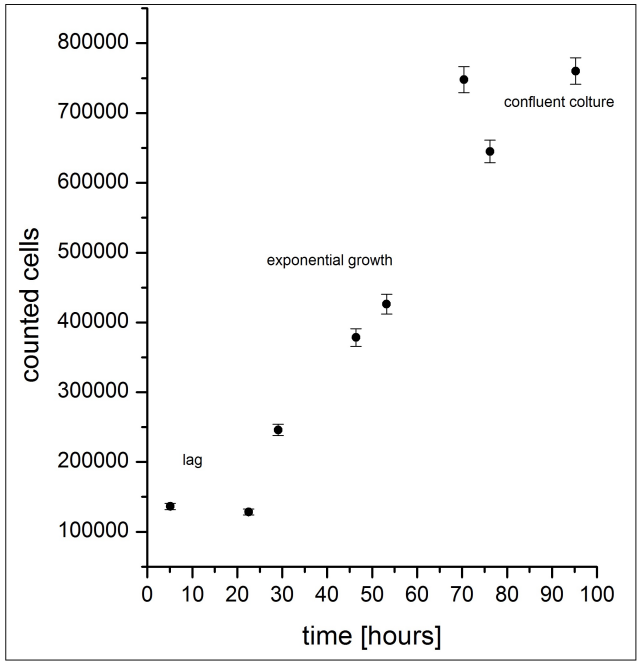

Figure 4.1: $\frac{n(t)}{n0}$ of A549 cells as a function of time.

ple. After a period called lag time that represents the time required for cells to progress through the cycle, cell growth is exponential. After the exponential growth, the cell culture become confluent.
Data in the exponential region have been interpolated according to equation:

$$\frac{n(t)}{n0} = 2^{\frac{t}{t_d}} \tag{4.1}$$

where t_d is the doubling time. Fit have been performed with the software *OriginLab*, based on χ^2 minimization. Details on the fit procedure are reported in Appendix A.
The t_d values are reported in table 4.2 for each cell line.

cell line	t_d [hours]
A549	21.2 ± 0.2
U251MG	24 ± 1
DAOY	24 ± 1

Table 4.2: Doubling time (t_d) values for A549, U251MG and DAOY cells.

The measure of the doubling time was necessary to determine the duration of the treatment with Epothilone B, in order to guarantee that cells pass through all the phases of their cycle. For this reason, a treatment time of 24 hours has been chosen.

4.3 Epothilone B characterization

Epothilone B (Sigma-Aldrich) was dissolved in dimethyl sulfoxide (DMSO) to generate a 10μM stock solution. The stock solution was then diluted in medium at opportune concentrations. The final DMSO concentration were less then 0.1%, this DMSO concentration is known to have no effect on cell survival.

Before starting with the study of the effects of irradiation combined with Epothilone B, the drug has been tested in term of clonogenic survival, effects on cell invasive capacity and cell cycle, as described in the following paragraphs.

4.3.1 Clonogenic survival

Clonogenic survival vs Epothilone B concentration

Clonogenic survival has been measured by colony forming assay as a function of Epothilone B concentration. The experimental procedure of colony forming assay will be described in detail in the next chapter.
Cells (in the phase of exponential growth) have been treated for 24 hours with Epothilone B at different concentrations. In figure 4.2 the fraction of surviving cells is reported as a function of Epothilone B concentration for A549, U251MG and DAOY cells. Due to the different sensitivity of the three cell lines, different concentrations range have been chosen: 0-0.6 nM for U251MG cells, 0-0.2 nM for A549 cells, 0-0.08 nM for DAOY cells, which resulted to be the more sensitive to Epothilone B. As shown in figure 4.2, the last concentration used for each cell line leads to a surviving fraction of about 0.015. It is possible to see that no effect on cell survival occurred at concentrations lower than 0.05 nM for A549 0.075 nM for U251MG and 0.02 nM for DAOY cells, suggesting the presence of a threshold concentration (whose value depends on the cell line) under which the drug has basically no effect on cell proliferative capacity. For concentrations greater than the threshold value, cells clonogenic survival decreases. This behavior is typical of cells treated with chemical cytotoxic agents.

This preliminary test was necessary to choose the drug concentration to be used in conjunction with radiation. A concentration corresponding to a survival level of about 40% has been chosen for each cell line. In table 4.3 the chosen Epothilone B concentration

are reported.

cell line	Epothilone B concentration [nM]
A549	0.075
U251MG	0.125
DAOY	0.035

Table 4.3: Epothilone B concentrations chosen for the combination Epothilone B - irradiation for each cell line. This concentrations correspond to about the 40% of cell clonogenic survival.

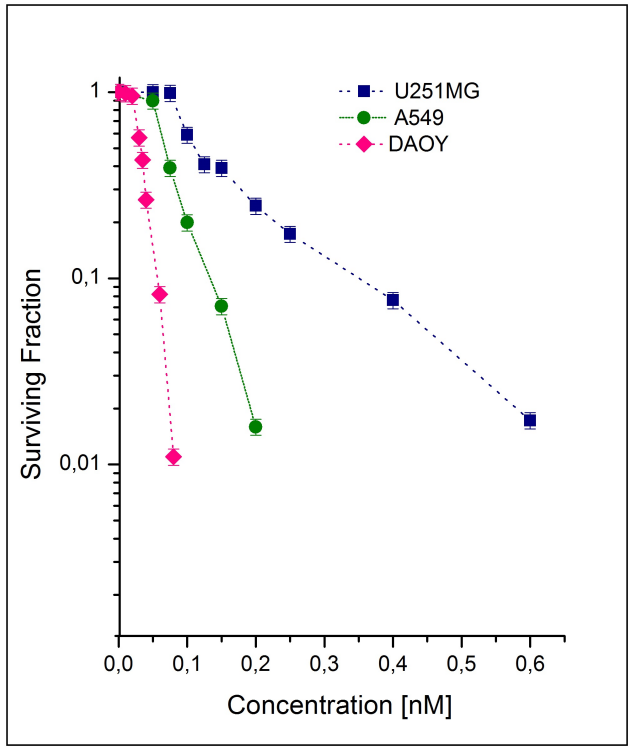

Figure 4.2: Surviving fraction as a function of Epothilone B concentration for U251MG cells (blue), A549 cells (green), DAOY cells (pink)

Clonogenic survival vs Epothilone B treatment time

Clonogenic survival was measured for cells treated with Epothilone B at the concentration chosen to be used in combination with radiation for different treatment time (18, 24 and 33 hours).
Collected data highlight that there are no significant cell survival variations in the treatment time interval 18-33 hours.

4.3.2 Epothilone B effects on invasive capacity

As mentioned in Chapter 3, Epothilone B is known to inhibits cells invasive capacity. We tested this property in A549 and U251MG cells (that are very invasive) at the concentration chosen for the evaluation of the effects of the combined treatment (0.075 nM for A549 cells and 0.125 for U251MG cells).
This analysis was performed through invasion assays. The complete procedure for invasion assay will be described in the next Chapter.
The invasive capacity was measured as the ratio between invading cells and the total number of cells initially seeded (see Chapter 4 for details). Obtained values were then normalized to the control ones.
In figure 4.3 the invasion rate of A549 and U251MG cells relative to the control sample (cells not treated with Epothilone B) is displayed. Epothilone B at these concentrations resulted to inhibit the invasive capacity, reducing the basal invasion rate of A549 to 55% and of U251MG to 68%.

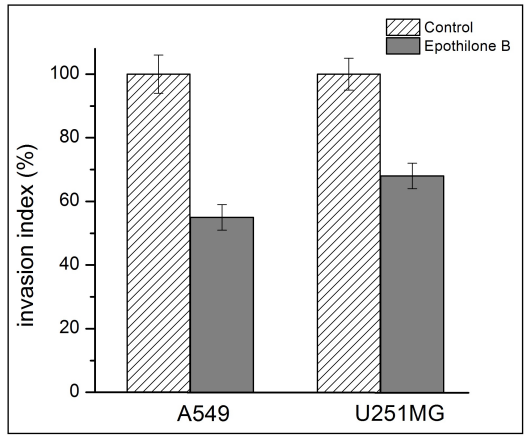

Figure 4.3: Relative invasion rate for A549 and U251MG cells treated with Epothilone B (0.075 nM and 0.125 nM, respectively) or not (control sample)

4.3.3 Epothilone B effects on cell cycle

The effects of Epothilone B on cell cycle were investigated on A549 and U251MG cells at different concentrations.
The analysis of cell cycle was performed through flow-cytometry in collaboration with the "DOSMM - Servizio di Citometria e Cell Sorting" at the Fondazione IRCCS Istituto Nazionale dei Tumori (Milano).
In flow-cytometry for cell cycle analysis, cells are stained with fluorescent probes able to intercalate in DNA double-helix. Fluorescence measurements permit to distinguish the different phases of the cell-cycle. In fact, in the G2 phase, DNA is duplicated in respect with the G1 phase, so that a double fluorescence intensity is detected. In the S phase intermediate fluorescence intensity values are found. Moreover, when apoptosis occurs, DNA is fragmented so that a sub-G1 peak can be identified. A detailed description of flow-cytometer is given in Appendix B.

For our measurements, we used the Propidium Iodide as fluorescent probe; its excitation length is in the green region and its emission spectrum is in the red region and has a peak correspondent to 610 nm. This fluorochrome is non fluorescent when free in solution, while its fluorescence intensifies when it is intercalated in DNA molecules.
In order to fix samples for cytofluorimetric analysis, we followed this procedure: after treatment with Epothilone B at different concentrations, cells were centrifuged (1500 rounds per minute, 10') in order to remove the medium. After this procedure they were re-suspended in PBS (Phosphate buffered saline, a tampon solution), re-centrifuged and then suspended in absolute ethanol (3 ml).
About 13 hours before cytofluorimetric analysis, the ethanol was removed through sample centrifuge; samples were then suspended in PBS and re-centrifuged. Cell pellet was suspended with Ribonuclease A (100 μg/ml; SIGMA ALDRICH) and incubated at 37^oC for 30'. The use of this enzyme is necessary to degrade the RNA; in fact the fluorochrome intercalating in RNA could affect the fluorescence measurements.
Samples were then re-centrifuged and suspended in Propidium Iodide (50 μg/ml; SIGMA ALDRICH) (0.5 ml for samples with $5*10^5$ cells, 1 ml for samples with 10^6 cells) for about 12 hours.
Samples were then analyzed with the cytometer, in order to obtain fluorescence histograms for cell cycle analysis. The analysis was performed through the software *ModFit LT*.
First of all, a gate in the plane fluorescence signal area vs. fluorescence signal height was applied in order to discard doublets and to select a correct cells population. An example of gate is shown in figure 4.4.

After this gating, fluorescence histograms were analyzed to determine the percentage of cells in each phase of the cycle and to individuate cells in apoptosis, when it occurs.
With the *ModFit LT* software it is possible to identify and symmetrize the fluorescence peaks corresponding to the G1, G2 phase and apoptosis (when present). The percentage of cells in each cycle phase is proportional to the correspondent area in the histogram. The software calculates the areas of the G1, G2 and apoptosis peaks and expresses it as a percentage of the total area. Considering that cells in the S phase have a DNA content intermediate between G1 and G2, the software calculates the percentage of histogram area corresponding to cells in S-phase.
Moreover, it calculates the ratio between the abscissa of the G2 and G1 peak; this value can be used as a check for the analysis, in fact its value must be proximum to 2, consid-

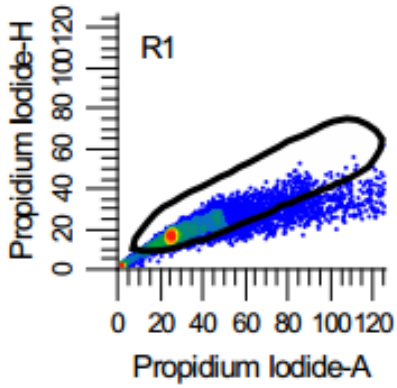

Figure 4.4: Example of gate to eliminate doublets in the cell cycle analysis. The cell population to be analyzed must be close to the diagonal.

ering that in the G2 phase the DNA content is twice the G1 ones.

In figures from 4.5 to 4.8 the fluorescence histograms are displayed. Moreover, the intensity of the G1, G2 and apoptosis (when present) peaks are reported, as well as the ratio G2/G1, which represents the ratio between the abscissa of the G2 and G1 peaks.
It is possible to notice that at the concentrations chosen for our experiments (0.075 nM for A549 cells and 0.125 nM for U251MG cells) very small variations in the G2 peaks occur in respect with the control sample, but for U251MG cells an apoptosis peak is detected. Despite we detect very small cell-cycle variations at these concentrations, in literature an enhanced radiosensitivity in A549 cells pretreated with Epothilone B (0.075 nM) and irradiated with photon beams was found (Baumgart et al., 2012a). Probably, this is due to the fact that, even at low concentration, Epothilone B is able to modify DNA repair mechanisms, as mentioned in Chapter 3. Moreover, other mechanisms induced by Epothilone B might be involved in radiosensitization.
The presence of the apoptosis peak shows that Epothilone B induces cell death via apoptosis; this cell-death mechanism is cell line dependent.
At the highest concentration studied (0.1 nM and 0.2 nM for A549 and U251MG cells, respectively), an apoptosis peak is detected even for A549 cells and in U251MG cells the apoptosis peak is more pronounced. Moreover in this cell line an higher G2 peak is detected and the percentage of cells in the S phase increases while the G1 peak reduces.
We can observe that Epothilone B seems to weakly increase the number of cells in the S-phase and this effect is more pronounced in the higher concentrations studied. Hofstetter et al. (2005) observed a supra-additive effect of Epothilone B combined with irradiation at concentrations that did not cause an accumulation of cells in the G2-M phase and they found that Epothilone B treatment induces a transient accumulation of cells in S phase, effect that became more marked when it is combined with irradiation. They conclude that an accumulation of cells in S phase in combined treatment may indicate that a decelerated S-phase transgression-related mechanism might cause the radiosensitizing effect they observed for the combination of Epothilone B and irradiation.

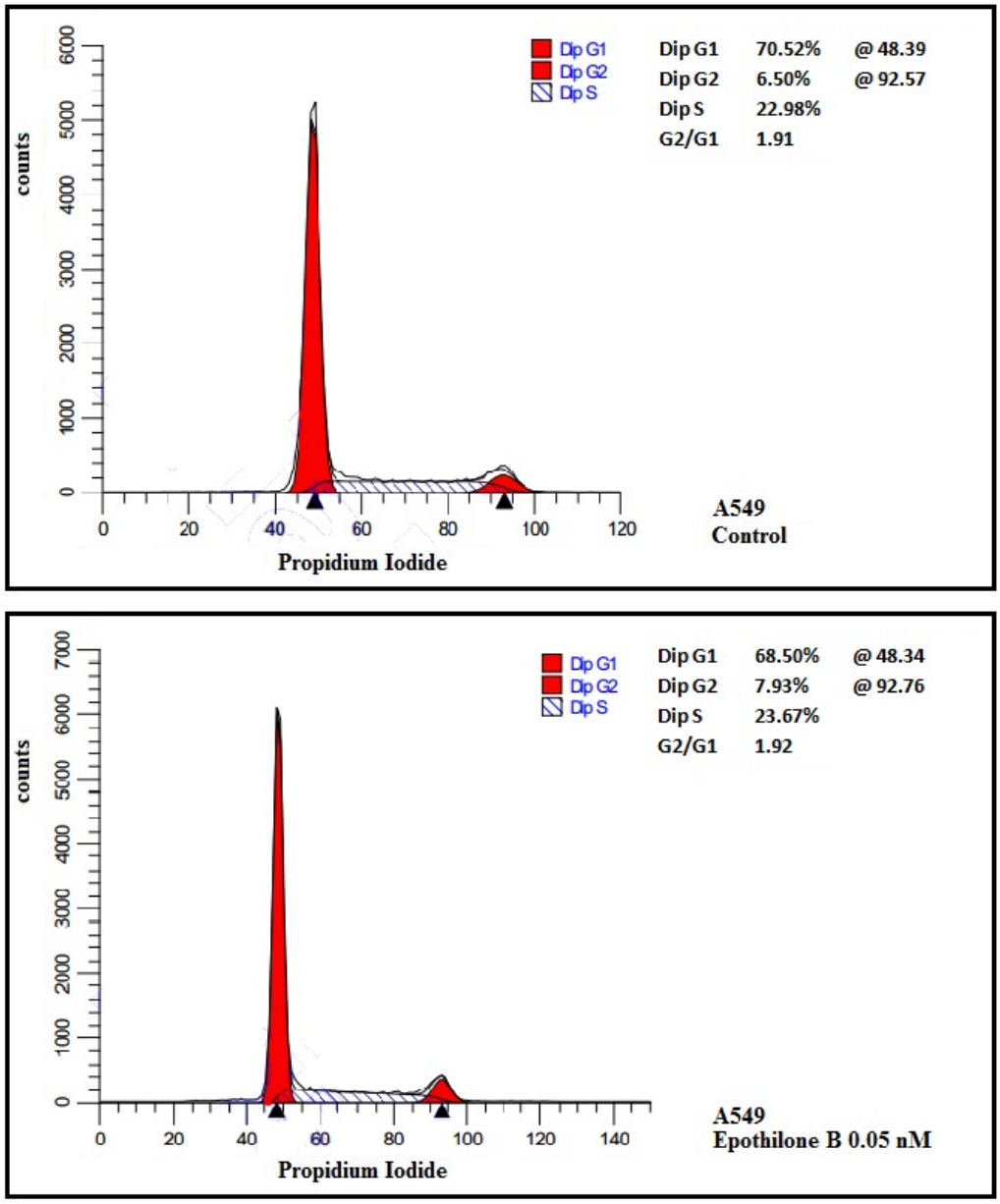

Figure 4.5: Cell cycle analysis through flow-cytometry of A549 cells (control sample and sample treated with Epothilone B 0.05 nM).

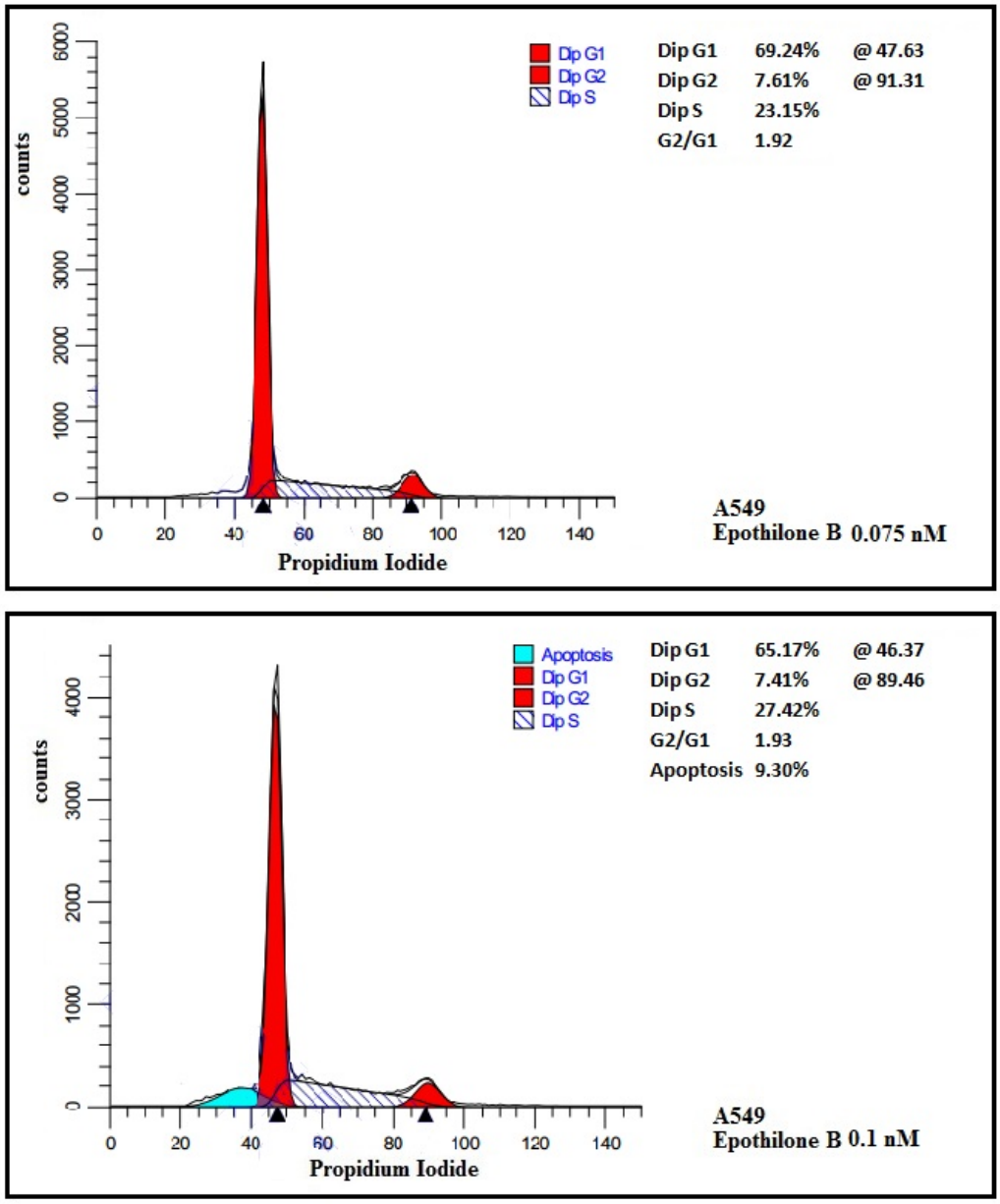

Figure 4.6: Cell cycle analysis through flow-cytometry of A549 cells (sample treated with Epothilone B 0.075 and 0.1 nM).

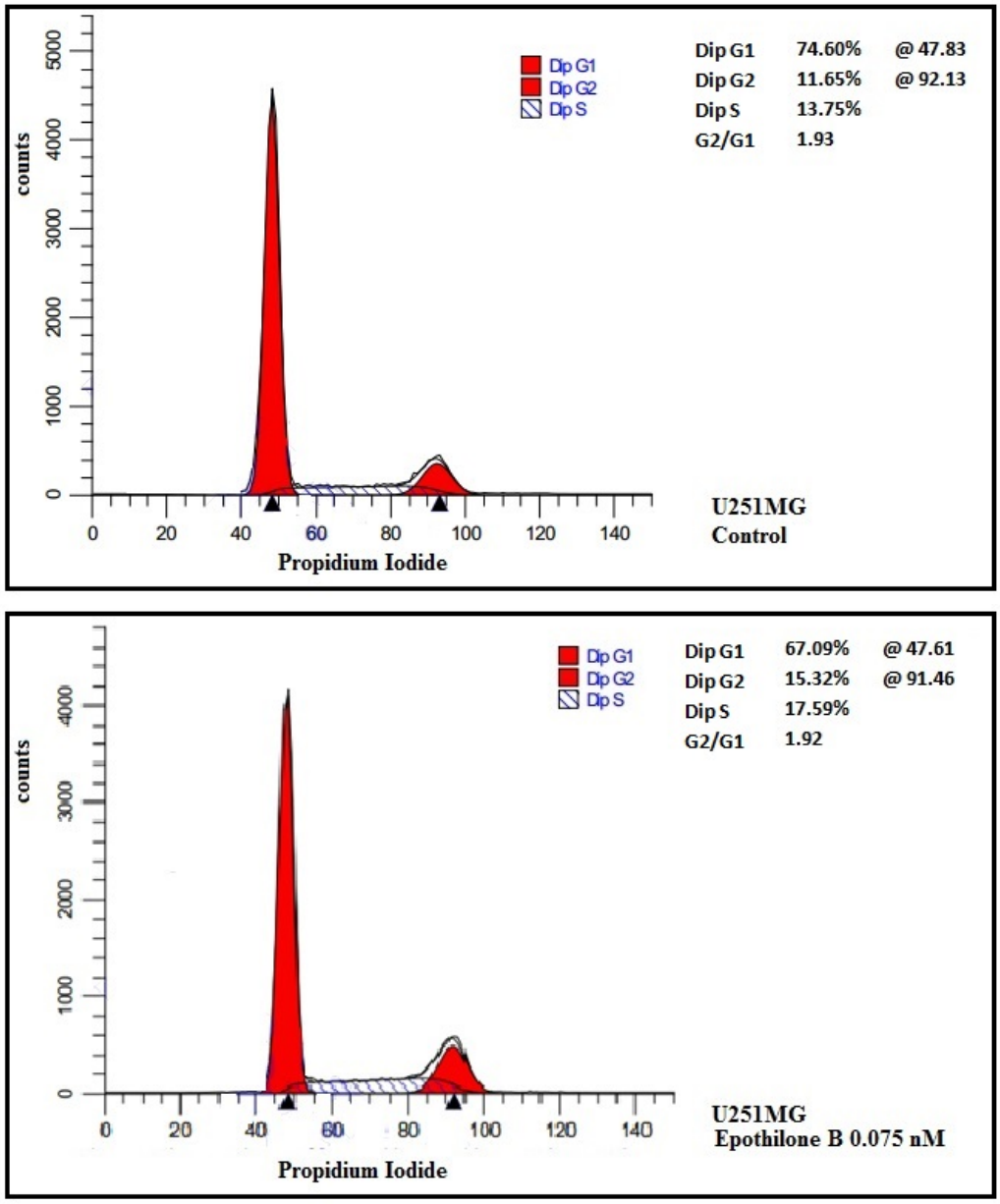

Figure 4.7: Cell cycle analysis through flow-cytometry of U251MG cells (control sample and sample treated with Epothilone B 0.075 nM).

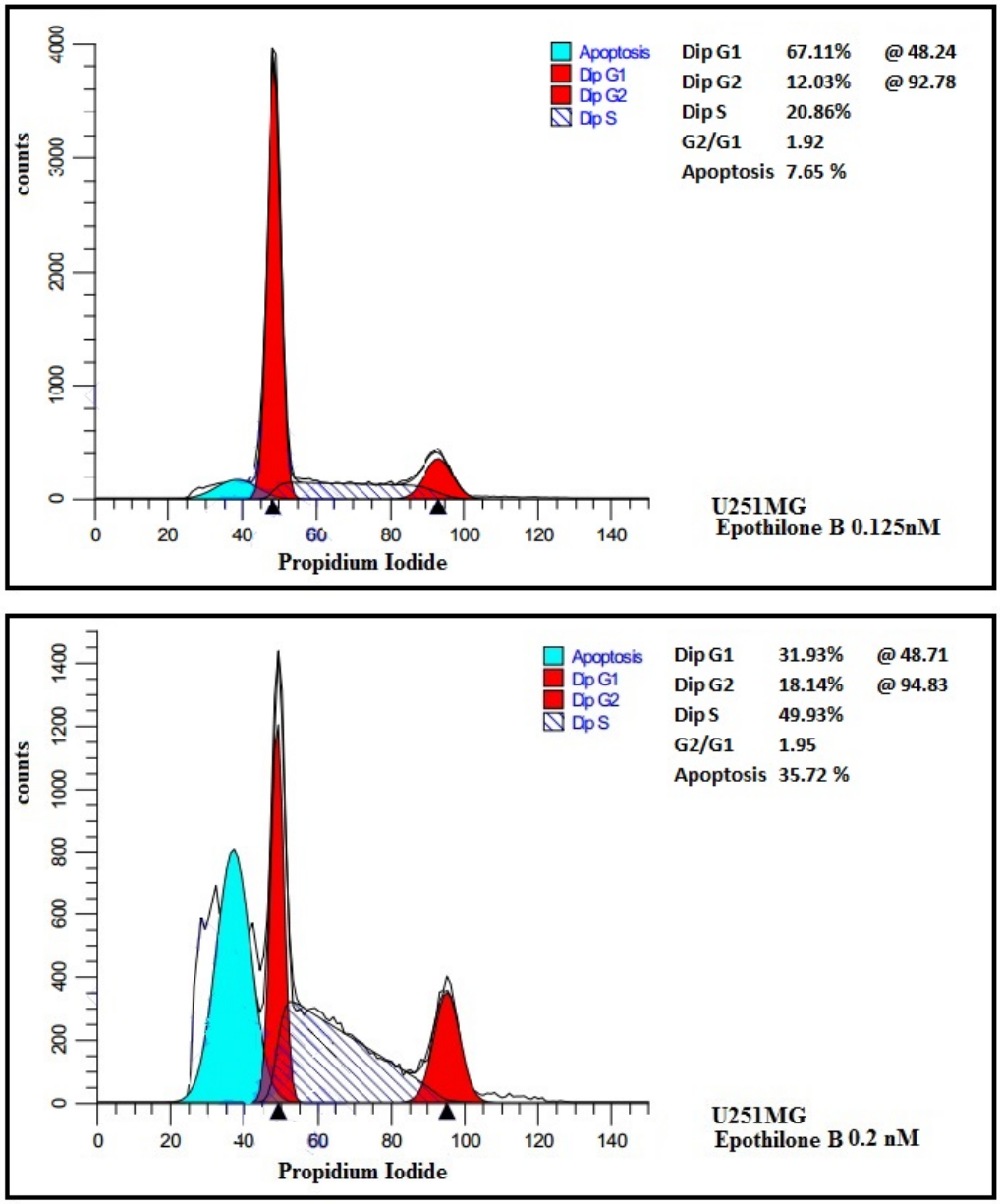

Figure 4.8: Cell cycle analysis through flow-cytometry of U251MG cells (sample treated with Epothilone B 0.125 and 0.2 nM).

CHAPTER 5

Experimental Procedure

In this Chapter the experimental procedure followed to measure the effects of irradiation with protons, carbon ions or photons combined with Epothilone B is described.
In figure 5.1, a very schematic description of the experimental procedure is displayed. Before undergoing irradiation, cells and Epothilone B were prepared as described in Section 5.1. The irradiation procedure followed with photon, proton or carbon ion beams is described in Section 5.2; while Section 5.3 is dedicated to the treatments performed on irradiated cells. The last Section is dedicated to the description of the assays performed to investigate the different biological end points (clonogenic survival, invasive capacity and cell growth).

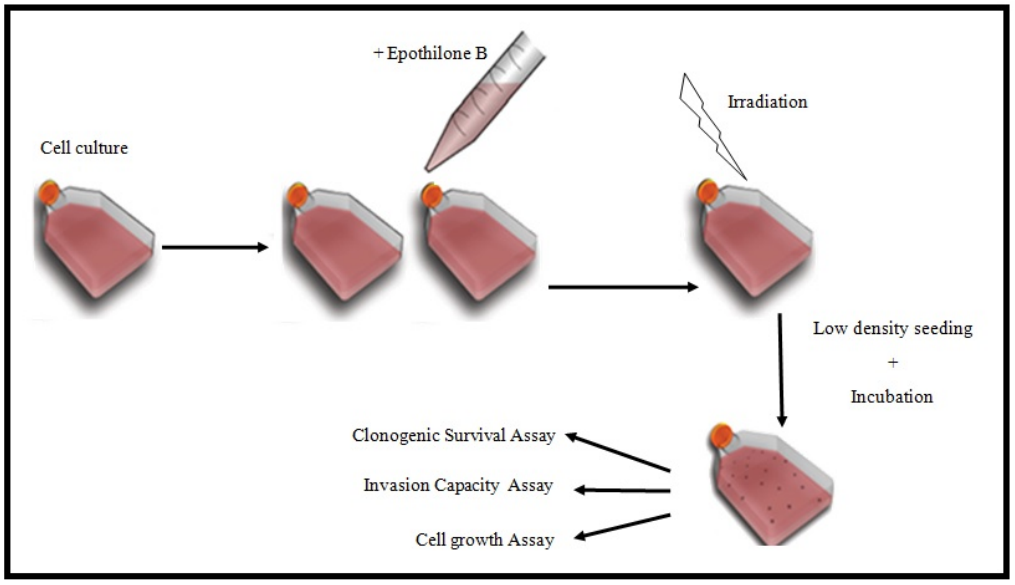

Figure 5.1: Schematic description of the experimental procedure for the measure of the effects of irradiation combined with Epothilone B.

5.1 Cell culture and drug preparation

In order to prepare samples undergoing irradiation, we followed the procedure described in this section.

As described in the previous Chapter, cells were stored in liquid nitrogen, in a solution containing 40% of medium, 50% of fetal bovine serum and 10% of DMSO. After thawing, cells were maintained at 37^oC in humidified atmosphere containing 5% CO_2.

48 hours before irradiation, cells were seeded in flasks T25 (growth area equal to 25 cm^2) and maintained at 37^oC in humidified atmosphere containing 5% CO_2 in air, as exponentially growing cultures in medium (DMEM for A549 cells and EMEM for U251MG and DAOY cells), as described in Chapter 4.
24 hours before irradiation, a fraction of the cells was treated with Epothilone B at opportune concentrations (0.075 nM for A549 cells, 0.125 nM for U251MG cells and 0.035 nM for DAOY cells); the procedure followed for the drug preparation is fully described in Chapter 4.
Just before irradiation, Epothilone B was removed and all the flasks were completely filled with medium.

5.2 Irradiation

5.2.1 Photon Irradiation

Photon beam irradiation was performed using a 6 MV linear accelerator (VARIAN Clinac 2100C, Varian Medical Systems, Palo Alto, USA) at the Fondazione IRCCS Istituto Nazionale dei Tumori, Milano. This linear accelerator is daily used for radiotherapy treatments.
Linear accelerators (LINAC) accelerate electrons, typically with voltage between 4 MV and 25 MV, exploiting radiofrequency fields. Electrons are further accelerated through waveguides and then they hit a Tungsten target, producing a bremmstrahlung photon spectrum.
In order to compensate the Heel effect, according to which X-rays generated at greater depth in the target undergo greater attenuation, compensation filters are used. Other filters are used in order to eliminate the soft component of the photon beam and to uniform the photon beam intensity in the whole field size.
Beam homogeneity and delivered dose are monitored using ionization chambers.

In figure 5.2 a picture of the photon beam irradiation setting is shown.
The flasks containing cells undergoing irradiation were placed horizontally at the isocenter in a water phantom at 5 cm depth and were irradiated using a vertical beam 20x20 cm^2 field.
Samples were irradiated at different doses with a dose rate equal to 3 Gy/min.

Despite we used a maximum dose of 7 Gy for photon irradiation, we chose 5 Gy as maximum dose for the irradiation of cells pretreated with Epothilone B, in order to analyze range of similar cytotoxicity for the standard treatment and for the combined one.

Figure 5.2: Photon beam irradiation setting: Varian 2100C linear accelerator at the Fondazione IRCCS Istituto Nazionale dei Tumori, Milano. The red circle points out the water phantom in which the flasks are placed.

5.2.2 Hadrons Irradiation

Proton and carbon Ion beams irradiation was performed using the synchrotron-based clinical scanning beams at the Centro Nazionale di Adroterapia Oncologica (CNAO), Pavia (Rossi, 2015).
Beams features have been reported in a publication by Mirandola et al. (2015).
In this section a brief description of the main beam characteristic and of the configuration used for sample irradiation will be given.

At CNAO proton and light ion beams can be provided. Particles are accelerated by a synchrotron (figure 5.3) and an active scanning pencil beam technique is exploited.
The following information were taken from (Mirandola et al., 2015).
The scanning magnets are located 5.5 m from the isocenter, providing a small divergence, so that CNAO beams are *quasiparallel*.
In treatment planning, the target volume is sectionated into isoenergy layers and the desired dose at a given depth is delivered spot-by-spot, selecting the opportune energy. For each energy layer two magnets scans the beam till all the spots are irradiated and then they move to the following layer.
The maximum beam intensity that can be reached is equal to $3 * 10^9$ and $6 * 10^7$ particles per second for protons and carbon ions, respectively.
Three treatment rooms are available, in the one we used for irradiation there is a single horizontal fixed beam line.

As reported in table 2.1 in Chapter 2, the CNAO beams energy ranges from 62.73

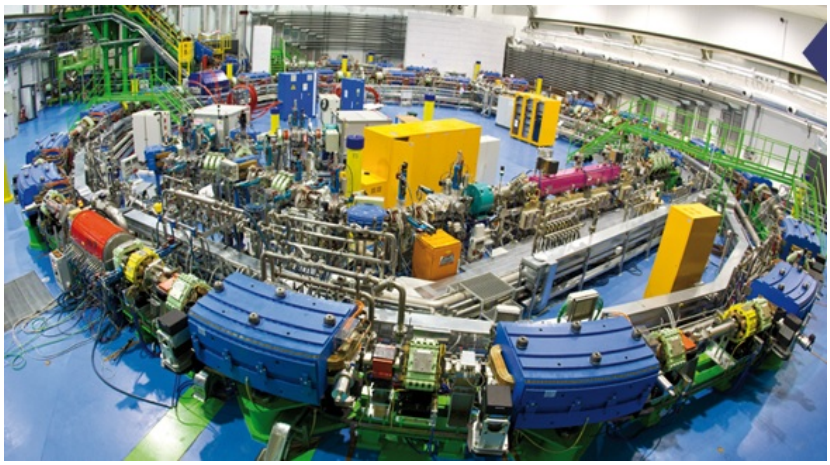

Figure 5.3: CNAO synchrotron (http://fondazionecnao.it).

to 228.57 MeV and 115.23 to 398.84 MeV/u for proton beams and carbon Ion beams, respectively. Bragg peak widths are also reported in this table in terms of FWHM.

Spot size in air

The spot sizes (in terms of FWHM) resulted to be energy-dependent (FWHM decreases with energy) and at the isocenter they vary from 2.2 to 0.7 cm for protons and from 0.8 to 0.4 cm for carbon Ions.
Moreover, the spot size dependence on its position resulted to be negligible.

Dose homogeneity

Dose homogeneity in 2D is evaluated in daily quality assurance along the main axes and diagonals with EB3 films placed at the isocenter and irradiated with monoenergetic uniform field (6 cm x 6 cm).
Homogeneity H is calculated as:

$$H = 100 * \frac{D_{max} - D_{min}}{D_{max} + D_{min}}$$

were D_{max} and D_{min} are the maximum and the minimum measured dose.

Energy constancy

Energy constancy is daily monitored in quality assurance using radiochromic films placed into solid slab phantom.

Irradiation configuration

The flasks containing cells undergoing irradiation were placed vertically inside a water phantom, which was put at the isocenter on the treatment table (as shown in figure 5.4), at the depth of 15 cm, corresponding to the mid Spread-Out Bragg Peak (SOBP). The SOBP had a width of 6 cm (ranging from 12 to 18 cm depth) and it was obtained with active beam energy modulation.

Figure 5.4: Water phantom for cell irradiation in the treatment rooms at CNAO.

PROTONS IRRADIATION

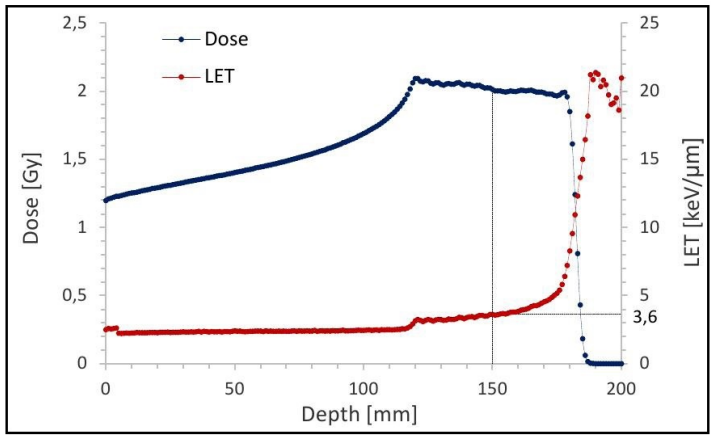

Figure 5.5: Proton SOBP and dose-averaged LET as a function of depth, evaluated with a Monte Carlo Fluka simulation. (Courtesy of Ciocca M., Mairani A. and Magro G. (CNAO))

The flasks were put in the center of an uniform scanned field. The field had a size of 10 x 10 cm^2 and the scanning step was equal to 3 mm.
The SOBP was achieved using 16 different energies from 131.5 to 164.8 MeV.
The dose-averaged Linear Energy Transfer (LET) in the mid SOBP, evaluated with Monte Carlo FLUKA simulation, was 3.6 $keV/\mu m$, as shown in figure 5.5. Samples were irradiated at different doses (0-5 Gy). We chose 3 Gy as maximum dose for the irradiation of cells pretreated with Epothilone B, in order to analyze range of similar cytotoxicity for the standard treatment and for the combined one.

carbon IONS IRRADIATION

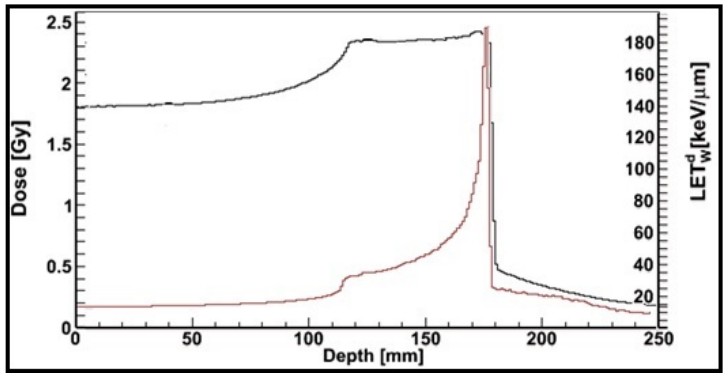

Figure 5.6: carbon Ion SOBP and dose-averaged LET as a function of depth, evaluated with a Monte Carlo Fluka simulation. (Courtesy of Ciocca M. and Mairani A. (CNAO))

The flasks were put in the center of an uniform scanned field. The field had a size of 10 x 10 cm^2 and the scanning step was equal to 2mm.
The SOBP(uniform in physical dose) was achieved using 31 different energies from 246 to 312 MeV/u.
The dose-averaged Linear Energy Transfer (LET) in the mid SOBP, evaluated with Monte Carlo FLUKA simulation, was about 45 $keV/\mu m$, as shown in figure 5.6.
Samples were irradiated at different doses (0-3 Gy). We chose 2 Gy as maximum dose for the irradiation of cells pretreated with Epothilone B, in order to analyze range of similar cytotoxicity for the standard treatment and for the combined one.

5.3 Post-irradiation treatments

Just after irradiation, the medium was removed and cells were detached from flasks using Trypsin-EDTA (0.25%). They were then counted using a portable Scepter cell counter in experiments performed at CNAO, or a Beckmann Coulter Counter in experiments performed at the Fondazione IRCCS Istituto Nazionale dei Tumori. The functioning of these instruments for cell count is described in the next paragraph.

5.3.1 Instruments for cell count

Beckmann Coulter Counter

This instrument is based on the Coulter principle: suspended particles passing through a pipe with an orifice produce an impedance variation when a voltage is applied.

Cells are suspended at low concentration in a solution containing an electrolyte. Specifically, 0.5 ml or 1 ml cell suspension is added to 19.5 ml or 19 ml of Isoton (dilution factor 40 or 20). A thin tube containing two electrodes is immersed in this solution; in the tube a small hole is present. In figure 5.7 a picture of the tube immersed in the solution

is shown.

Figure 5.7: Beckmann Coulter Counter. The tube is immersed in the glass containing the isotonic solution with cells to be counted.

The sensitive volume of the instrument is between the two electrodes, which in the presence of current provide an impedance measure. The solution is aspirated within the sensitive volume: the passage of a cell in this region induces an impedance variation, in fact the cell double lipid membrane opposes to the current passage.
Each impedance variation is recorded as a count and the amplitude of the signal is proportional to the cell volume. It is possible to set a gate on volumes, excluding impedance variations that may not be due to the passage of a cell (for example due to debris passage).
The instrument calculates the cell density (cell/ml) as the average value of the counts made on the solution.

Scepter Handheld Automated Cell Counter

The functioning of this instrument is the same of the Beckmann Coulter Counter. The main advantage is the small dimension, that permits to carry the instrument in other laboratories.
The sensitive volume in this case is a tip, that is immersed in a pipe containing cells to be counted. After the counting the tip must be discarded.
Also in this instrument it is possible to set a gate in order to exclude counting not associated to a cell passing within the sensitive volume.
In figure 5.8 a picture of the Scepter Handheld Automated Cell Counter is shown.

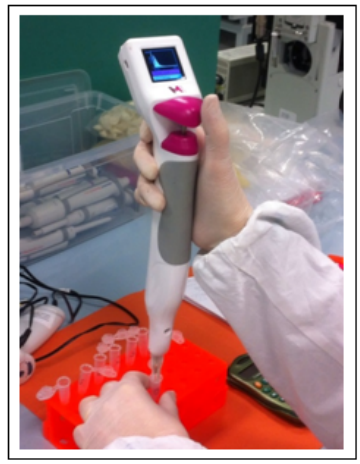

Figure 5.8: Scepter Handheld Automated Cell Counter used during an experiment at CNAO.

After counting, cells were prepared for the study of different biological end points, as described in the following section.

5.4 Biological end-points

In the present study, we investigated different biological end-points: cell clonogenic survival, invasive capacity and cell growth of irradiated cells pretreated or not with Epothilone B at the chosen concentrations.
Invasion rate and cell growth were investigated only for A549 and U251MG cells and for carbon Ions and Photons irradiation.
In the following paragraphs the assays performed for the study of these end-points will be described.

5.4.1 Clonogenic survival assay

Clonogenic (colony forming) assay is widely applied in order to study cell proliferative capacity. The original paper by Puck and Marcus (1956) described the technique for this assay.
For the measure of clonogenic survival, irradiated cells were plated into five flasks T25 for each dose at different inocula, calculated considering the expected survival that was estimated taking into account the dose and the Epothilone B concentration.
After seeding, cells were incubated for about 13 days and after this period they were fixed with ethanol, stained with 10% Giemsa solution and counted.
Colonies consisting of more than 50 cells were scored as survivors. An example of colonies generated from survived cells after the fixing and staining procedure is displayed in figure 5.9.

For each dose, the number of survived cells was determined as the mean of the counts obtained for the five flasks. The plating efficiency PE was then determined as the ratio

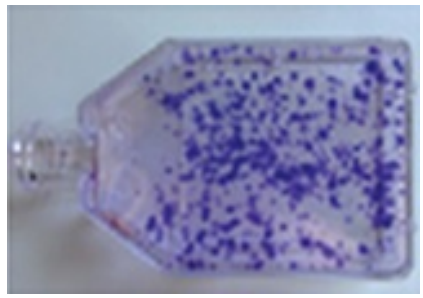

Figure 5.9: Colonies generated from survived cells after the fixing and staining procedure.

between the mean number of survived cells and the number of cells initially plated. Surviving fractions at dose D (S(D)) were determined as the ratio between the plating efficiency (PE(D)) of the irradiated sample and the control one (PE(0)):

$$S = \frac{PE(D)}{PE(0)}.$$

Survival curves for irradiated cells (pretreated or not with Epothilone B) were obtained plotting the surviving fraction as a function of dose.

At least three independent experiments have been performed for each radiation type and cell line. The final survival values were obtained as the mean of the surviving fractions measured in each experiment.
An example of survival data for cells irradiated with photons, pretreated or not with Epothilone B, is reported in figure 5.10.

5.4.2 Cell invasion assay

Cell invasion was investigated only in A549 and U251MG cells pretreated or not with Epothilone B and irradiated at three doses: 0 Gy, 1.5 Gy and 3 Gy for photon beams, 0 Gy, 0.75 Gy and 1.5 Gy for carbon Ions.
Cells invasion rate was measured using the CHEMICON Cell Invasion Assay Kit (QCM ECMatrix Cell Invasion Assay, Merck-Millipore).
After irradiation, about 10^6 cells were plated in each insert in serum-free medium. In the lower chamber of every insert $500\mu l$ of medium containing 10% fetal bovine serum were dropped.
The inserts contain an $8\mu m$ pore size polycarbonate membrane, over which a layer of $ECMatrix^{TM}$ is deposited. This thin layer occludes the membrane pores, preventing non-invasive cells from migrating, while invasive cells can migrate through the ECMatrix layer, reaching the bottom of the polycarbonate membrane in about 24 hours, as shown in figure 5.11.

After 24 hours of incubation, non-invasive cells and the ECMatrix were removed from the interior of the insert, while the invasive cells (migrated to the bottom of the membrane) were stained with Chrystal Violet stain and then counted by photographing the membrane through a microscope.
The invasion rate has been determined as the ratio between the invasive counted cells

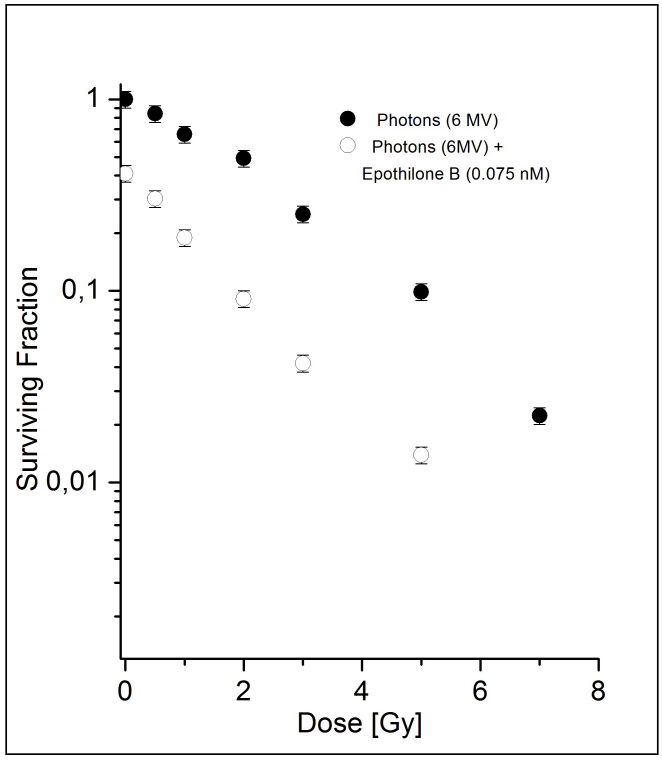

Figure 5.10: Surviving fraction of A549 cells as a function of dose for cells pretreated or not with Epothilone B.

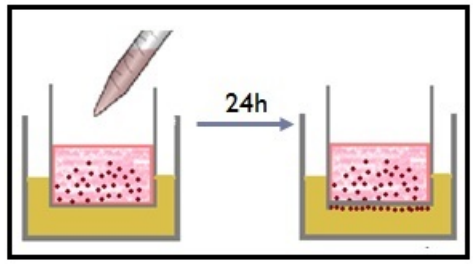

Figure 5.11: Schematic description of the invasion assay.

and the total number of plated cells. Values obtained for cells irradiated and/or treated with Epothilone B were then normalized to the control one, in order to obtain the relative invasion rate.

At least two independent experiments have been performed.

5.4.3 Cell growth

Cell growth was measured only in U251MG cells pretreated or not with Epothilone B and irradiated with carbon ion beams at three doses: 0 Gy, 0.75 Gy and 1.5 Gy.
Just after irradiation cells were plated at different inocula in flasks T25 and then incubated.
At different time from irradiation cells were detached from flasks using Trypsin-EDTA (0.25%). They were then counted using a Beckmann Coulter Counter.
Growth curves were obtained plotting the ratio between the number of counted cells n(t) and the number of cells initially plated n_0 as a function of time.
Two independent experiments have been performed.

CHAPTER 6

Data analysis

The aim of this thesis is the study of the effects obtained combining radiations and Epothilone B in human cancer cell cultured *in vitro*, investigating different biological end-points.
In particular, the main goal of this study is to determine if the Epothilone B has a radiosensitising effect when combined with photon, proton or carbon ion irradiation.
In this Chapter the analysis of data relative to cell clonogenic survival, Relative Biological Effectiveness, cell invasive capacity, and cell growth will be described.
Moreover, the analysis of the radiation-drug interaction performed in order to determine if radiation and Epothilone B interact in an additive way, or in a synergic one will be explained.
The procedures described in the following sections were applied to the data obtained for all cell lines and radiation types. For brevity, in this Chapter only the analysis performed on A549 cells (or U251MG cells in the case of cell growth) will be described, by way of example. The results obtained for all cell lines and radiations will be exposed in Chapter 7.

In the first section the analysis of surviving fraction performed to obtain the survival-dose curves will be shown. Afterwards, the procedure followed to determine the Relative Biological Effectiveness will be described. In the third section the analysis of radiation-drug interaction according to the model of Luttjeboer et al. (2010) will be presented. Section 4 and 5 will be dedicated to the analysis of cell invasive capacity and growth.

6.1 Survival curves

The mean surviving fractions obtained as described in Chapter 5 and plotted as a function of dose were used to determine dose-survival curves. It was estimated that an error on survival lower than 10% could underestimate the real uncertainty in clonogenic survival measurements, given the biological variability and the uncertainties in the post-irradiation treatments and on the inoculum. Thus, the error on survival was determined as the greatest value between the standard error of the mean and the 10% of the survival value:

$$\sigma_S = max\left(\sqrt{\frac{\sum_{i=1}^{N}(S_i - < S >)}{N(N-1)}}; 10\%\right)$$

Given the great uncertainties on surviving fractions, the uncertainties on the absorbed dose were considered to be negligible.

Survival data as a function of radiation dose were fitted with the software *OriginLab* according to the Linear Quadratic (LQ) model (described in Chapter 1) for all cell lines and radiations type. A weighted fit was performed using error bars as weight: $w_i = \frac{1}{\sigma_i^2}$. More details about the fit are exposed in Appendix A.

The obtained curves were exploited for RBE determination and for the analysis of radiation-drug interaction mechanism.

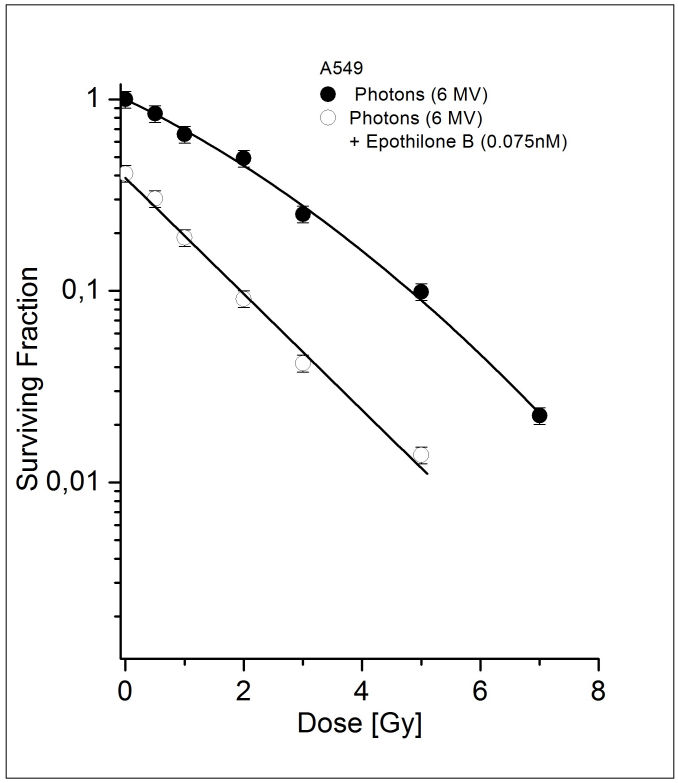

Figure 6.1: Survival curves of A549 cells pretreated (empty circles) or not (full circles) with 0.075 nM Epothilone B and irradiated with photon beams. Reported data are the mean of 5 independent experiments.

In figure 6.1 survival curve of A549 cells exposed to radiation alone (full circles) and combined with 0.075 nM Epothilone B (empty circles) are reported, as an example.
The curve relative to radiation alone represents the interpolation of the experimental points according to the linear quadratic model:

$$S = e^{-\alpha D - \beta D^2} \tag{6.1}$$

where S is the Surviving fraction and D the radiation dose.
We can observe that data relative to cells treated with Epothilone B and then irradiated show a different radiation dose-dependence: surviving fraction exponentially decreases with dose, without any shoulder. In fact, the β parameter of the LQ fit is consistent with 0. Thus data are interpolated with a linear function:

$$S = S_0 e^{-\alpha D} \tag{6.2}$$

The parameter S_0 represents the clonogenic survival of cells treated with Epothilone B and not irradiated.

Analogous results were found with proton beams and for all the cell lines, while, as expected, survival curves relative to cell simply irradiated with carbon Ions shows a linear trend , the β parameter being negative. The obtained results will be presented and discussed in the next Chapter.

6.2 Relative Biological Effectiveness (RBE)

RBE (defined in Chapter 1) was calculated as the ratio between the dose of reference radiation (6MV photons) and that of protons or carbon Ions necessary to produce the same biological effect. The end-point we decided to use for RBE determination is the 10% of survival. RBE was calculated as the ratio between the doses of photons and that of protons or carbon Ions that lead to a surviving fraction equal to 0.1, as displayed in figure 6.2, where the surviving fractions of A549 cells exposed to photons (circles) or protons (triangles) are shown.
RBE at 10% of survival ($RBE_{10\%}$) was calculated according to equation 6.3.

$$RBE_{10\%} = \left(\frac{D_{photons}}{D_{radiation}} \right)_{S=0.1} \tag{6.3}$$

The radiation doses $D_{0.1}$ necessary to obtain a surviving fraction of 0.1 were calculated starting from the survival curves, according to equation 6.4 and 6.5 for linear-quadratic curves and linear curves, respectively.

$$D_{0.1} = \frac{-\alpha + \sqrt{\alpha^2 - 4\beta ln(0.1)}}{2\beta} \tag{6.4}$$

$$D_{0.1} = \frac{-\alpha}{ln(0.1)} \tag{6.5}$$

RBE uncertainty was determined according to error propagation:

$$\begin{aligned} \sigma_{RBE_{10\%}} &= \sqrt{\left(\frac{\partial RBE_{10\%}}{\partial D_{photons}} \right)^2 \sigma^2_{D_{photons}} + \left(\frac{\partial RBE_{10\%}}{\partial D_{radiation}} \right)^2 \sigma^2_{D_{radiation}}} \\ &= RBE_{10\%} \sqrt{\left(\frac{\sigma_{D_{photons}}}{D_{photons}} \right)^2 + \left(\frac{\sigma_{D_{radiation}}}{D_{radiation}} \right)^2} \end{aligned} \tag{6.6}$$

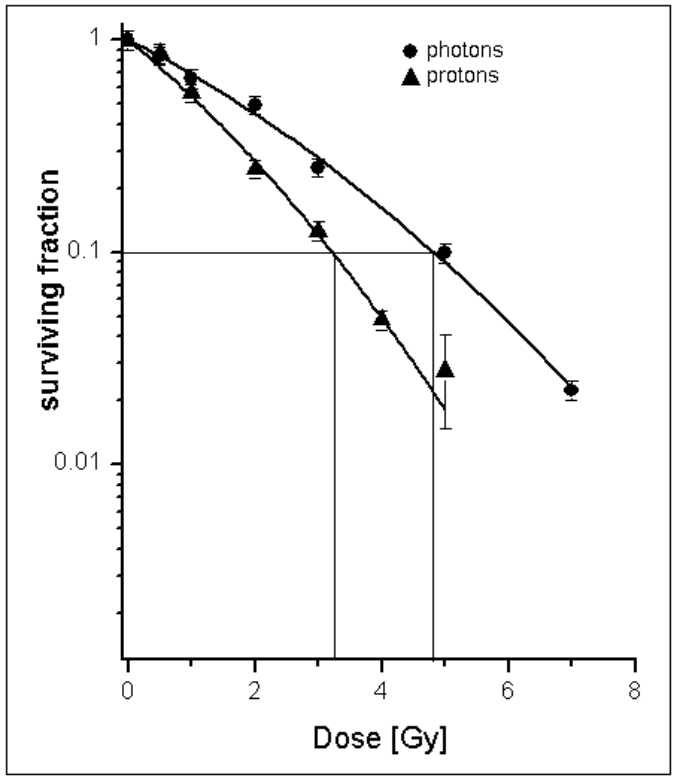

Figure 6.2: Surviving fractions of A549 cells exposed to photons (circles) or protons (triangles) are shown. 10% of survival and the dose of photons and protons that lead to this survival level are highlighted in order to show the procedure followed to calculate the $RBE_{10\%}$.

Dose uncertainties are determined according to error propagation through relations 6.7 and 6.8 for linear quadratic curves and linear curves, respectively.

$$\sigma_D = \sqrt{\left(\frac{\partial D}{\partial \alpha}\right)^2 \sigma_\alpha^2 + \left(\frac{\partial D}{\partial \beta}\right)^2 \sigma_{beta}^2 + 2cov(\alpha,\beta)\frac{\partial D}{\partial \alpha}\frac{\partial D}{\partial \beta}} \tag{6.7}$$

$$\sigma_D = \frac{\partial D}{\partial \alpha}\sigma_\alpha \tag{6.8}$$

where α and β are the fit parameters and D the dose of radiation.

In equation 6.7 the covariance of α and β appears, since the parameter of the linear quadratic fit cannot be considered completely uncorrelated. $cov(\alpha,\beta)$ resulted to be always negative for all the linear quadratic curves. The fact that the covariance is negative is coherent with the fact that α and β are weakly anti-correlated, since when α increases β decreases and viceversa.
We can notice that the product $\frac{\partial D}{\partial \alpha}\frac{\partial D}{\partial \beta}$ is negative. In fact, the partial derivatives of dose D with respect to α and β are:

$$\frac{\partial D}{\partial \alpha} = -\frac{D}{\alpha + 2\beta D}$$
$$\frac{\partial D}{\partial \beta} = -\frac{D^2}{\alpha + 2\beta D}.$$

Thus, the product of the two derivatives is:

$$\frac{\partial D}{\partial \alpha}\frac{\partial D}{\partial \beta} = \frac{D^3}{(\alpha + 2\beta D)^2} > 0$$

As a consequence, the product $2cov(\alpha, \beta)\frac{\partial D}{\partial \alpha}\frac{\partial D}{\partial \beta}$ is negative, given the values of $cov(\alpha, \beta)$, and can lead to an underestimation of the real RBE uncertainties. For this reason, we decided to neglect this term in the calculation of doses uncertainties, considering the parameters α and β as independent .

6.3 Radiation-drug interaction mechanism

As mentioned in Chapter 3, the model proposed by Luttjeboer et al. (2010) was applied in order to analyze radiation-drug interactions, basing on changing in clonogenic capacity induced by radiation modifying agents, like Epothilone B.
Different quantitative analysis of dose-effects relations have been published, for our analysis we decided to exploit this model because it is the nearest to our experimental approach.
This model started from the analysis of Lam (1989) in which the final effect of the combination of two cytotoxic agents on the biological system is produced in a certain time through a series of intermediate lesions. As a consequence, two extreme definition of additivity are proposed: on the one hand, two additive cytotoxic agents can act through completely independent mechanism, while, on the opposite, they can act mainly in the same way, causing the same intermediate lesions. A schematic description of this two additive modalities of interaction is given in figure 6.3. In the first case (a) agents A and B product different intermediate lesions leading to the final effect AB. In case b, the agents A and B products the same kind of intermediate lesions, leading to the final effect AB.

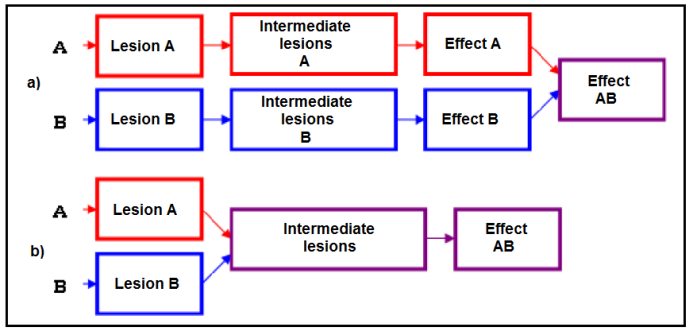

Figure 6.3: Schematic description of the Lam approach.

Basing on this approach, in the model Luttjeboer et al. (2010) an area of additiv-

ity is built in the survival-dose plane. This region is delimited by two curves obtained supposing two different modalities of additivity between cytotoxic agents: the *independent* and the *overlapping* additivity. In the independent additivity, the only action of the chemotherapy is the reduction of the number of clonogenic cells on which radiation will act and drug and radiation act completely independently. Thus, the final surviving fraction is simply the product of the surviving fractions obtained exposing cells to radiation and drug separately. Looking at the survival curves, this action cause a downward shift of starting point of the survival curve relative to irradiation alone. The curve of independent additivity is so built starting from survival curve for irradiation alone, according to equation 6.9.

$$S = S_0 e^{-\alpha D - \beta D^2} \tag{6.9}$$

Where S_0 is the surviving fraction of cells treated with Epothilone B and not irradiated, used as starting point for the irradiation, while α and β are the parameter of the survival curve of cells just irradiated, reported in equation 6.1.
In the case of overlapping additivity, the drug is supposed to act as an additional radiation dose, $D^\star$, defined as the radiation dose giving a citotoxicity equal to that obtained with the drug alone (i.e. leading to a surviving fraction equal to S_0). Looking at survival curves, the overlapping additivity reflects in a left-shift of the survival curve relative to irradiation alone. Thus, the curve of overlapping additivity is built starting from survival curve for irradiation alone, according to equation 6.10.

$$S = e^{-\alpha(D+D^\star) - \beta(D+D^\star)^2} \tag{6.10}$$

α and β are the parameter of the survival curve of cells just irradiated, reported in equation 6.1, while $D^\star$ is calculated from survival curve for irradiation alone, imposing a surviving fraction equal to S_0:

$$\begin{cases} S = e^{-\alpha D - \beta D^2} \\ S = S_0 \end{cases}$$

$$D^\star = \frac{-\alpha + \sqrt{\alpha^2 - 4ln(S_0)\beta}}{2\beta} \tag{6.11}$$

Experimental curves obtained for the radiation-drug combination falling within the additivity area (delimited by the independent and overlapping additivity curves) indicate a simply additive interaction between the two agents, otherwise experimental data that fall below this region, indicate a synergic interaction.

α	0.343 Gy^{-1}
β	0.028 Gy^{-2}
S_0	0.390
$D^\star$	2.31 Gy

Table 6.1: Parameters used to calculate the independent and overlapping additivity curves for A549 cells irradiated with photon beams.

In figure 6.4 the analysis of interaction of photon beams and Epothilone B (0.075 nM) according to the described model is displayed for A549 cells, as an example. The relative

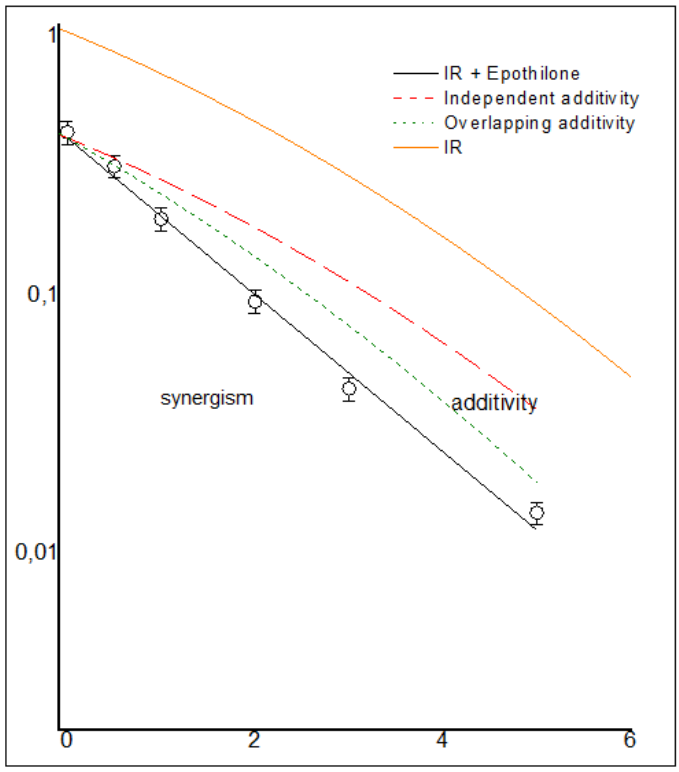

Figure 6.4: Analysis of the interaction between photons and Epothilone B (0.075 nM) in A549 cells. The region of "partial common action" (corresponding to an additive interaction) is bounded by the independent (red, dashed line) and overlapping (green, dotted line) curves. These curves were built shifting downwards or on the left the curve relative to irradiation alone (orange, solid line). The curve relative to the combined treatment of photons and Epothilone B (black, solid line) that fits the experimental data (empty circles) falls below the additivity region, indicating a synergism in radiation-drug interaction.

survival curves are shown in figure 6.1. We can notice that the experimental points and the curve relative to irradiation combined to the Epothilone B treatment fall below the additivity region delimited by the red (independent) and the green (overlapping) curves, indicating a synergic interaction modality. The overlapping curve is parallel to the curve relative to irradiation alone, while the independent curve seems to have a different slope, due to the presence of the factor S_0 in equation 6.9. It is important to underline that in this representation a different slope with respect to that of irradiation alone does not indicate a non-additive interaction.
In table 6.1 the values of the parameter used to calculate the independent and overlapping additivity curves (according to equations 6.9 and 6.10) are reported.

In case of linear curve relative to irradiation alone, like for high-LET radiation survival curves ($S = e^{-\alpha D}$), the independent and the overlapping curves, calculated according to equations 6.9 and 6.10 with $\beta = 0$, coincide and the area of partial common action degenerates in a straight line, below which the radiation-drug interaction can be

considered synergic.

In order to quantify the effectiveness of the combined treatment with respect to irradiation alone, the Dose Enhancement Factor (DEF), was determined. The DEF is defined as the ratio between the radiation doses used alone (D_{ir}) and combined to the drug ($D_{ir+drug}$) to obtain the same biological end point (i.e. the same survival level). It is important to highlight that with linear-quadratic survival curves a DEF value greater than 1 is not an indication of a synergistic interaction according to the model we applied, but simply a quantification of the greater effectiveness of the combined treatment with respect to irradiation alone.
We calculated the DEF at 10% of survival for all radiation types and cell lines:

$$DEF_{10\%} = \left(\frac{D_{ir}}{D_{ir+drug}} \right)_{S=10\%}$$

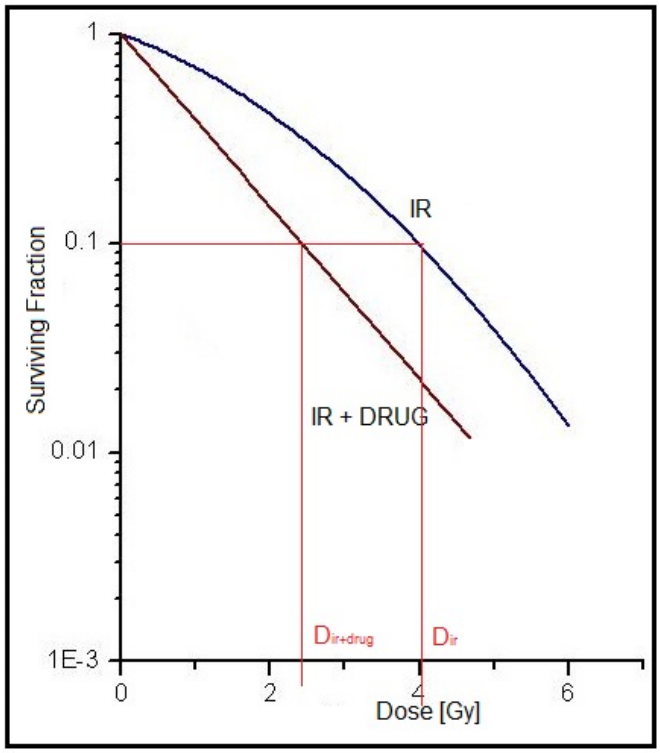

Figure 6.5: Example of DEF calculation.

For this calculation the curve relative to the combined treatment was normalized to the surviving fractions of cells pretreated with Epothilone B and not irradiated (S_0), in order to compare this curve with the one relative to irradiation alone, as shown in figure 6.5. Results obtained for all radiation types and cell lines are reported in Chapter 7.

6.4 Invasion rate

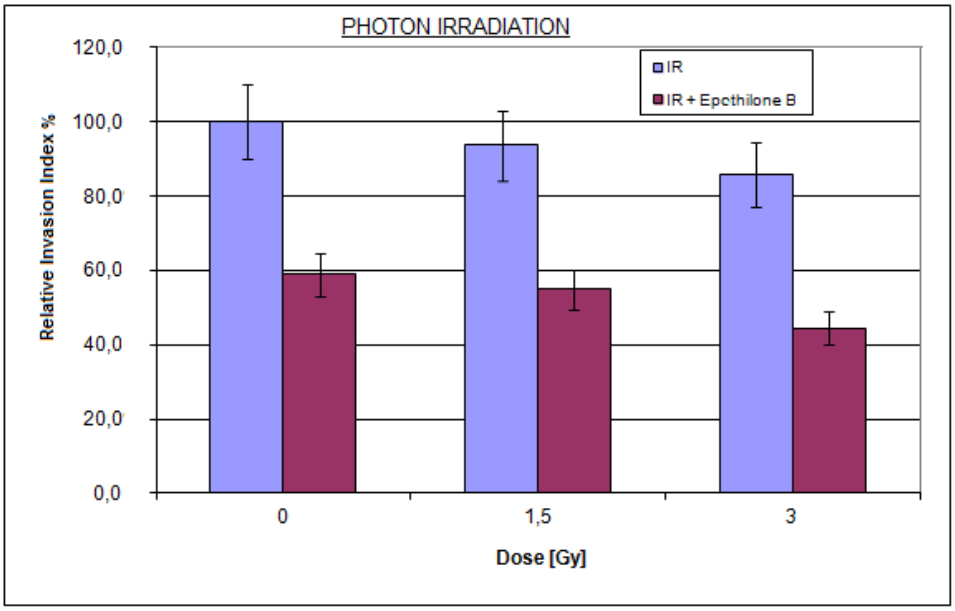

Figure 6.6: Relative Invasion Index of A549 cells irradiated with photons at different doses pretreated or not with Epothilone B 24 hours before irradiation. (I.I. values have been normalized to the control sample).

As described in the previous Chapter, Invasion Index (I.I.) was measured as the ratio between the number of invading cells, passed through the ECMatrix, and the total number of seeded cells. Obtained I.I. values were then normalized to the control sample, in order to obtain the relative invasion index for every dose for both Epothilone B treated and untreated samples.
Results were plotted in histograms, as the one reported in figure 6.6 in which the relative I.I. of A549 irradiated with photon beams combined to 0.075 nM Epothilone B or not is reported.
Error bars were determined as the greatest value between the standard error and 10% of the relative I.I., as in the case of Surviving fractions, due to analogous considerations.

6.5 Cell growth

Cell growth was measured only for U251MG cells irradiated with carbon ions.
The mean ratio between the number of cells counted at time t $n(t)$ and the number of plated cells n_0 has been plotted as a function of time for each dose of radiation combined to Epothilone B or not. In order to calculate the uncertainties on time and on the ratio $\frac{n(t)}{n_0}$ the standard error was calculated.
Obtained curves were then compared with the aim of evaluating the effects of irradiation and Epothilone B on cell growth.

Data relative to cells in the phase of exponential growth were then fitted according to equation 4.1. Looking at data relative to cells irradiated with carbon ions, we noticed a delay in the growth curves which resulted shifted with respect to the curve relative to the control sample. In this case, data were fitted according to equation 6.12

$$\frac{n(t)}{n_0} = 2^{\frac{(t-x)}{t_D}} \tag{6.12}$$

where x is the delay and t_D the doubling time.
Also in this case, error bars were determined as the greatest value between the standard error and 10% of the relative I.I., as in the case of Surviving fractions, due to analogous considerations.
Weighted fits were performed with the software *OriginLab*. Details on the fitting procedure with this software are reported in Appendix 3.

CHAPTER 7

Experimental results: description and interpretation

In this Chapter the results obtained after the analysis presented in Chapter 6 will be described and discussed.

First of all, dose-survival curves will be shown for cells irradiated, treated or not with Epothilone B and a comparison between the effects induced by photons, protons and carbon ions will be performed. Then, the values obtained for proton and carbon ion Relative Biological Effectiveness will be presented and discussed. The results of the analysis of radiation-drug interaction will be then described and commented. Data obtained in experiments with photon and proton beams on A549 and U251MG cells have been reported in an already submitted paper (Bettega et al.).
In the following sections, results obtained on cell growth and invasion will be described for cells irradiated and exposed or not to Epothilone B.

7.1 Dose-survival curves

Dose-survival curves will be presented for each cell line, comparing the results obtained with the different radiation types combined or not with Epothilone B. Data are reported in semilogarithmic plots and error bars were estimated following the procedure described in Chapter 6.
In the following paragraphs survival data (mean of at least 3 independent experiments) of A549, U251MG and DAOY cells exposed to 6MV LINAC photon, proton (dose-averaged LET $= 3.6 keV/\mu m$) or carbon ion (dose-averaged LET $= 45 keV/\mu m$) beams pretreated or not with Epothilone B will be displaied. The reported curves are the fit to the experimental points according to the LQ model (equations 6.1 and 6.2 for cells simply irradiated or even treated with the drug, respectively). The fit parameters are reported in table 7.4.

7.1.1 A549 cells

Figure 7.1 shows survival curves of A549 cells simply irradiated. As expected, the curve relative to C-ions irradiation is linear, in fact the β parameter in equation 6.1 is negative. A negative β-value has no physical meaning according to the LQ model, for this reason data were fitted with a pure exponential function (imposing $\beta = 0$). This behavior is typical of cells irradiated with High-LET radiation.
Looking at survival curves relative to photon and proton irradiation, we can notice that

the latter are more effective in inducing clonogenic cell death; this fact reflects on a proton RBE value higher than 1 (more details are discussed in Section 7.2).

Figure 7.2 shows survival data of A549 cells pretreated with 0.075 nM Epothilone B and irradiated. We can observe that data obtained for cells treated with Epothilone B and irradiated with photons or protons show a dose dependency different from the one of cells simply irradiated. In fact, the surviving fraction decreases exponentially with dose, without any shoulder. This is a first clue of the fact that Epothilone B modifies cell response to irradiation, removing the shoulder (described by the quadratic term in equation 6.1) typical of low-LET irradiation. This aspect will be investigated in Section 7.3.

In table 7.1 the mean surviving fractions are reported for each dose. Data collected in each experiment are reported in Appendix C.

Irradiation								
photon irradiation			proton irradiation			C-ion irradiation		
Dose [Gy]	$\overline{S}$	error	Dose [Gy]	$\overline{S}$	error	Dose [Gy]	$\overline{S}$	error
0	1.00	0.10	0	1.00	0.10	0	1.00	0.1
0.5	0.84	0.08	0.5	0.87	0.09	0.5	0.57	0.06
1	0.66	0.07	1	0.56	0.06	0.75	0.30	0.05
2	0.49	0.05	2	0.25	0.02	1	0.15	0.02
3	0.25	0.03	3	0.13	0.01	1.5	0.071	0.007
5	0.10	0.01	4	0.05	0.00	2	0.031	0.003
7	0.022	0.002	5	0.03	0.01	3	0.010	0.001
Irradiation + Epothilone B								
Dose [Gy]	$\overline{S}$	error	Dose [Gy]	$\overline{S}$	error	Dose [Gy]	$\overline{S}$	error
0	0.41	0.04	0	0.39	0.04	0	0.40	0.04
0.5	0.30	0.03	0.5	0.26	0.03	0.5	0.20	0.02
1	0.19	0.02	1	0.12	0.01	0.75	0.10	0.01
2	0.091	0.009	2	0.062	0.006	1	0.05	0.01
3	0.042	0.004	3	0.023	0.003	1.5	0.026	0.007
5	0.014	0.001	4	0.012	0.002	2	0.009	0.002

Table 7.1: Mean surviving fractions of A549 cells irradiated with photon, proton and carbon ion beams with or without 0.075 Epothilone B.

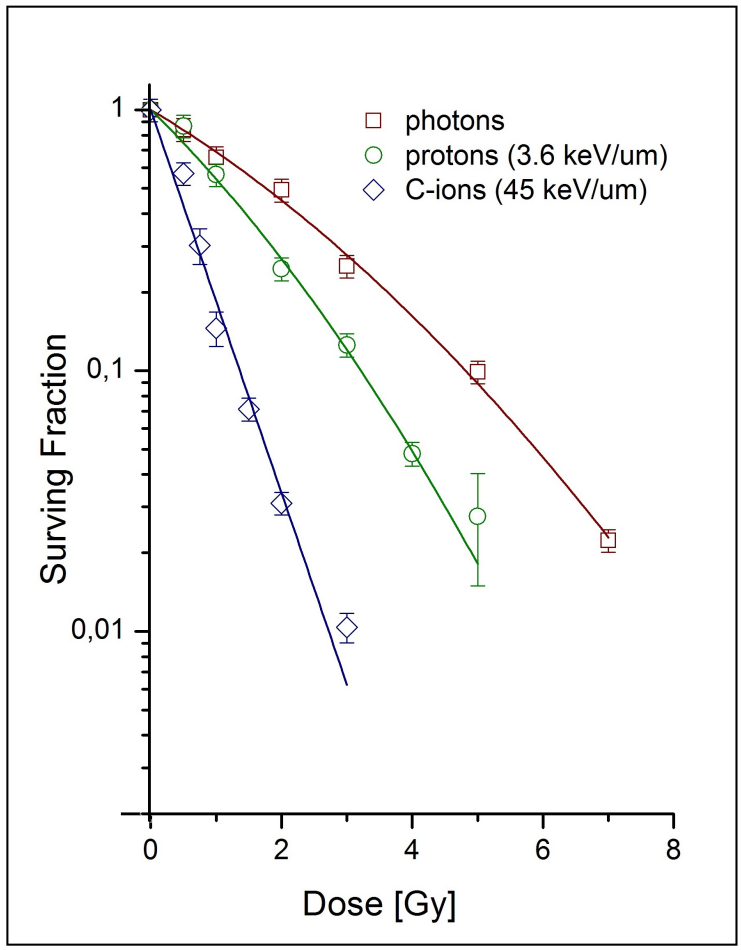

Figure 7.1: Surviving fraction of A549 cells exposed to photons (mean of 5 independent experiments), protons (mean of 4 independent experiments) and carbon ions (mean of 3 independent experiments). Solid lines are the fit of the experimental data according to equations 6.2. In the case of C-ions irradiation the quadratic term was set to 0. Error bars represent the maximum value between the Standard Error and the 10% of Survival.

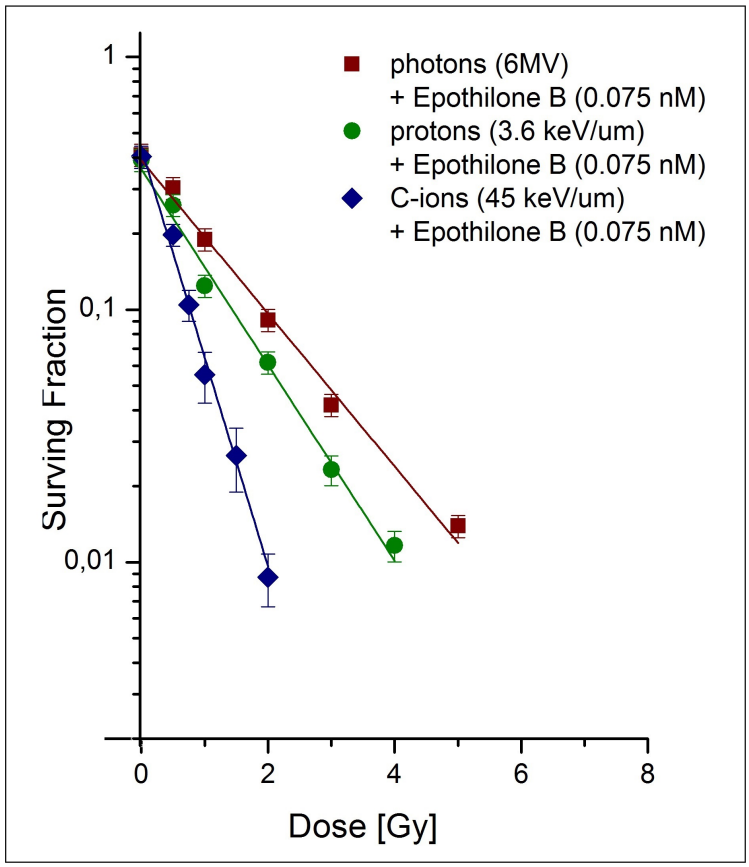

Figure 7.2: Surviving fractions of A549 cells pretreated with 0.075 nM Epothilone B and exposed to photons (mean of 5 independent experiments), protons (mean of 3 independent experiments) and carbon ions (mean of 3 independent experiments). Solid lines are the fit of the experimental data according to equations 6.2. Error bars represent the maximum value between the Standard Error and the 10% of Survival.

7.1.2 U251MG cells

Figures 7.3 and 7.4 show survival curves of U251MG cells simply irradiated or irradiated and pretreated with 0.125 nM Epothilone B, respectively.

Considerations analogue to those relative to A549 cells can be done.

In table 7.2 the mean surviving fractions are reported for each dose. Data collected in each experiment are reported in Appendix C.

Irradiation								
photon irradiation			proton irradiation			C-ion irradiation		
Dose [Gy]	$\overline{S}$	error	Dose [Gy]	$\overline{S}$	error	Dose [Gy]	$\overline{S}$	error
0	1.0	0.1	0	1.0	0.1	0	1.0	0.10
0.5	0.90	0.09	0.5	0.80	0.08	0.5	0.61	0.07
1	0.72	0.07	1	0.53	0.05	0.75	0.35	0.04
2	0.48	0.05	2	0.25	0.03	1	0.17	0.02
3	0.22	0.02	3	0.10	0.01	1.5	0.09	0.01
5	0.07	0.02	4	0.043	0.004	2	0.041	0.004
7	0.019	0.004	5	0.011	0.001	3	0.012	0.002
Irradiation + Epothilone B								
Dose [Gy]	$\overline{S}$	error	Dose [Gy]	$\overline{S}$	error	Dose [Gy]	$\overline{S}$	error
0	0.411	0.041	0	0.41	0.04	0	0.42	0.04
0.5	0.241	0.024	0.5	0.23	0.03	0.5	0.24	0.04
1	0.127	0.013	1	0.11	0.02	0.75	0.13	0.02
2	0.064	0.006	2	0.043	0.004	1	0.050	0.007
3	0.029	0.003	3	0.015	0.001	1.5	0.023	0.003
5	0.007	0.001	4	0.0059	0.0006	2	0.0082	0.0008

Table 7.2: Mean surviving fractions of U251MG cells irradiated with photon, proton and carbon ion beams with or without 0.125 Epothilone B.

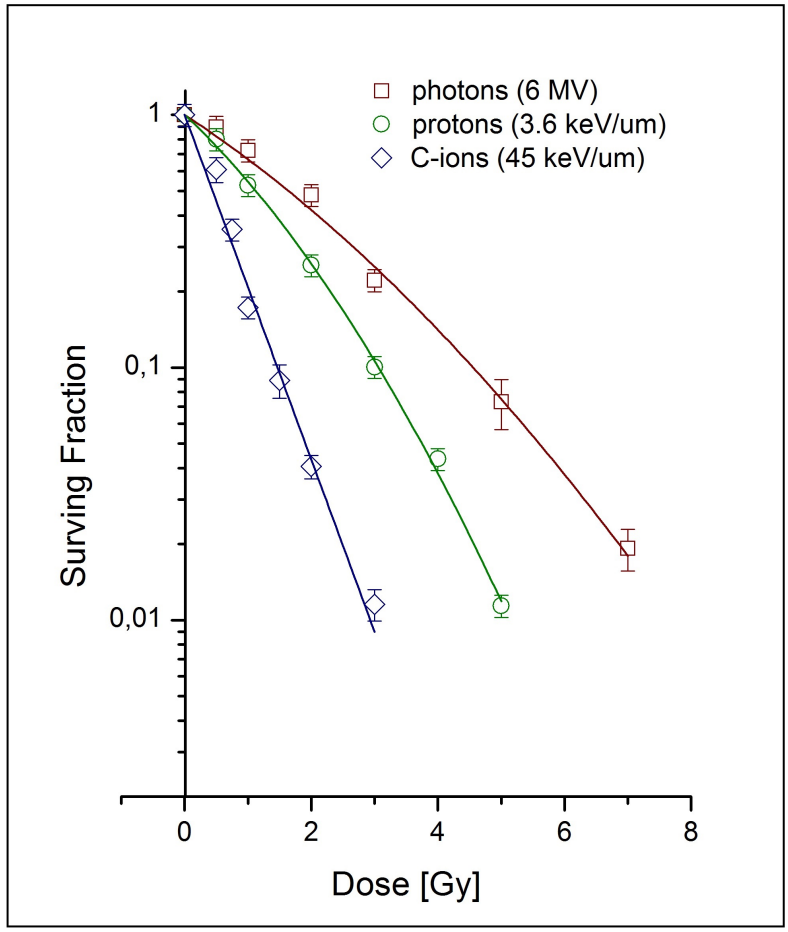

Figure 7.3: Surviving fractions of U251MG cells exposed to photons (mean of 4 independent experiments), protons beams (mean of 4 independent experiments) and carbon ions (mean of 3 independent experiments). Solid lines are the fit of the experimental data according to equations 6.2. In the case of C-ions irradiation the quadratic term was set to 0. Error bars represent the maximum value between the Standard Error and the 10% of Survival.

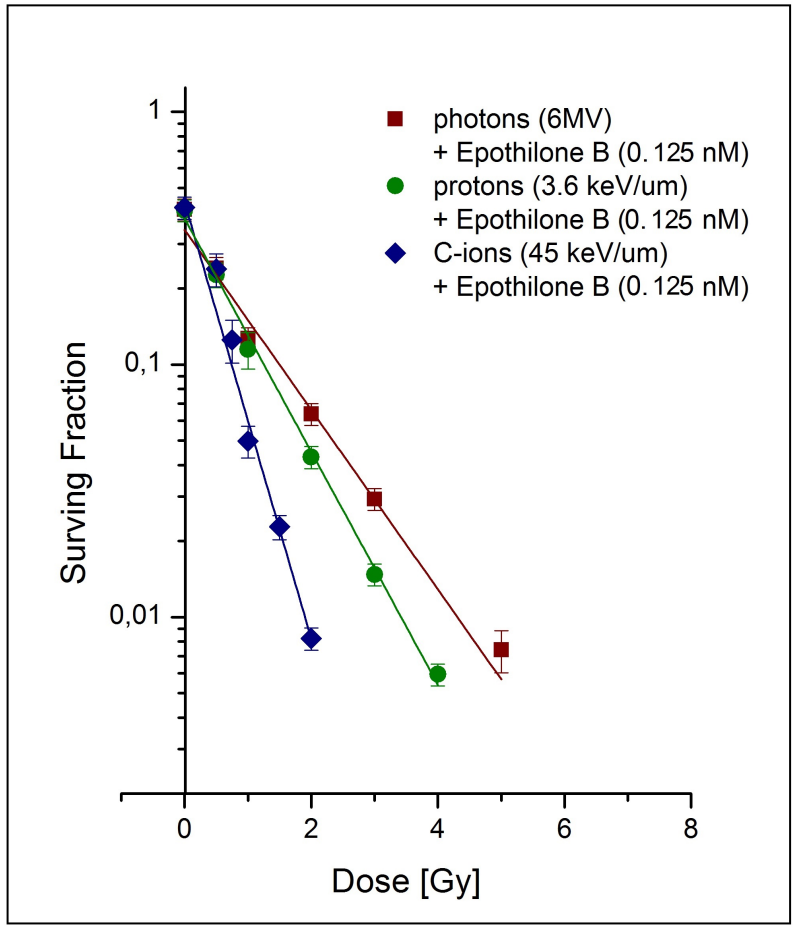

Figure 7.4: Surviving fractions of U251MG cells pretreated with 0.125 nM Epothilone B and exposed to photon (mean of 3 independent experiments), proton beams (mean of 4 independent experiments) and carbon ions (mean of 3 independent experiments). Solid lines are the fit of the experimental data according to equations 6.2. Error bars represent the maximum value between the Standard Error and the 10% of Survival.

7.1.3 DAOY cells

DAOY cells were treated only with low-LET radiation (protons and photons), as mentioned in the previous chapters. Figure 7.5 shows survival data of DAOY cells simply irradiated. We can notice that this cell line is more radiosensitive than the A549 and the U251MG and that protons and photons survival curves are quite similar. This behavior is typical of very radiosensitive cell-lines.
Figure 7.6 shows survival data of cells pretreated with 0.035 nM Epothilone B and irradiated.
We can observe that also in this cell line, Epothilone B remove the dose-survival curve shoulder, modifying cell response to irradiation. Moreover, due to the high radiosensitity of this cells even to photon irradiation, the curves relative to the combination of protons or photons to Epothilone B are very similar.

In table 7.3 the mean surviving fraction are reported for each dose. Data collected in each experiment are reported in Appendix C.

Irradiation					
photon irradiation			proton irradiation		
Dose [Gy]	$\overline{S}$	error	Dose [Gy]	$\overline{S}$	error
0	1	0.1	0	1	0.1
0.5	0.83	0.08	0.5	0.80	0.08
1	0.70	0.07	1	0.55	0.06
2	0.37	0.04	2	0.26	0.03
3	0.17	0.02	3	0.13	0.01
5	0.041	0.004	4	0.058	0.006
7	0.010	0.001	5	0.022	0.002
Irradiation + Epothilone B					
Dose [Gy]	$\overline{S}$	error	Dose [Gy]	$\overline{S}$	error
0	0.42	0.04	0	0.39	0.04
0.5	0.27	0.03	0.5	0.27	0.03
1	0.13	0.01	1	0.13	0.01
2	0.053	0.005	2	0.062	0.006
3	0.025	0.002	3	0.025	0.002
5	0.005	0.002	4	0.013	0.004

Table 7.3: Mean surviving fractions of DAOY cells irradiated with photon and proton beams with or without 0.035 Epothilone B.

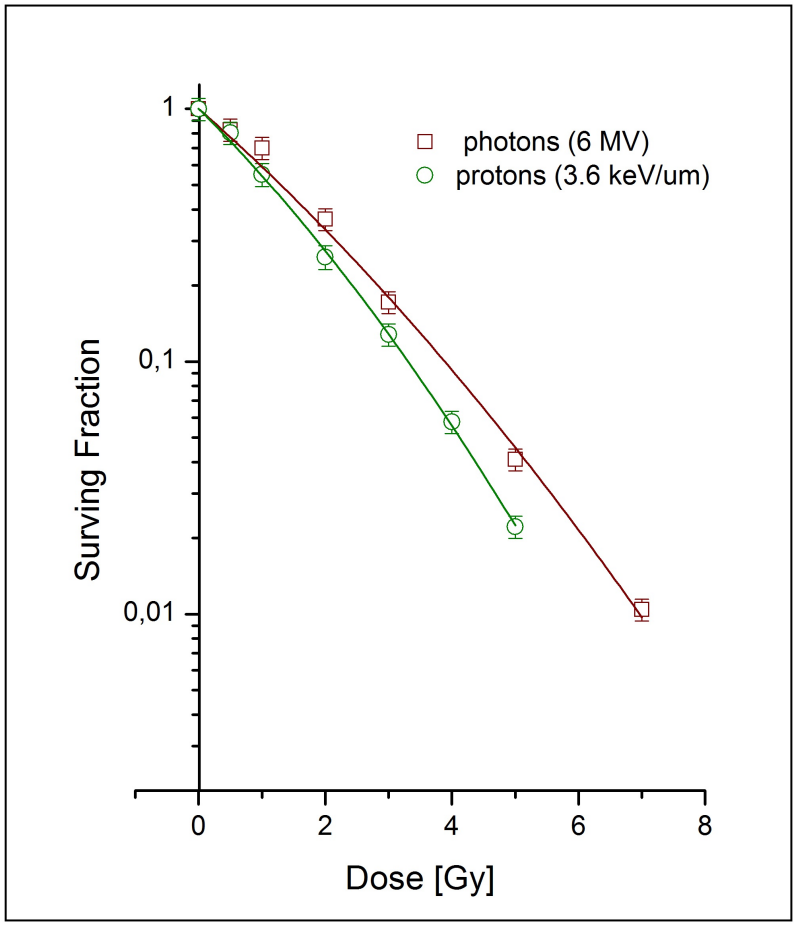

Figure 7.5: Surviving fractions of DAOY cells exposed to photon (mean of 3 independent experiments) and proton beams (mean of 4 independent experiments). Solid lines are the fit of the experimental data according to equations 6.1. Error bars represent the maximum value between the Standard Error and the 10% of Survival.

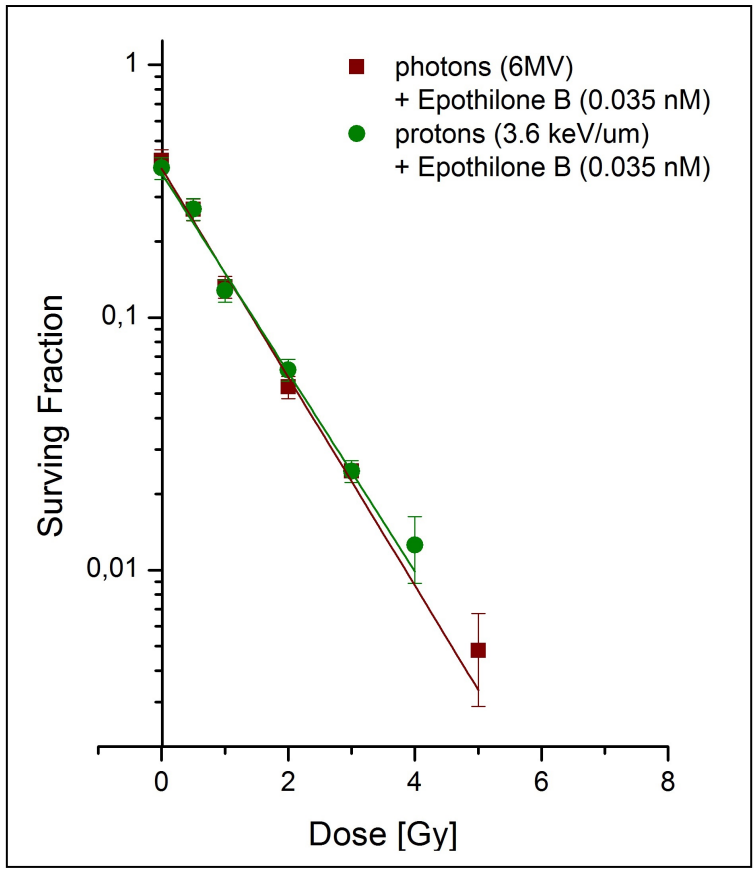

Figure 7.6: Surviving fractions of DAOY cells pretreated with 0.035 nM Epothilone B and exposed to photon (mean of 3 independent experiments) and proton beams (mean of 4 independent experiments). Solid lines are the fit of the experimental data according to equations 6.2. Error bars represent the maximum value between the Standard Error and the 10% of Survival.

Fit Parameters

Parameter	A549	U251MG	DAOY
Photon irradiation			
$\alpha[Gy^{-1}]$	0.34 ± 0.04	0.38 ± 0.04	0.51 ± 0.04
$\beta[Gy^{-2}]$	0.028 ± 0.009	0.028 ± 0.006	0.022 ± 0.007
Photon irradiation + Epothilone B			
S_0	0.39 ± 0.03	0.34 ± 0.02	0.38 ± 0.03
$\alpha[Gy^{-1}]$	0.70 ± 0.04	0.82 ± 0.04	0.94 ± 0.04
Proton irradiation			
$\alpha[Gy^{-1}]$	0.56 ± 0.07	0.54 ± 0.05	0.57 ± 0.05
$\beta[Gy^{-2}]$	0.05 ± 0.02	0.07 ± 0.01	0.04 ± 0.01
Proton irradiation + Epothilone B			
S_0	0.36 ± 0.03	0.38 ± 0.03	0.37 ± 0.03
$\alpha[Gy^{-1}]$	0.89 ± 0.04	1.06 ± 0.03	0.90 ± 0.04
C-ions irradiation			
$\alpha[Gy^{-1}]$	1.69 ± 0.03	1.57 ± 0.03	/
C-ions irradiation + Epothilone B			
S_0	0.43 ± 0.03	0.44 ± 0.04	/
$\alpha[Gy^{-1}]$	1.9 ± 0.1	1.99 ± 0.07	/

Table 7.4: Dose-survival curve parameters of A549, U251MG and DAOY cells irradiated with photons, protons or carbon ions combined or not with Epothilone B.

7.2 Relative Biological Effectiveness

Proton and C-ion RBE was calculated according to equation 6.3 starting from dose-survival curves using a survival level of 10% as end point, as described in the previous Chapter. In this Section, the RBE values obtained for protons and C-ions will be presented and compared with values published in literature.

7.2.1 Proton RBE

Proton (dose-averaged LET 3.6 keV/μm) RBE was calculated using 6MV LINAC photon beams as reference radiation and resulted to be cell line dependent. The doses of photons and protons producing a surviving fraction equal to 10% are 4.82 and 3.22 for A549 cells, 4.56, 3.06 for U251MG cells and 3.88 and 3.31 for DAOY cells. In table 7.5 proton $RBE_{10\%}$ values for A549, U251MG and DAOY cells are reported.

Cell line	RBE
A549	1.5 ± 0.2
U251MG	1.5 ± 0.2
DAOY	1.2 ± 0.1

Table 7.5: proton $RBE_{10\%}$ for A549, U251MG and DAOY cells.

A549 and U251MG cell RBE is greater than the value nowadays assumed in proton therapy, equal to 1.1 (ICRU, 2007), while the RBE value obtained for DAOY, is compatible with the clinical value. The proton RBE value 1.1 represents the mean value derived from widely different data*in vitro* and *in vivo* data. *In vitro* measured values of proton RBE show significant variations as reported in reviews by Jones (2016) and Paganetti (2014), ranging from 0.9 to 2.1 (Paganetti et al., 2002). These RBE variations may be due to different experimental conditions (beam energy, active scanning techniques or passive beam modulation, methods for RBE calculation, cell lines, reference radiation). Recent reviews indicate that for many end points cell biological response is differently modulated by proton or photon irradiation (Tommasino and Durante, 2015; Girdhani et al., 2013). Recently, many results concerning the differences in DSB induction and repair between photon and proton irradiation have been reported in literature; in particular it was found that proton irradiation induces an increased number of DSBs and Clustered Lesions when compared to photons ($^{137}Cs\gamma$ rays) (Calugaru et al., 2011). Moreover, recent studies investigated the impact of homologous and nonhomologous end-joining pathways in repairing DSB after photon or charged particle irradiation: it was reported that proton-induced DSBs preferentially follow the homologous-recombination repair pathway in A549 and glioblastoma cells(Fontana et al., 2015); this pathway is believed to be followed in the repair of more complex lesions.
In addition, it is known that the biological effect of irradiation are also influenced by free-radicals production, in particular Reactive Oxygen Species (ROS): Mitteer et al. (2015) showed that when compared to photons, protons induce greater cytotoxicity, DNA damages and cell cycle alteration through ROS in glioma stem cells.
For all this reason, proton RBE is still widely studied and debated.

The RBE value we measured for DAOY cells does not significantly differ from the clinically assumed value. We conjecture that this different behavior with respect to A549 and U251MG cells is due to the different radiosensitivity of these cell lines. As a matter of fact, DAOY cells resulted to be more radiosensitive, as shown in the dose-survival curves reported in the previous section. Thus, it is probable that in this cell line the DNA repair mechanisms are less efficient than in A549 and U251MG cells.

Combined treatment biological effectiveness

For the combination of irradiation and Epothilone B, proton effectiveness relative to photons was calculated as the ratio between the slopes of the two combined treatment survival curves ($\frac{\alpha_p}{\alpha_X}$). Since the curves are exponential, this ratio did not depend on the survival level and its value resulted 1.3 $\pm$ 0.1 for A549 and U251MG cells, suggesting that the combination of Epothilone B with proton beams can lead to a greater effectiveness with respect to its combination with photon beams.
The relative effectiveness in DAOY cells resulted equal to 0.96 $\pm$ 0.06, indicating that for this cell line there are no significative differences in therms of treatment efficacy when Epothilone B is combined with photon or proton beams.

7.2.2 C-ion RBE

C-ion (dose-averaged LET 45 keV/μm) RBE was measured only for A549 and U251MG cells using 6MV LINAC photon beams as reference radiation and resulted to be cell line dependent. In table 7.6 the obtained $RBE_{10\%}$ values at the mid SOBP are reported.
The doses of photons and carbon ions producing a surviving fraction equal to 10% are 4.82 and 1.46 for A549 cells 4.56 and 1.46 for U251MG cells.

Cell line	RBE
A549	3.5 $\pm$ 0.3
U251MG	3.1 $\pm$ 0.3

Table 7.6: C-ion $RBE_{10\%}$ for A549 and U251MG cells.

In literature different carbon ion RBE values are reported ranging from 2 to 5. C-ion RBE varies with LET, as mentioned in Chapter 1. Moreover differences in RBE values can be caused by different experimental conditions (beam line, active or passive beam modulation and so on). It is important to underline that, as previously reported, carbon ions effectiveness is much greater than that of photons in the Bragg Peak region, where the LET increases.
Schlaich et al. (2013) using a SOBP carbon ion beam (rasterscanning technique, dose-averaged LET 103 keV/μm) found that C-ions RBE at 10% of survival is equal to 3.6 $\pm$ 0.8 in A549 cells. Niemantsverdriet et al. (2011) using a 90 MeV/u carbon ions (dose-averaged LET equal to 189 keV/μm) and γ produced by a ^{137}Cs source as reference radiation found that A549 RBE at 10% of survival is equal to 3.4. These RBE values are compatible with the one we measured for the same cell line, but in our measurements the dose-averaged LET is smaller, so that it is difficult to compare this values.

Tsuboi et al. (1998), using a monoenergetic carbon ion beam and γ rays from ^{137}Cs as reference radiation, measured the RBE of different glioblastoma cell lines, varying the ions LET. They found that U251MG RBE at 10% of survival ranges from 1.65 (LET 20 keV/μm) to 2.95 (LET 105 keV/μm), also in this case, despite the different LET, this latter RBE value is compatible with the one we measured for the same cell line, but the irradiation configurations are very different.

Combined treatment biological effectiveness

For the combination of irradiation and Epothilone B, C-ions effectiveness relative to photons was calculated as the ratio between the slopes of the two exponential survival curves ($\frac{\alpha_C}{\alpha_X}$). Also in this case, the ratio did not depend on the survival level and its value resulted 2.7 $\pm$ 0.2 and 2.4 $\pm$ 0.1 for A549 and U251MG cells, respectively.

7.3 Radiation-drug interaction

The interaction mechanism between radiation and Epothilone B was investigated applying the model proposed by Luttjeboer et al, as described in Chapter 6, in order to determine if they interact in an additive way or if the drug acts enhancing radiation effect (synergic interaction).
For each cell line and radiation (proton, carbon ion, photon beams), the additivity region delimited by the overlapping and independent additivity curves was represented in the dose-survival plane. The independent additivity (IA) curve and the overlapping one (OA) were built starting from the parameters of the dose-survival curves relative to irradiation alone and combined to Epothilone B, as described in Chapter 6.
In this section the analysis performed for photon, proton and carbon ion irradiation for each cell line will be presented.

7.3.1 Photon-drug interaction

In figures from 7.7 to 7.9 the graphs showing the analysis of the photon-Epothilone B interaction for A549, U251MG and DAOY cells are displayed: the additivity region is delimited by the dotted (independent additivity) and the dashed (overlapping additivity) lines. Experimental values of surviving fractions (full symbols) of cells irradiated and treated with Epothilone B are represented and associated with error bars. The solid line represents the fit to the experimental data according to equation 6.2.
In table 7.7 the parameters α, β, S_0 and $D^\star$ used to calculate the independent and overlapping additivity curves (equations 6.9 and 6.10) are reported. Details for this calculation are reported in Chapter 6. In the same table, the Dose Enhancement Factor values, calculated according to equation 6.3 are reported.
The experimental data relative to the combined treatment (photon beams and Epothilone B) are located below the additivity region for each cell line, indicating a synergic radiation-drug interaction.
The area of the additivity region obtained for DAOY cells is smaller than that of the other cell lines studied. This is due to the fact that the survival curve present a small shoulder

with respect to A549 and U251MG cell curves.

Parameter	A549	U251MG	DAOY
Photon-drug interaction			
$\alpha[Gy^{-1}]$	0.34	0.38	0.51
$\beta[Gy^{-2}]$	0.028	0.028	0.022
S_0	0.39	0.34	0.38
$D^{\star}[Gy]$	2.3	2.4	1.8
$DEF_{10\%}$	1.5 ± 0.1	1.6 ± 0.2	1.6 ± 0.2

Table 7.7: Parameters for the calculation of the independent and overlapping additivity curves for the analysis of photon-drug interaction and Dose Enhancement Factor (DEF) values.

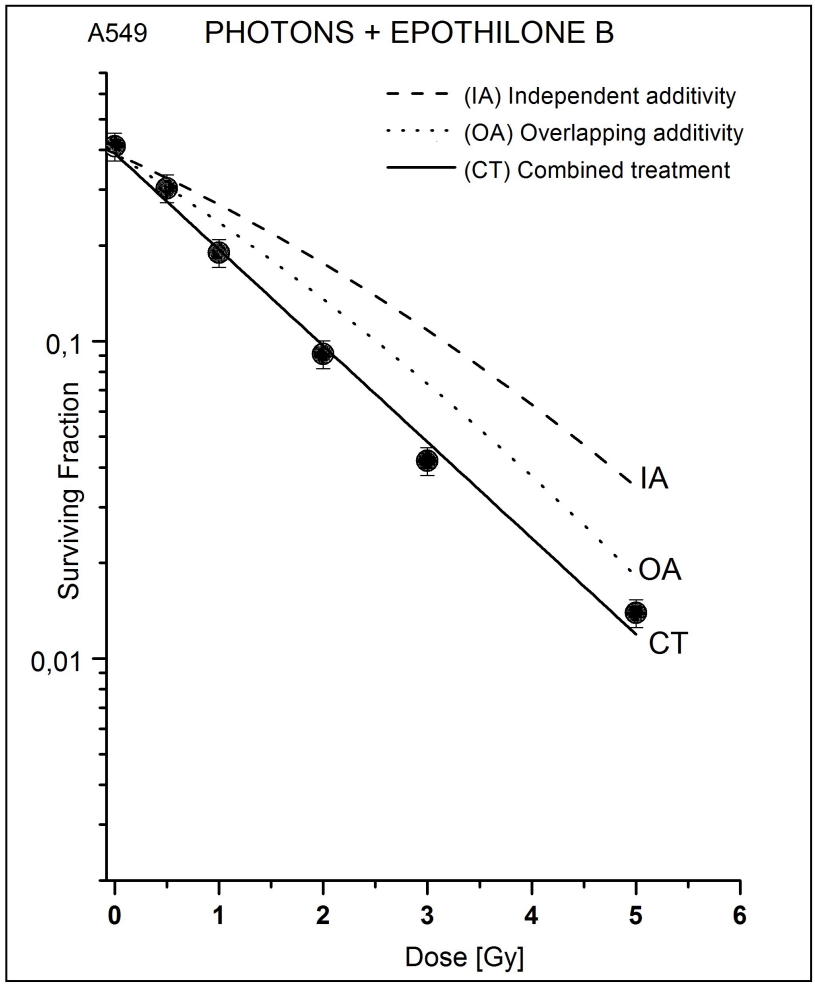

Figure 7.7: Analysis of photon-drug interaction in A549 cells. Experimental data relative to photon irradiation combined with 0.075 nM Epothilone B are reported and fitted with the solid line (CT). The dotted line (IA) represents the independent additivity; the dashed line (OA) is relative to the overlapping additivity.

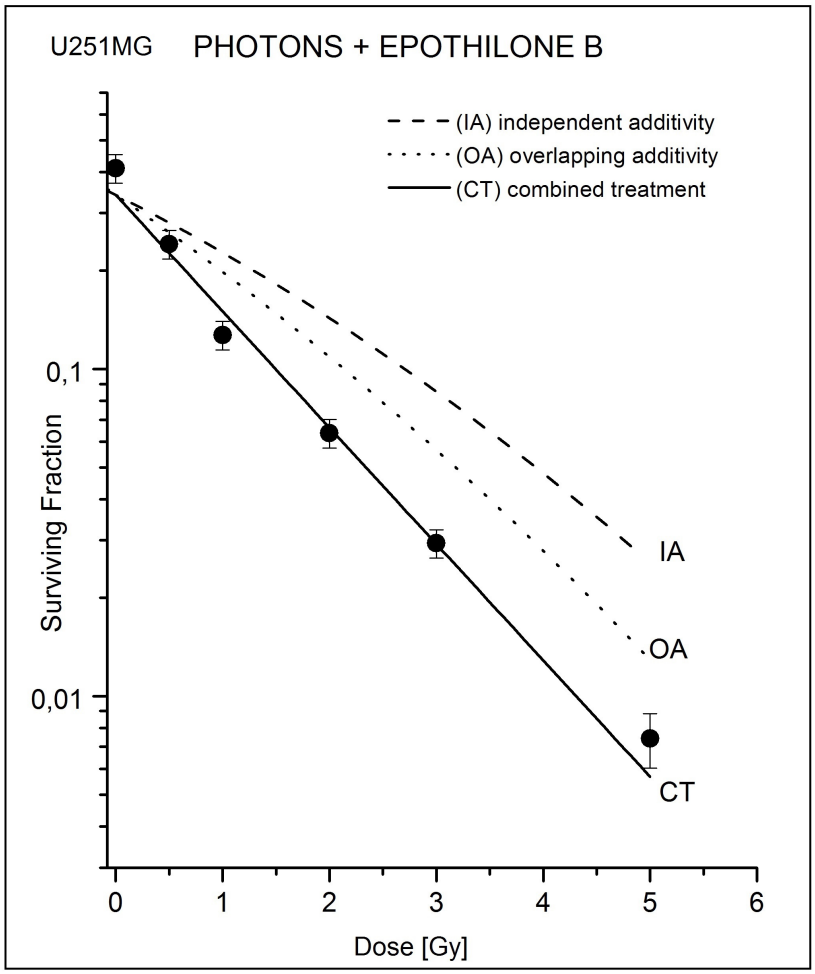

Figure 7.8: Analysis of photon-drug interaction in U251MG cells. Experimental data relative to photon irradiation combined with 0.125 nM Epothilone B are reported and fitted with the solid line (CT). The dotted line (IA) represents the independent additivity; the dashed line (OA) is relative to the overlapping additivity.

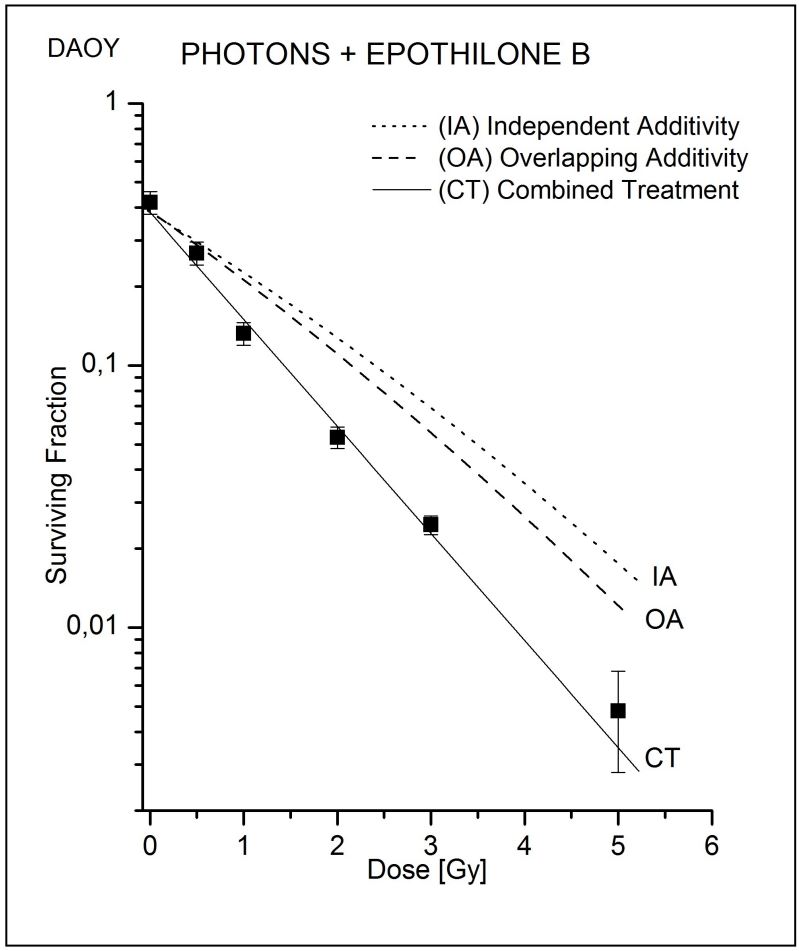

Figure 7.9: Analysis of photon-drug interaction in DAOY cells. Experimental data relative to photon irradiation combined with 0.035 nM Epothilone B are reported and fitted with the solid line (CT). The dotted line (IA) represents the independent additivity; the dashed line (OA) is relative to the overlapping additivity.

Parameter	A549	U251MG	DAOY
Proton-drug interaction			
$\alpha[Gy^{-1}]$	0.56	0.54	0.57
$\beta[Gy^{-2}]$	0.05	0.07	0.04
S_0	0.36	0.38	0.37
$D^{\star}[Gy]$	1.6	1.5	1.6
$DEF_{10\%}$	1.2 ± 0.1	1.4 ± 0.1	1.3 ± 0.1

Table 7.8: Parameters for the calculation of the independent and overlapping additivity curves for the analysis of proton-drug interaction and Dose Enhancement Factor (DEF) values.

7.3.2 proton-drug interaction

In figures from 7.10 to 7.12 the graphs showing the analysis of the proton-Epothilone B interaction for A549, U251MG and DAOY cells are displayed: the additivity region is delimited by the dotted (independent additivity) and the dashed (overlapping additivity) lines. Experimental values of surviving fractions (full symbols) of cells irradiated and treated with Epothilone B are represented and associated with error bars. The solid line represent the fit to the experimental data according to equation 6.2.
In table 7.8 the parameters α, β, S_0 and $D^{\star}$ used to calculate the independent and overlapping additivity curves (equations 6.9 and 6.10) are reported. Details for this calculation are reported in Chapter 6. In the same table, the Dose Enhancement Factor values, calculated according to equation 6.3 are reported.
Also for proton beams, the experimental data relative to the combined treatment are located below the additivity region for each cell line, indicating a synergic radiation-drug interaction.

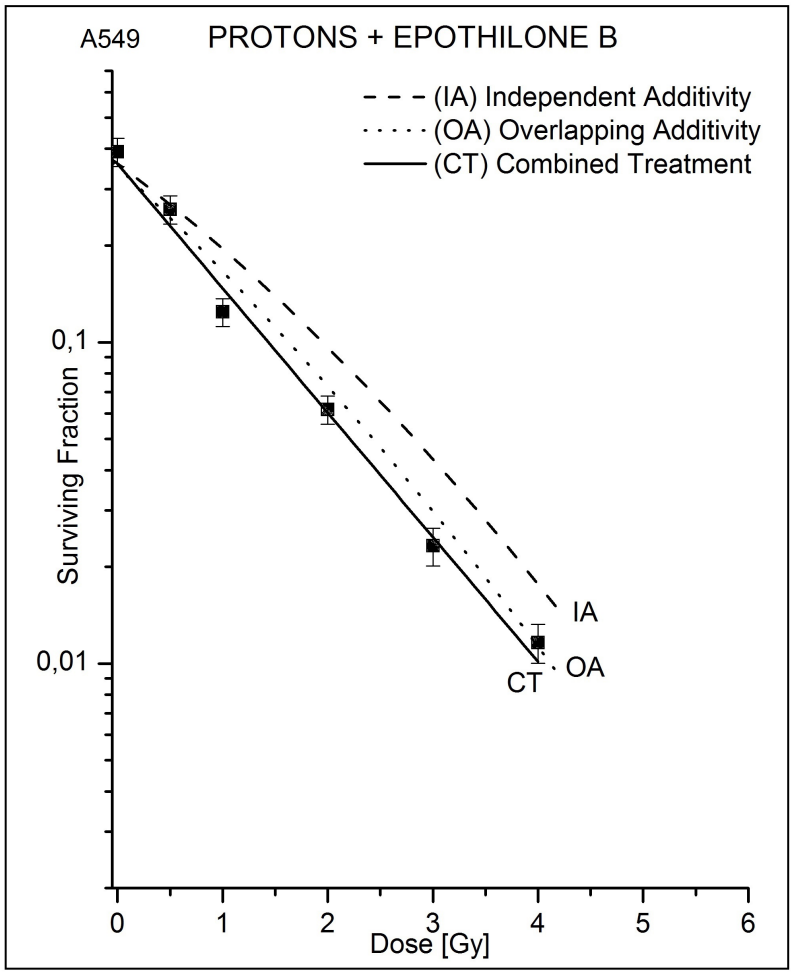

Figure 7.10: Analysis of proton-drug interaction in A549 cells. Experimental data relative to proton irradiation combined with 0.075 nM Epothilone B are reported and fitted with the solid line (CT). The dotted line (IA) represents the independent additivity; the dashed line (OA) is relative to the overlapping additivity.

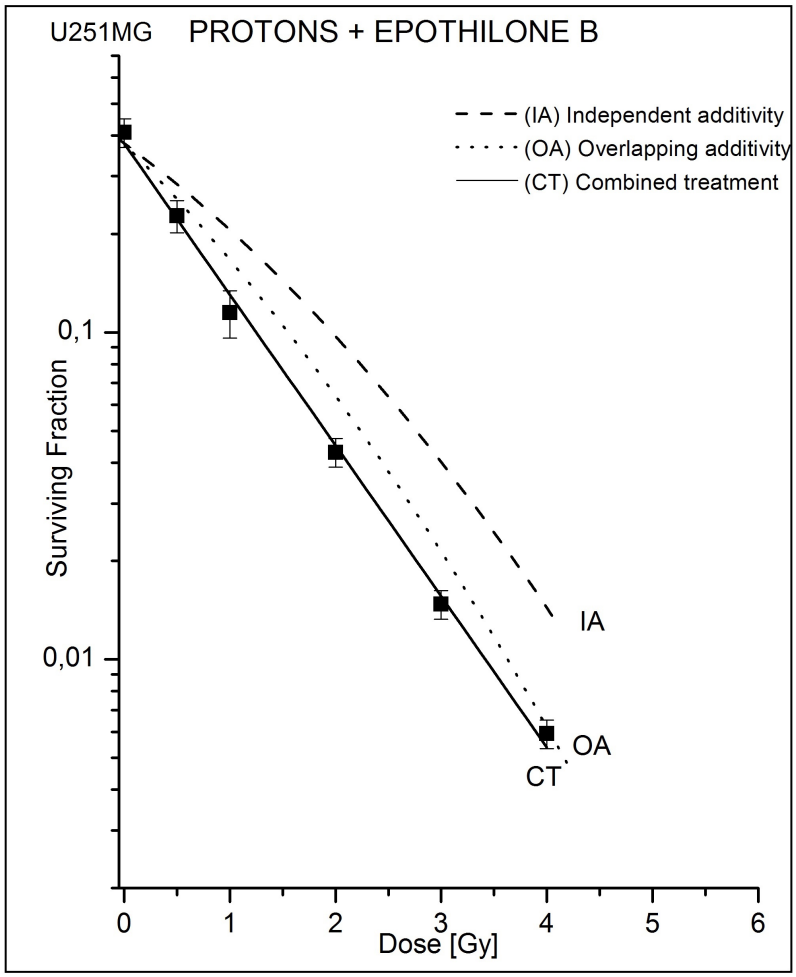

Figure 7.11: Analysis of proton-drug interaction in U251MG cells. Experimental data relative to proton irradiation combined with 0.125 nM Epothilone B are reported and fitted with the solid line (CT). The dotted line (IA) represents the independent additivity; the dashed line (OA) is relative to the overlapping additivity.

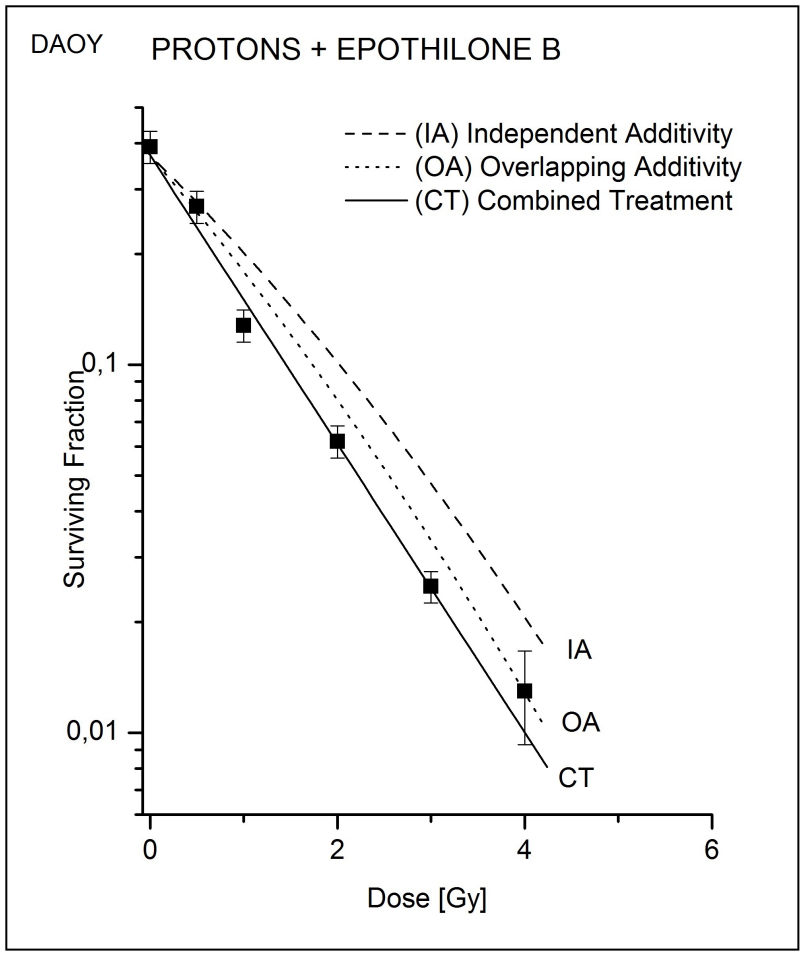

Figure 7.12: Analysis of proton-drug interaction in DAOY cells. Experimental data relative to proton irradiation combined with 0.035 nM Epothilone B are reported and fitted with the solid line (CT). The dotted line (IA) represents the independent additivity; the dashed line (OA) is relative to the overlapping additivity.

Parameter	A549	U251MG
Carbon ion-drug interaction		
$\alpha[Gy^{-1}]$	1.69	1.57
S_0	0.43	0.44
$D^{\star}[Gy]$	0.49	0.53
DEF	1.13 ± 0.06	1.26 ± 0.05

Table 7.9: Parameters for the calculation of the independent and overlapping additivity curves for the analysis of C-ion-drug interaction and Dose Enhancement Factor (DEF) values.

7.3.3 Carbon ion-drug interaction

In figure 7.13 and 7.14 the graphs showing the analysis of the carbon ion-Epothilone B interaction for A549 and U251MG cells are displayed. In the case of carbon ion irradiation, the dose-survival curves are purely exponential, thus the independent and overlapping additivity curves (obtained shifting downwards and to the left the survival curve relative to irradiation alone as previously described) coincides: the independent and overlapping additivity curves are represented with the dotted line. Experimental values of surviving fractions (full symbols) of cells irradiated and treated with Epothilone B are represented and associated with error bars. The solid line represent the fit to the experimental data according to equation 6.2.
In table 7.9 the parameters α, S_0 and $D^{\star}$ used to calculate the independent and overlapping additivity curves (equations 6.9 and 6.10 where the β parameter was set to 0) are reported. Details for this calculation are reported in Chapter 6. In the same table, the Dose Enhancement Factor values, calculated according to equation 6.3 are reported. Since the curves are purely exponential, the DEF value does not depend on the survival level, but can be simply evaluated as the ratio between the slopes of the curves relative to irradiation alone or in combination with Epothilone B.
Experimental data relative to the combined treatment for A549 cells are very close to the curve of additivity, indicating a purely additive radiation-drug interaction. Data relative to U251MG show two different behaviors: at the lower doses they are very close (or even over) to the additivity curve, but at the higher doses they deviate, indicating a slightly more than additive interaction. Since only three independent experiments have been performed with carbon ion beams, it is desirable to perform other experiments with carbon ions to consolidate the obtained results.

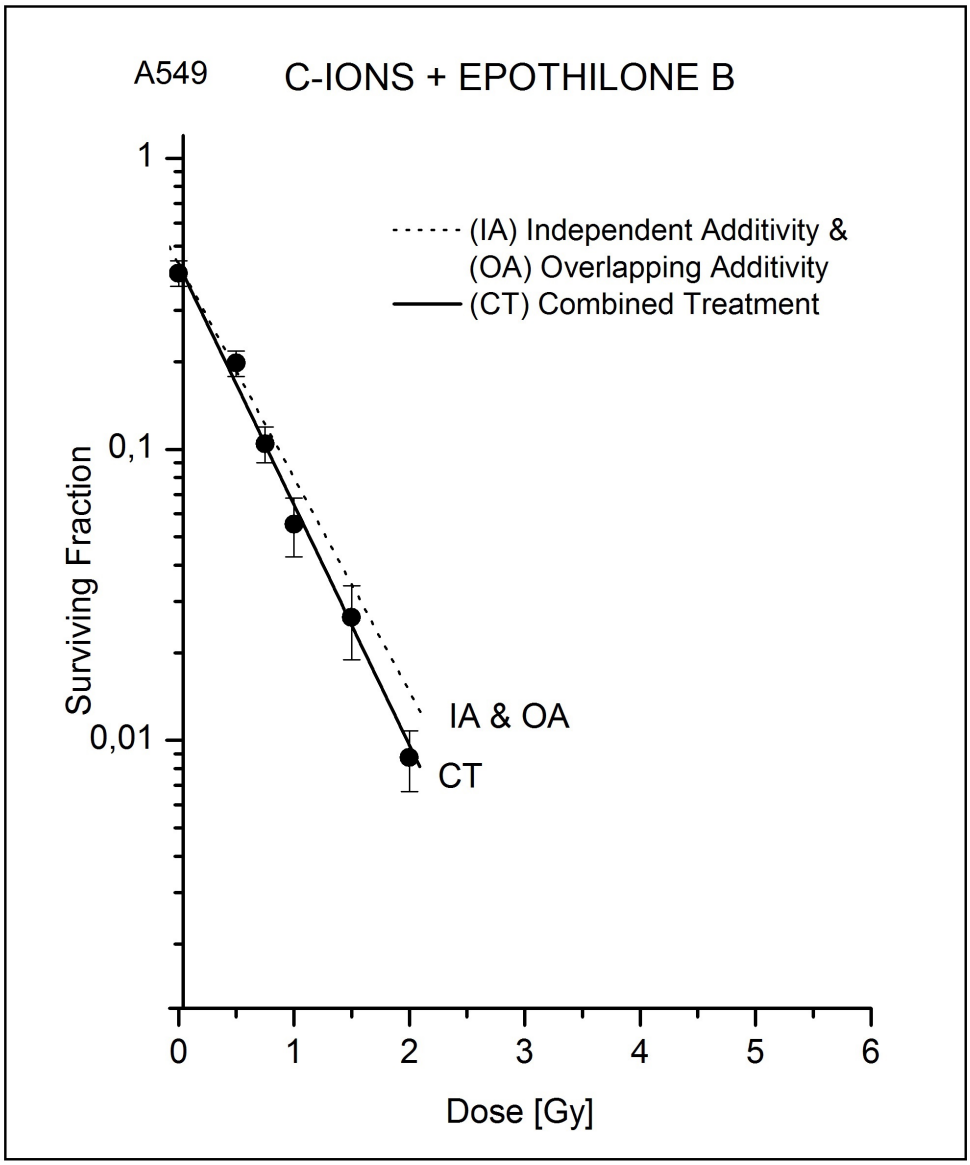

Figure 7.13: Analysis of C-ion-drug interaction in A549 cells. Experimental data relative to C-ion irradiation combined to 0.075 nM Epothilone B are reported and fitted with the solid line (CT). The dotted line (IA) represents the independent additivity; the dashed line (OA) is relative to the overlapping additivity.

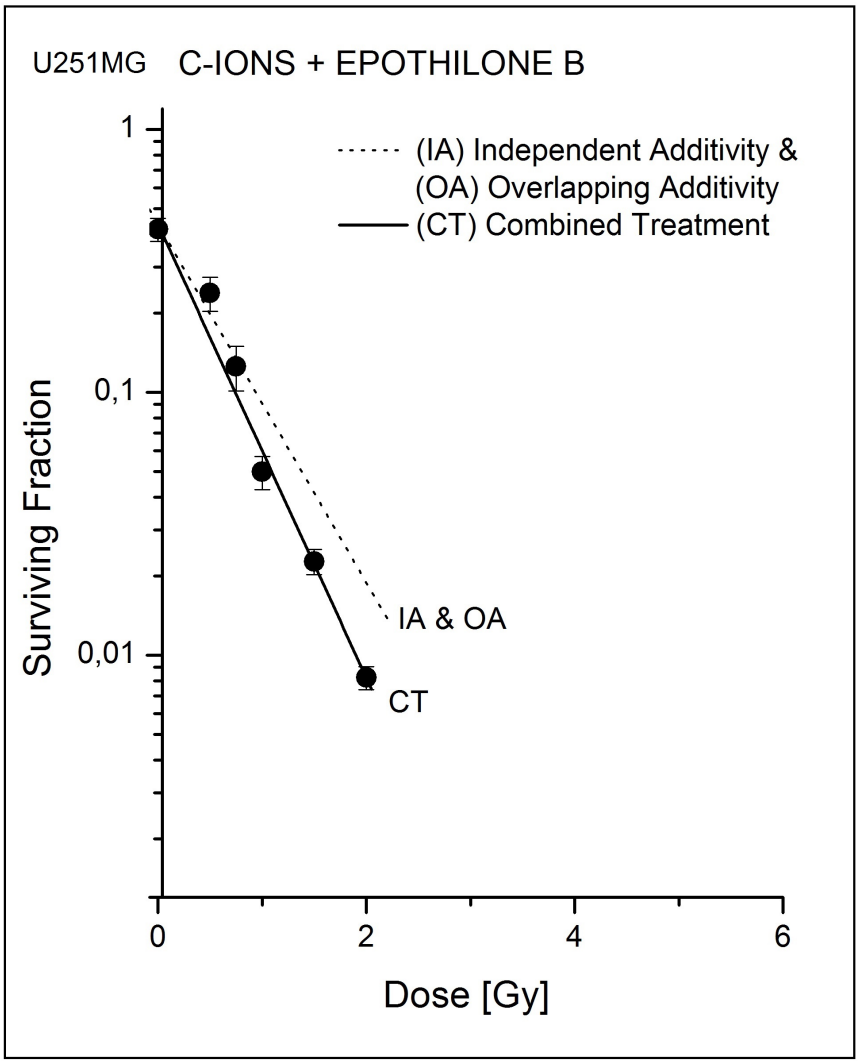

Figure 7.14: Analysis of C-ion-drug interaction in U251MG cells. Experimental data relative to C-ion irradiation combined to 0.125 nM Epothilone B are reported and fitted with the solid line (CT). The dotted line (IA) represents the independent additivity; the dashed line (OA) is relative to the overlapping additivity.

7.3.4 Result interpretation

As shown in the previous figures, experimental data relative to the combined treatment of low-LET radiations (photons and protons) and Epothilone B fall below the additivity region, indicating a slightly synergic interaction between radiation and drug. Thus, with photon and proton beams Epothilone B act as a radiosensitizing agent in all the cell lines analyzed, enhancing the cell radiation sensitivity.
Our results relative to the irradiation of A549 cells with photon beams are in agreement with those of Baumgart et al. (2012a), who found for the same cell line a synergic effect of Epothilone B combined to photon beams. Roher-Bley et al. (Roher Bley et al., 2013, 2009) found an at least additive effect for the combination of Epothilone B with X-rays irradiation on A549 cells. (Oehler et al., 2011) observed that Epothilone B is effective against different medulloblastoma cell lines and that at picomolar concentrations and combined with X-rays it reduces cell clonogenic survival. Hofstetter et al. (2005) found that Epothilone B combined with X-rays has a radiosenziting effect in human colon adenocarcinoma cells (SW480) and in p53-null MEF cells.
To our knowledge no data are published on the combination of Epothilone B with proton irradiation.

Interestingly the radiosensitizing effect we observed, occur at concentrations that did not cause a G2/M block. Thus, the radiosensitizing effect of Epothilone B is not necessarily only related to a G2-M arrest, but other mechanisms occurring at sub-nanomolar concentrations can be involved in radiosensitization and might be studied. As reported in Chapter 4, Hofstetter et al. (2005) found that the supra-additive effect of the combination of Epothilone B with irradiation occurs at concentrations not leading to a G2/M cell accumulation (as in our case) and they conjecture that the radiosensitization can be due to an S-phase related mechanism, stating that some microtubule-associated proteins have been discovered modulating cell stress response after irradiation also in other phases of the cell cycle, such as the S one.

Looking at the previously reported graphs, the reader can observe that the synergism results weaker for proton than for photon beams, especially in A549 cells. Also the DEF values resulted to be smaller for proton beams when compared to the correspondent photon values.
We conjecture that the differences in correctly-reparable damages induced by photon or proton irradiation may explain the weaker synergism found for protons. Indeed, as mentioned in Chapter 3, it was shown that Epothilone B reduces DNA repair of cancer cells and this property may be less relevant in the case of drug interaction with radiation inducing more complex and less reparable lesions.
Moreover the fact that after DSBs induced by photons or protons, different repair pathways can be followed (i.e. Homologous Recombination and Non Homologous End Joining, as discussed in the previous section) might explain the different action of Epothilone B on cells irradiated with photon or proton beams. For this reason, it can be interesting to study the DNA repair mechanism after Epothilone B exposure and proton irradiation, to well understand the differences in the Epothilone B-radiation interaction found with photons and protons.

The previous considerations are confirmed by the fact that with high-LET radiation (i.e. carbon ions) the radiation enhancement caused by Epothilone B resulted weaker and the radiation-drug interaction resulted to be simply additive in A549 cells and slightly

more than additive in U251MG cells. Indeed, as discussed in the previous section, survival curves of high-LET irradiation lack the shoulder that is correlated to the repair capacity. Thus, the DNA repair inhibition caused by Epothilone B might be negligible when it is combined to carbon ions.
This behavior is typical of carbon ion irradiation when combined with chemotherapy drugs. By way of example, Schlaich et al. (2013) found that independent cytotoxicities occur when different chemotherapy drugs are combined with C-ion irradiation. Combs et al. (2009) reported that the combination of TMZ and irradiation showed an additive effect in glioblastoma cell lines (LN229 and U87MG).

Despite the weaker synergism with respect to photons, proton beams are very promising to be combined with a non tumor-specific drug (such as Epothilone B), due to their good conformability to the tumor volume. Carbon ion irradiation resulted significantly more effective than photon irradiation and the addition of Epothilone B even to high-LET radiation may lead to better results in different tumors.

7.4 Cell invasion rate

Cell invasion rate relative to the control sample (not irradiated and not exposed to Epothilone B) was measured for A549 and U251MG cells irradiated with photons and carbon ions, with or without Epothilone B at the same concentration used for survival assays (0.075 and 0.125 nM, respectively).
Obtained results are reported for both the cell lines in the next paragraphs.

7.4.1 A549 cells

In figure 7.15 the relative invasion index of A549 cells exposed to photons (at doses of 1.5 and 3 Gy)and carbon ions (at doses of 0.75 and 1.5 Gy) treated or not with 0.075 nM Epothilone B is displayed. Reported data are the mean of two independent experiments. Data collected in each experiment are reported in Appendix C.
In table 7.10 the relative invasion index values and the error bars (calculated as described in Chapter 6) are reported.
Reported results show that the use of Epothilone B significantly reduces the basal invasion rate. Photon irradiation alone at these doses seems not to have effects on cells invasive capacity; conversely carbon ion irradiation alone reduces the invasion rate.
Obtained results will be discussed in Section 7.4.3.

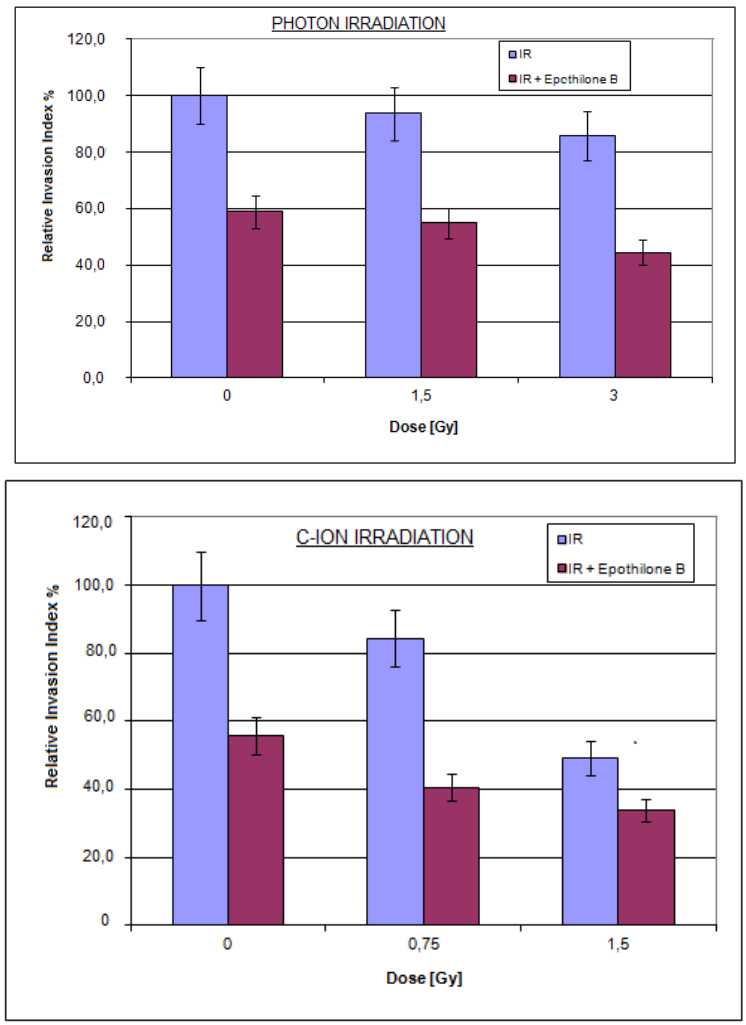

Figure 7.15: Invasion Index relative to the control sample of A549 cells irradiated with photons or carbon ions combined with 0.075 nM Epothilone B.

Dose [Gy]	Relative I.I. [%]	error [%]
Photon beams		
0	100	10
1.5	93.7	9.4
3	86.0	8.6
Photon beams + Epothilone B		
0	61.7	6.2
1.5	54.9	5.5
3	44.5	4.4
C-ion beams		
0	100	10
0.75	84.5	8.5
1.5	49.3	4.9
C-ion beams + Epothilone B		
0	55.8	5.6
0.75	40.7	4.1
1.5	33.9	3.4

Table 7.10: Invasion Index relative to the control sample of A549 cells irradiated with photons and carbon ions combined with 0.075 nM Epothilone B.

7.4.2 U251MG cells

Dose [Gy]	Relative I.I. [%]	error [%]
Photon beams		
0	100	10
1.5	91.2	12.8
3	88.6	11.9
Photon beams + Epothilone B		
0	65.9	6.6
1.5	57.9	5.8
3	49.1	4.9
C-ion beams		
0	100	10
0.75	71.1	7.1
1.5	60.0	6.0
C-ion beams + Epothilone B		
0	63.7	6.4
0.75	53.4	6.6
1.5	40.5	4.0

Table 7.11: Invasion Index relative to the control sample of U251MG cells irradiated with photons and carbon ions combined with 0.125 nM Epothilone B.

In figure 7.16, the relative invasion index of U251MG cells exposed to photons (at doses of 1.5 and 3 Gy, mean of two independent experiments)and carbon ions (at doses of 0.75 and 1.5 Gy, mean of three independent experiments) treated or not with 0.125 nM

Epothilone B is reported. Data collected in each experiment are reported in Appendix C. In table 7.11 the relative invasion index values and the error bars (calculated as described in Chapter 6) are reported.
Reported results show that also for this cell line the use of Epothilone B significantly reduces the basal invasion rate. Also in this cell line photon irradiation at these doses seems not to have effects on cells invasive capacity; conversely carbon ion irradiation alone reduces the invasion rate. Obtained results will be discussed in Section 7.4.3.

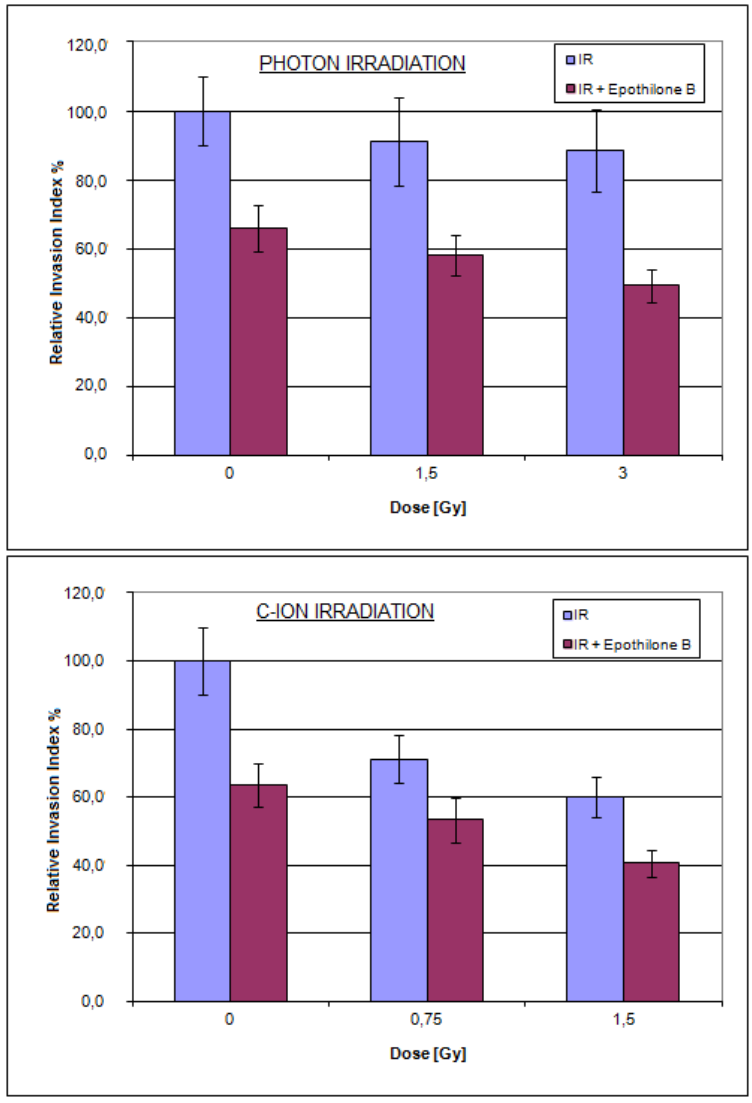

Figure 7.16: Invasion Index relative to the control sample of U251MG cells irradiated with photons or carbon ions combined with 0.125 nM Epothilone B.

7.4.3 Result interpretation

The obtained results show that for both the cell lines the use of Epothilone B reduces the invasion rate, as described in Chapter 4.
An invasion rate reduction was observed also in cells irradiated with carbon ions and not treated with the drug, suggesting that high-LET irradiation may reduce cancer invasive capacity.
This effect was not observed in cells simply irradiated with photon beams: despite an invasion reduction at 3 Gy of X-rays was observed in both cell lines, it is not statistically significative.
In literature there are some studies that show that carbon ion irradiation inhibits cell invasion: by way of example, Akino et al. (2009) found that carbon ion irradiation reduces migration and invasion in NSC lung cancer cells (among wich the A549 line, used in the present study); Fujita et al. (2015) reported that carbon ions suppress migration and invasion in human pancreatic carcinoma cells.

Our results suggest that the combination of Epothilone B and carbon ion irradiation can lead to advantages even in the suppression of cancer cell metastatic potential.

7.5 Cell growth

U251MG cell growth after carbon ion irradiation combined or not with Epothilone B was investigated according to the procedure described in Chapter 6.
In figures 7.17 the ratio between the number of cells at time t ($n(t)$) and the number of cells initially plated ($n0$) is reported as a function of time (mean of two independent experiments, data are reported in table 7.13) for cell simply irradiated (a) and irradiated and treated with 0.125 nM Epothilone B.
The results of the single experiments are reported in Appendix C.
Data were fitted according to equations 4.1 and 6.12, for the control and the treated samples respectively. The fit parameters are reported in table 7.13.

We can observe that, despite the great uncertainties due to the fact that there are few experimental points, C-ion irradiation induces a significant delay in cell growth and that this delay is enhanced when radiation is combined with Epothilone B. After this delay, cell growth re-start with a slope that is very similar to the control sample one.
The observed growth delay can be due to the fact that damage signaling and attempts to repair need more time, due to the complexity of the damages induced by high-LET irradiation alone. Moreover, as previously said, when irradiation is combined with the chemotherapy drug, DNA repair is partially inhibited, so that growth delay is enhanced.
It can be interesting to compare these results with a cell-cycle analysis of samples irradiated with carbon ions and treated or not with Epothilone B, in order to better understand the effects we found on cell growth. For this reason a cytofluorimetric analysis of samples irradiated with carbon ions (pretreated or not with Epothilone B) is planned.
Moreover similar experiments on cell growth with photon beams are planned in order to make a comparison with the results obtained with carbon ion irradiation. As a matter of fact, high-LET irradiation effects on cell growth have been widely debated in the past and light ion irradiation seems to be more effective in inducing cell growth delay with respect to conventional radiotherapy.

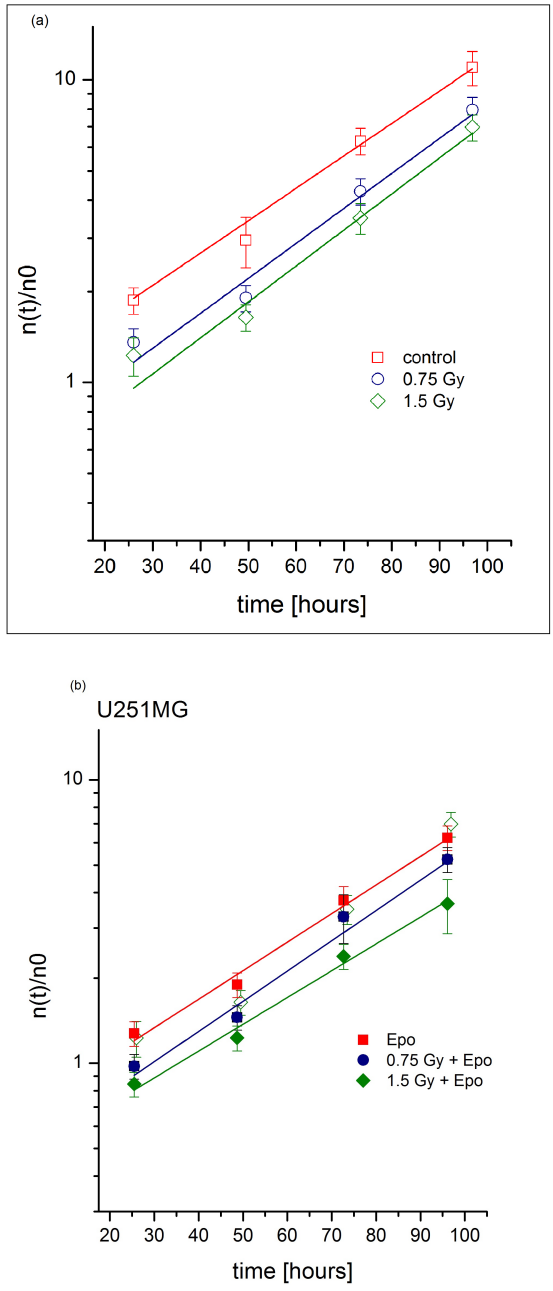

Figure 7.17: Cell growth of U251MG cells simply irradiated (a) or pretreated with 0.125 nM Epothilone B (b)

U251MG					
Irradiation			Irradiation + Epothilone B (0.075 nM)		
time [hours]	$\frac{n(t)}{n0}$	error	time [hours]	$\frac{n(t)}{n0}$	error
control sample					
26.00	1.87	0.19	25.50	1.27	0.13
49.50	2.96	0.56	48.67	1.89	0.19
73.46	6.29	0.63	72.66	3.76	0.44
96.88	11.00	1.43	96.09	6.25	0.62
0.75 Gy					
26.00	1.36	0.15	25.50	0.98	0.10
49.50	1.90	0.19	48.67	1.45	0.15
73.46	4.28	0.43	72.66	3.29	0.64
96.88	7.95	0.80	96.09	5.24	0.52
1.5 Gy					
26.00	1.23	0.18	25.50	0.84	0.08
49.50	1.64	0.16	48.67	1.23	0.12
73.46	3.50	0.41	72.66	2.38	0.22
96.88	6.98	0.70	96.09	3.66	0.79

Table 7.12: U251MG cell growth data: ratio between the number of cell at time t ($n(t)$) and cells initially seeded $n0$. Error bars are the maximum value between the standard error and the 10% of the ratio. Reported data are the mean of two independent experiments.

U251MG					
Irradiation			Irradiation + Epothilone B (0.075 nM)		
control sample					
t_D	28.1	$\pm$ 1.1	t_D	29.9	$\pm$ 2.6
			x	17.6	$\pm$ 4.2
0.75 Gy					
t_D	26.1	$\pm$ 2.1	t_D	28.2	$\pm$ 2.3
x	20.2	$\pm$ 3.9	x	29.5	$\pm$ 3.3
1.5 Gy					
t_D	25.3	$\pm$ 2.3	t_D	31.8	$\pm$ 4.3
x	27.6	$\pm$ 4.0	x	35.5	$\pm$3.4

Table 7.13: U251MG cell growth fit parameters.

Conclusions and outlook

Recently, the use of charged hadron beams in oncological treatments is rapidly growing and new cancer therapy modalities are being studied with the aim of achieving better tumor local control and reducing the metastasis probability.
In particular, treatments that combine the use of radiation and chemotherapy attracted a lot of interest due to the possibility of combining a very local therapy (i.e. radiotherapy) to a systemic one (i.e. chemotherapy) and to the challenge of exploiting eventual radiosensitizing effects of the chemotherapy drug.

In this work the interaction of charged hadron (carbon ion and proton) Spread-Out-Bragg-peak beams used in oncological treatments combined with the the microtubule-stabilizing agent Epothilone B was investigated and compared with the interaction of LINAC photon beams with this drug.
Epothilone B is known to stop cells in the G2/M phase, the more radiosensitive of cell cycle, and to inhibit DNA repair mechanism, for this reason it is promising to be used as radiosensitizer.
The study was performed *in vitro* on three human cancer cell lines: A549 (non small cell lung adenocarcinoma), U251MG (glioblastoma multiforme) and DAOY (pediatric medulloblastoma).
Despite in literature there are different study on the combination of Epothilone B with photon beam irradiation, to our knowledge no data are published on its interaction with charged hadrons.

The experiments described in this thesis were performed with proton and carbon ion beams at CNAO (Pavia) or with photon beams at the Fondazione IRCCS - Istituto Nazionale dei Tumori (Milano). Cell clonogenic survival, invasion rate and growth were studied after irradiation and treatment with Epothilone B at sub-nanomolar concentrations.

For all the three cell lines, survival curves after photon and proton irradiation alone showed a linear quadratic behavior with a proton RBE at 10% survival, equal to 1.5 ± 0.2 for A549 and U251MG cells and to 1.2 ± 0.1 for DAOY cells. Differently, the survival curves for the combined treatment Epothilone B - radiation showed a linear trend and the analysis of the interaction of Epothilone B with photons or protons, performed according to the method proposed by Luttjeboer et al. (2010), indicated a synergism. This result suggests that Epothilone B at sub-nanomolar concentration can act as a radiosensitizer on this cancer cell lines. The synergism in radiation-drug interaction resulted

weaker for protons than for photons; this difference is probably due to different amount of correctly-reparable damages induced by photons and protons, as discussed in the previous Chapter.
Due to the high radiosensitivity of the pediatric medulloblastoma (DAOY) cells, the combination of carbon ions and Epothilone B was studied only for A549 and U251MG cells. As typical of curve obtained after high-LET irradiation, dose-survival curves after carbon ion irradiation alone showed a linear trend, without any shoulder in both these cell lines. The same behavior was found on cells irradiated and treated with Epothilone B. The analysis of the radiation-drug mechanism showed a simply additive interaction in A549 cells and a slightly supra-additive interaction in U251MG cells. A549 and U251MG RBE at 10% of survival resulted equal to 3.5 ± 0.3 and 3.1 ± 0.3, respectively.

The cytofluorimetric analysis performed on cells treated with Epothilone B at different sub-nanomolar concentrations do not show an accumulation in the G2/M phase, reported in literature at higher concentrations. Despite this fact, in the present study a radiosensitizing effect was found at low concentrations, when the drug is combined with low-LET irradiation. This results are in agreement with results reported in literature on the combined use of Epothilone B and photon irradiation, as discussed in the previous Chapter.

Furthermore, Epothilone B alone or combined with photon and carbon ion irradiation resulted to inhibit A549 and U251MG cell invasive capacity (experiments on DAOY cells not performed). A reduction of the invasion rate was found even on cells simply irradiated with carbon ions, suggesting that high-LET irradiation can reduce cancer cell metastatic potential. This effect was not observed in cells simply irradiated with photon beams.

Carbon ion irradiation alone resulted to induce a growth delay in U251MG cells and this effect is enhanced when irradiation is combined with Epothilone B.

We can conclude that Epothilone B acts as a radiosensitizing agent on the three cell lines studied and that the interaction resulted synergic with low-LET radiations (photons and protons) and additive (or slightly supra-additive, in the case of U251MG cells) with carbon ions. For this reason it is promising to be used even in combination with charged hadrons. Moreover it induces a growth delay and it reduces the invasion capacity, especially when combined to carbon ion irradiation, suggesting that the combination of Epothilone B and carbon ions can lead to advantages even in reducing cancer cell metastatic potential.

In order to better understand the interaction between radiation and Epothilone B, other studies will be performed. In particular cell cycle analysis of irradiated cells pretreated or not with Epothilone B are planned in order to study more in detail the effect of the combination of Epothilone B and radiation on cycle progression.
Moreover experiments on cell growth after photon irradiation (combined or not with Epothilone B) are programmed, in order to compare this results with those obtained with carbon ions.
Since in literature there are some evidence that high-LET radiation inhibit cancer cell invasive capacity (as commented in Chapter 7), in this Thesis we gave the priority to the study of cell invasion after carbon ion irradiation and to the comparison of the results with those obtained with photon beams, considered to be the reference radiation. In the

next future it can be desirable to perform analogue study on cell invasion even after proton irradiation (combined or not with Epothilone B).

Results published in this thesis and the ones that will be reported in the next publications provide a radiobiological basis for further experiments on the combination of charged hadrons and Epothilone B, as well as for clinical studies.

Appendices

APPENDIX A

Fit details

In this Appendix a schematic description of the fit performed with the software *OriginLab* (version: *OriginPro 7.5*) will be given.
Curves fitting was performed exploiting the method of least squares. In particular, for survival curves the software minimizes the chi-square function:

$$\chi^2 = \sum_{i=1}^{n} \left(\frac{y_{exp,i} - y_{calc,i}(x_i, \alpha, \beta)}{\sigma_i} \right)^2 \tag{A.0.1}$$

where n is the number of experimental points, $y_{exp,i}$ are the measured y values at x_i and $y_{calc,i}$ are the correspondent calculated values.

In order to find the parameters that minimize this function, the software applies the Levenberg-Marquardt algorithm, a numeric minimization algorithm. A very schematic description of this algorithm is given in the following lines.
This iterative procedure consists of different steps:

1. Once the initial parameter vector b is set, the software solves the Levenberg-Marquardt equation A.0.2 for δ, in order to correct the initial b values:

   $$(J^T J + \lambda I)\delta = J^T r \tag{A.0.2}$$

   where r is the residual vector, whose components are:

   $$r_i = y_{exp,i} - y_{calc,i}$$

   λ is the damping parameter, chosen by the software as a balance between a step and the following one and **J** is the jacobian matrix of derivatives of the residuals with respect to the parameters.

2. Once δ is found, $\chi^2(b + \delta b)$ is evaluated. If $\chi^2(b + \delta b) \geq \chi^2(b)$, the step is rejected, λ is incremented and the software goes back to point 1. Otherwise, the b values and the residual vector are updated to the new ones ($b_{new} = b + \delta b$), λ is reduced and the software goes back to step 1 with the new parameter vector b_{new} and the new residuals.

3. The procedure iterates and stops when the χ^2values computed in two successive iterations are small enough, compared with the tolerance (the fit converges).

$$Tolerance = |\frac{\chi'^2 - \chi^2}{\chi'^2 + \chi^2}|$$

where χ'^2 is the chi-square of the last iteration and χ^2 is the chi-square of the current iteration.

In weighted fits the function to be minimized becomes

$$\chi^2 = \sum_{i=1}^{n} w_i \left(\frac{y_{exp,i} - y_{calc,i}(x_i, \alpha, \beta}{\sigma_i} \right)^2 \tag{A.0.3}$$

where w_i are the weights.

Survival curve fitting

For the fit of dose-survival curves according to the LQ model ($S = S_0 exp(-\alpha D - \beta D^2)$), a weighted fit was performed, minimizing the function A.0.3, that in this case is given by:

$$\chi^2 = \sum_{i=1}^{n} w_i \left(\frac{S_{exp,i} - S_{calc,i}(D_i, \alpha, \beta}{\sigma_i} \right)^2$$

where n is the number of experimental points, $S_{exp,i}$ are the measured surviving fractions at dose D_i and $S_{calc,i}$ are the correspondent calculated values.
Error bars were used as weights: $w_i = \frac{1}{\sigma_i^2}$.

Growth curve fitting

Growth curves (cell number relative to the initial number of seeded cells vs. time) were fitted performing a weighted fit according to equation:

$$\frac{n(t)}{n_0} = 2^{\frac{t}{T_D}}$$

for cells not irradiated and not treated with Epothilone B; or

$$\frac{n(t)}{n_0} = 2^{\frac{t-x}{T_D}}$$

for treated samples, as described in Chapter 6. $n(t)$ is the cell number at time t, n_0 is the number of cells initially plated, T_D is the doubling time and x the delay induced by cell treatment/irradiation.
In this case, the function to be minimized is:

$$\chi^2 = \sum_{i=1}^{n} w_i \left(\frac{\left(\frac{n(t)}{n_0}\right) - \left(\frac{n(t)}{n_0}\right)(t_i, x, T_D)}{\sigma_i} \right)^2$$

where n is the number of experimental points, $\left(\frac{n(t)}{n_0}\right)_{exp,i}$ are the measured ratios between the cell number at time t_i and the number of cell initially seeded and $(\frac{n(t)}{n_0})(t_i, x, T_D)$ are the correspondent calculated values.
Error bars were used as weights: $w_i = \frac{1}{\sigma_i^2}$.

APPENDIX B

Flow cytometry

Flow cytometry is a technique widely used in biotechnology and employed in cell counting, cell sorting and so on.
Flow cytometers analyze thousands particles per second in real time. The basic structure of a flow cytometer is made up of five components:

1 Fluidic system: a sheath fluid that carries and aligns cells into a stream of single particles.

2 Optical system made up of lasers. The cells passes through the optical system: light scattering or fluorescence emission (if cells are labeled with fluorochromes) provides information about cell properties.

3 Detectors and analogue-to-digital converters.

4 Amplification system.

5 Computer to analyze signals.

In the next paragraphs this five components will be briefly described, basing on the guide by Raman et al. (2014).

Fluidic system. The fluidic system is made up of a central channel in which the sample is injected; this channel is enclosed by an outer sheath that contains a faster flowing fluid that creates a massive drag effect on central chamber, altering the velocity of the central fluid.
The fluid flow front becomes parabolic with greatest velocity at its center, creating a single stream of particles (hydrodynamic focusing).
This focusing permits to collect and analyze single particle signals.

Optical system and detectors.

Light scattering. When single particles passes through the optical system, they are hit by light that is scattered in different directions.
Light scattered in the forward direction, is collected by a lens (forward scatter channel, FSC). The FSC intensity is related to the particle size and moreover it can be used to distinguish between cellular debris and living cells.
Light measured at about 90^o angle to the excitation line is collected by the side scatter channel (SSC) and gives information on the granular content within a particle.

Fluorescence measurements. When cells are labeled with fluorescent probes (as in our case for the measurements of cell cycle) and they are hit by laser light at opportune wavelengths, they emit fluorescence light whose intensity typically has a peak at a wavelenght different from the absorbed light one (Stokes shift). Flow cytometers use separate fluorescence (FL) channels to detect light emitted. The specificity of detection is controlled by optical filters. Typically photomultiplier tubes (PMTs) and silicon photodiodes are used as detectors.

Signal amplification and processing. The signal is amplified with PMT, converted with an analogue-to-digital converter and sent to the computer. Signals are collected and processed for each detectors (FSC and SSC, as well as for fluorescence detectors FL): signal area, height and width are recorded. By way of example, for the analysis of cycle with Propidium Iodide, whose emission spectrum is in the red region and has a peak correspondent to 610 nm, fluorescence signals recorded in the fluorescence channel correspondent to the emission region of Propidium Iodide are processed: the signal area is proportional to the fluorescence emission intensity so that fluorescence histograms are built and analyzed, as described in Chapter 4.

In order to select the cell population to be analyzed or to distinguish debris from living cells, different gates can be applied. For example, gates can be applied according to physical characteristics. For instance, debris and aggregates can be distinguished from single cells by size, that can be evaluated by forward scatter: a gate can be applied selecting an opportune region in the plane SSC vs FSC. Moreover, in order to eliminate doublets in fluorescence histograms, a gate can be applied in the plane signal height vs. signal area, as shown in Chapter 4.

In the present study, flow cytometry was exploited for cell cycle analysis in cell treated with Epothilone B at different concentrations, but lots of different cell characteristics can be analyzed with this technique, such as study of ploidy and cell proliferation, immunophenotypic analysis, analysis of apoptosis and so on. A schematic view of the flow cytometer setup is displayed in figure A.0.

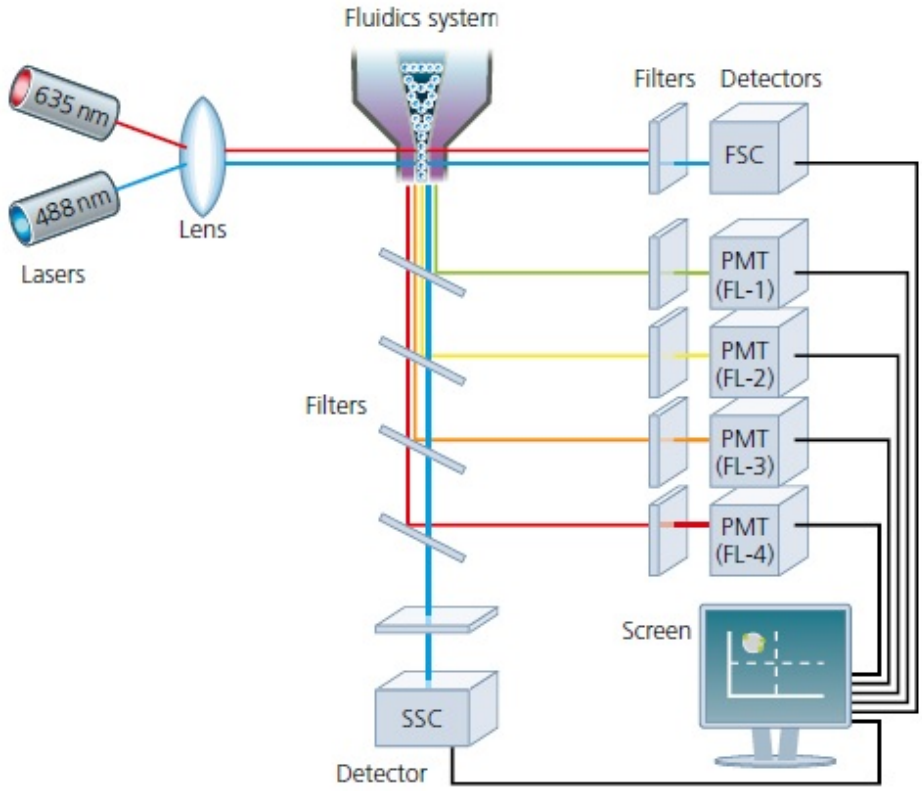

Figure A.0: Schematic view of the flow cytometer setup (Raman et al., 2014)

.

APPENDIX C

Single experiment results

In Chapter 7 the presented results are the mean of different experiments (at least 3 for survival curves and at least 2 for Invasion rate and growth curves). In this Appendix the results obtained in each experiment will be reported.

C.1 Dose-survival curves

In this section the results of the clonogenic survival assays described in Chapter 6 will be reported for each irradiation condition (photon, proton or carbon ion beams combined or not with the use of Epothilone B) and cell line.

C.1.1 Photon irradiation

In table C.1, C.2 and C.3 the surviving fractions (S) obtained through the clonogenic survival assays performed on cells irradiated with photon beams are reported, as well as the mean values ($\overline{S}$) and the error bars (obtained as explained in Chapter 6).

C.1.2 Proton irradiation

In table C.4, C.5 and C.6 the surviving fractions (S) measured in each experiment through clonogenic survival assays, the mean surviving fractions ($\overline{S}$) and error bars are reported for cells irradiated with protons.

C.1.3 Carbon ion irradiation

In table C.7 and C.8 the surviving fractions (S) of the clonogenic survival assays performed on A549 and U251MG cells irradiated with proton beams are reported, as well as the mean values ($\overline{S}$) and the error bars (obtained as explained in Chapter 6).

A549 cells							
Photons							
Dose [Gy]	S1	S2	S3	S4	S5	$\overline{S}$	error
0	1	1	1	1	1	1	0.1
0.5	0.83	0.83	0.83	0.86	0.86	0.84	0.08
1	0.68	0.68	0.65	0.61	0.66	0.66	0.07
2	0.48	0.49	0.50	0.50	0.50	0.49	0.05
3	0.26	0.28	0.28	0.21	0.23	0.25	0.03
5	0.098	0.106	0.113	0.09	0.087	0.10	0.01
7	0.023	0.022	0.024	0.020	0.023	0.022	0.002
Photons + Epothilone B							
0	0.41	0.41	0.41	0.41	0.40	0.41	0.04
0.5	0.30	0.30	0.31	0.28	0.32	0.30	0.03
1	0.19	0.21	0.21	0.15	0.20	0.19	0.02
2	0.087	0.097	0.115	0.073	0.083	0.091	0.009
3	0.038	0.047	0.054	0.031	0.039	0.042	0.004
5	0.014	0.015	0.015	0.011	0.014	0.014	0.001

Table C.1: Surviving fractions (S) of A549 cells photon-irradiated and pretreated or not with 0.075 nM Epothilone B. The mean surviving fraction ($\overline{S}$) and error bars are also reported.

U251MG cells						
Photons						
Dose [Gy]	S1	S2	S3	S4	$\overline{S}$	error
0	1.00	1.00	1.00	1.00	1.00	0.10
0.5	0.85	0.86	0.84	1.04	0.90	0.09
1	0.74	0.74	0.77	0.66	0.72	0.07
2	0.54	0.54	0.47	0.38	0.48	0.05
3	0.26	0.26	0.18	0.19	0.22	0.02
5	0.11	0.10	0.05	0.04	0.07	0.02
7	0.026	0.025	0.012	0.015	0.019	0.004
Photons + Epothilone B						
0		0.39	0.42	0.42	0.41	0.04
0.5		0.21	0.26	0.25	0.24	0.02
1		0.11	0.14	0.13	0.13	0.01
2		0.05	0.07	0.07	0.06	0.01
3		0.025	0.030	0.033	0.029	0.003
5		0.010	0.006	0.006	0.007	0.001

Table C.2: Surviving fractions (S) of U251MG cells photon-irradiated and pretreated or not with 0.125 nM Epothilone B. The mean surviving fraction ($\overline{S}$) and error bars are also reported.

DAOY cells					
Photons					
Dose [Gy]	S1	S2	S3	$\overline{S}$	error
0	1.00	1.00	1.00	1.00	0.10
0.5	0.89	0.85	0.75	0.83	0.08
1	0.69	0.71	0.70	0.70	0.07
2	0.38	0.38	0.34	0.37	0.04
3	0.17	0.18	0.17	0.17	0.02
5	0.039	0.041	0.044	0.041	0.004
7	0.010	0.010	0.011	0.010	0.001
Photons + Epothilone B					
0	0.45	0.40	0.40	0.42	0.042
0.5	0.31	0.25	0.25	0.27	0.027
1	0.14	0.13	0.13	0.13	0.013
2	0.05	0.05	0.06	0.05	0.005
3	0.03	0.02	0.03	0.02	0.002
5	0.003	0.003	0.009	0.005	0.002

Table C.3: Surviving fractions (S) of DAOY cells photon-irradiated and pretreated or not with 0.035 nM Epothilone B. The mean surviving fraction ($\overline{S}$) and error bars are also reported.

A549 cells						
Protons						
Dose [Gy]	S1	S2	S3	S4	$\overline{S}$	error
0	1.0	1.0	1.0	1.0	1.0	0.1
0.5	1.0	0.8	0.8	0.8	0.9	0.1
1	0.6	0.5	0.5	0.5	0.6	0.1
2	0.2	0.3	0.2	0.2	0.2	0.0
3	0.16	0.12	0.10	0.12	0.13	0.01
4	/	0.045	0.049	0.051	0.048	0.005
5	0.07	0.02	0.02	0.01	0.03	0.01
Protons + Epothilone B						
0	0.38		0.39	0.40	0.39	0.04
0.5	0.27		0.26	0.25	0.26	0.03
1	0.12		0.13	0.12	0.12	0.01
2	/		0.06	0.06	0.06	0.01
3	0.017		0.028	0.024	0.023	0.003
4	/		0.013	0.010	0.012	0.002

Table C.4: Surviving fractions (S) of A549 cells proton-irradiated and pretreated or not with 0.075 nM Epothilone B. The mean surviving fraction ($\overline{S}$) and error bars are also reported.

U251MG cells						
Protons						
Dose [Gy]	S1	S2	S3	S4	$\overline{S}$	error
0	1.00	1.00	1.00	1.00	1.00	0.10
0.5	0.85	0.86	0.84	1.04	0.90	0.09
1	0.74	0.74	0.77	0.66	0.72	0.07
2	0.54	0.54	0.47	0.38	0.48	0.05
3	0.26	0.26	0.18	0.19	0.22	0.02
5	0.11	0.10	0.05	0.04	0.07	0.02
7	0.026	0.025	0.012	0.015	0.019	0.004
Protons + Epothilone B						
0	0.42	0.39	0.41	0.42	0.41	0.04
0.5	0.15	0.25	0.25	0.26	0.23	0.03
1	0.06	0.14	0.14	0.13	0.11	0.02
2	0.031	0.046	0.046	0.050	0.043	0.004
3	0.012	0.017	0.017	0.013	0.015	0.001
4	0.006	0.006	0.006	0.006	0.006	0.001

Table C.5: Surviving fractions (S) of U251MG cells proton-irradiated and pretreated or not with 0.125 nM Epothilone B. The mean surviving fraction ($\overline{S}$) and error bars are also reported.

DAOY cells						
Protons						
Dose [Gy]	S1	S2	S3	S4	$\overline{S}$	error
0	1.00	1.00	1.00	1.00	1.00	0.10
0.5	0.70	0.81	0.82	0.88	0.80	0.08
1	0.38	0.60	0.61	0.61	0.55	0.06
2	0.18	0.28	0.28	0.30	0.26	0.03
3	0.11	0.13	0.13	0.14	0.13	0.01
4	0.06	0.06	0.05	0.06	0.06	0.01
5	0.025	0.026	0.020	0.018	0.022	0.002
Protons + Epothilone B						
0	0.31	0.43	0.41	0.41	0.39	0.04
0.5	0.23	0.29	0.27	0.29	0.27	0.03
1	0.123	0.143	0.122	0.123	0.128	0.015
2	0.065	0.067	0.057	0.059	0.062	0.006
3	0.031	0.025	0.023	0.020	0.025	0.002
4	0.015	0.012	0.011	/	0.013	0.003

Table C.6: Surviving fractions (S) of DAOY cells proton-irradiated and pretreated or not with 0.035 nM Epothilone B. The mean surviving fraction ($\overline{S}$) and error bars are also reported.

A549 cells					
C-ions					
Dose [Gy]	S1	S2	S3	$\overline{S}$	error
0	1.00	1.00	1.00	1.00	0.10
0.5	0.54	0.55	0.62	0.57	0.06
0.75	0.25	0.26	0.40	0.30	0.05
1	0.12	0.13	0.19	0.15	0.02
1.5	0.065	0.066	0.083	0.071	0.007
2	0.029	0.030	0.034	0.031	0.003
3	0.009	0.009	0.013	0.010	0.001
C-ions + Epothilone B					
0	0.41	0.39	0.41	0.40	0.04
0.5	0.19	0.19	0.21	0.20	0.02
0.75	0.09	0.09	0.13	0.10	0.01
1	0.04	0.04	0.08	0.06	0.01
1.5	0.018	0.020	0.042	0.026	0.008
2	0.007	0.007	0.013	0.009	0.002

Table C.7: Surviving fractions (S) of A549 cells carbon ion-irradiated and pretreated or not with 0.075 nM Epothilone B. The mean surviving fraction ($\overline{S}$) and error bars are also reported.

U251MG cells					
C-ions					
Dose [Gy]	S1	S2	S3	$\overline{S}$	error
0	1.00	1.00	1.00	1.00	0.10
0.5	0.75	0.56	0.52	0.61	0.07
0.75	0.41	0.31	0.33	0.35	0.04
1	0.21	0.16	0.16	0.17	0.02
1.5	0.12	0.08	0.07	0.09	0.01
2	0.049	0.036	0.036	0.041	0.004
3	0.014	0.012	0.009	0.012	0.002
C-ions + Epothilone B					
0	0.45	0.42	0.38	0.42	0.04
0.5	0.31	0.20	0.20	0.24	0.04
0.75	0.17	0.11	0.09	0.13	0.02
1	0.064	0.046	0.040	0.050	0.007
1.5	0.028	0.021	0.019	0.023	0.003
2	0.009	0.008	0.008	0.008	0.001

Table C.8: Surviving fractions (S) of U251MG cells carbon ion-irradiated and pretreated or not with 0.125 nM Epothilone B. The mean surviving fraction ($\overline{S}$) and error bars are also reported.

C.2 Cell-invasion rate

In this section the result of the invasion assays described in Chapter 6 will be reported for each irradiation condition studied (photon or carbon ion beams combined or not to the use of Epothilone B) and cell line (A549 and U251MG cells).
In table the invasion index relative to the control sample (I.I.r.) measured in each experiment as well as the mean invasion rates and the error bars are reported for A549 and U251MG cells irradiated with photons or carbon ions.

A549 cells				
photons				
Dose [Gy]	I.I.r1	I.I.r.2	$\overline{I.I.r.}$	error
0	1.00	1.00	1.00	0.10
1.5	0.97	1.07	1.02	0.10
3	0.86	0.76	0.81	0.08
photons + Epothilone B				
0	0.56	0.64	0.60	0.06
1.5	0.53	0.55	0.54	0.05
3	0.45	0.28	0.36	0.08

Table C.9: Relative invasion index of A549 cells irradiated with photon beams, pretreated or not with 0.075 nM Epothilone B. The mean invasion index ($\overline{S}$) and error bars are also reported.

U251MG cells				
photons				
Dose [Gy]	I.I.r1	I.I.r.2	$\overline{I.I.r.}$	error
0	1.00	1.00	1.00	0.10
1.5	0.97	1.07	1.02	0.10
3	0.86	0.76	0.81	0.08
photons + Epothilone B				
0	1.00	1.00	1.00	0.10
1.5	1.04	0.78	0.91	0.13
3	1.01	0.77	0.89	0.12

Table C.10: Relative invasion index of U251MG cells irradiated with photon beams, pretreated or not with 0.125 nM Epothilone B. The mean invasion index ($\overline{S}$) and error bars are also reported.

A549 cells				
C-ions				
Dose [Gy]	I.I.r1	I.I.r.2	$\overline{I.I.r.}$	error
0	1.00	1.00	1.00	0.10
0.75	0.86	0.83	0.85	0.08
1.5	0.47	0.52	0.49	0.05
photons + Epothilone B				
0	0.56	0.56	0.56	0.06
0.75	0.39	0.42	0.41	0.04
1.5	0.33	0.35	0.34	0.03

Table C.11: Relative invasion index of A549 cells irradiated with carbon ion beams, pretreated or not with 0.075 nM Epothilone B. The mean invasion index ($\overline{S}$) and error bars are also reported.

U251MG cells					
C-ions					
Dose [Gy]	I.I.r1	I.I.r.2	I.I.r.3	$\overline{I.I.r.}$	error
0	1.00	1.00	1.00	1.00	0.10
0.75	0.80	0.64	0.70	0.71	0.07
1.5	0.60	0.59	0.61	0.60	0.06
photons + Epothilone B					
0	0.67	0.61	0.63	0.64	0.06
0.75	0.67	0.46	0.48	0.53	0.07
1.5	0.42	0.38	0.41	0.40	0.04

Table C.12: Relative invasion index of U251MG cells irradiated with carbon ion beams, pretreated or not with 0.125 nM Epothilone B. The mean invasion index ($\overline{S}$) and error bars are also reported.

C.3 Cell growth

In this section the results of each experiment on cell growth for U251MG cells irradiated with carbon ion beams at different doses in combination or not with Epothilone B will be presented.
In table C.13, the ratio between the number of cells counted at time t $n(t)$ from irradiation and that of cells initially seeded is reported as a function of time for each experiment.

U251MG cells						
t1	t2	$\bar{t}$	$\frac{n(t)}{n_0}1$	$\frac{n(t)}{n_0}2$	$\overline{\frac{n(t)}{n_0}}$	error
Irradiation						
Control sample						
25	27	26.0	1.9	1.9	1.9	0.2
48.33	50.67	49.5	2.4	3.5	3.0	0.6
72.58	74.33	73.5	6.5	6.1	6.3	0.6
96.75	97	96.9	9.6	12.4	11.0	1.4
0.75 Gy						
25	27	26.0	1.5	1.2	1.4	0.1
48.33	50.67	49.5	1.8	2.0	1.9	0.2
72.58	74.33	73.5	4.7	3.9	4.3	0.4
96.75	97	96.9	8.5	7.4	8.0	0.8
1.5 Gy						
25	27	26.0	1.4	1.0	1.2	0.2
48.33	50.67	49.5	1.6	1.7	1.6	0.2
72.58	74.33	73.5	3.9	3.1	3.5	0.4
96.75	97	96.9	7.7	6.3	7.0	0.7
Irradiation + Epothilone B						
0 Gy						
24	27	25.5	1.1	1.4	1.3	0.1
47.67	49.67	48.7	1.9	1.9	1.9	0.2
72	73.17	72.66	4.2	3.3	3.8	0.4
96.17	96	96.1	5.7	6.8	6.2	0.6
0.75 Gy						
24	27	25.5	0.9	1.0	1.0	0.1
47.67	49.67	48.7	1.4	1.5	1.5	0.1
72	73.33	72.66	3.9	2.6	3.3	0.6
96.17	96	96.1	5.4	5.1	5.2	0.5
1.5 Gy						
24	27	25.5	0.8	0.9	0.8	0.1
47.67	49.67	48.7	1.3	1.2	1.2	0.1
72	73.33	72.66	2.3	2.5	2.4	0.2
96.17	96	96.1	2.9	4.5	3.7	0.8

Table C.13: Ratio between the number of cells counted at time t $n(t)$ from irradiation and that of cells initially seeded for U251MG cells irradiated with carbon ions combined or not with Epothilone B (0.125 nM) at different doses, measured in two independent experiments. The mean ratio and its error are also reported. t1 is the time from irradiation in experiment1, t2 is the same for experiment2. $\bar{t}$ is the mean time.

Bibliography

Akino, Y., Teshima, T., Kihara, A., et al. (2009). Carbon-ion beam irradiation effectively suppresses migration and invasion of human non-small-cell lung cancer cells. *Int J Radiat Oncol Biol Phys*, 75:475–481.

Altmann, K., Wartmann, M., and O'Reilly, T. (2000). Epothilones and related structures – a new class of microtubule inhibitors with potent in vivo antitumor activity. *Bichim Biophys Acta*, 1470:M79–M91.

Amaldi, U. (1999). Cancer therapy with particle accelerators. *Nucl Phys A*, 654:375c–399c.

Baumgart, T., Klautke, G., Kriesen, S., et al. (2012a). Radiosensitizing effect of Epothilone B on human epithelial cancer cells. *Strahlenther Onkol*, 188:177–184.

Baumgart, T., Kriesen, S., Hildebrandt, G., et al. (2012b). Effect of Epothilone B on cell cycle, metabolic activity, and apoptosis induction on human epithelial cancer cells - Under special attention of combined treatment with ionizing radiation. *Cancer Invest*, 30:593–603.

Baumgart, T., Kriesen, S., Neels, O., et al. (2015). Investigation of Epothilone B-induced cell death mechanisms in human epithelial cancer cells - in consideration of combined treatment with ionizing radiation. *Cancer Invest.*, 33:213–224.

Bentzen, S. M., Harari, P. M., and Bernier, J. (2007). Exploitable mechanisms for combining drugs with radiation: concepts, achievements and future directions. *Nat Clin Pract Oncol*, 4:172–180.

Bethe, H. (1930). Zur theorie des durchgangs schneller korpuskularstrahlen durch materie. *Ann Phys*, 397:325–400.

Bettega, D., Calzolari, P., Ciocca, M., et al. *Submitted*.

Bloch, F. (1933). Zur bremsung rasch bewegter teilchen beim durchgang durch materie. *Ann Phys*, 408:285–320.

Bocci, G., Nicolaou, K., Kerbel, R., et al. (2002). Protracted low-dose effects on human endothelial cell proliferation and survival in vitro reveal a selective antiangiogenic window for various chemotherapeutic drugs. *Cancer Res*, 62:6938–6943.

Calugaru, V., Nauraye, C., Noel, G., et al. (2011). Radiobiological characterization of two therapeutic proton beams with different initial Energy spectra used at the institut Curie Proton Therapy Center in Orsay. *Int J Rad Oncol Biol Phys*, 113:6–43.

Carabe, A., Moteabbed, M., Depauw, N., et al. (2012). Range uncertainty in proton therapy due to variable biological effectiveness. *Phys Med Biol*, 57:1159–1172.

Combs, S. E., Bohl, J., Elsässer, T., et al. (2009). Radiobiological evaluation and correlation with the local effect model (LEM) of carbon ion radiation therapy and temozolomide in glioblastoma cell lines. *Int J Radiat Biol*, 85:126–136.

Cottingham, W. N. and Greenwood, D. A. (2001). *An introduction to Nuclear Physics*. Cambridge University Press, 2nd edition edition.

Ferretti, S., Allegrini, P., O'Reilly, T., et al. (2011). Patupilone induced vascular disruption in orthotopic rodent tumor models detected by magnetic resonance imaging and interstitial fluid pressure. *J Surg Res*, 11:7773–7784.

Fogh, S., Machtay, M., Werner-Wasik, M., et al. (2010). Phase I trial using Patupilone (Epothilone B) and concurrent radiotherapy for central nervous system malignancies. *Int J Radiat Oncol Biol Phys*, 77:1009–1016.

Fontana, A., Augsburger, M., Grosse, N., et al. (2015). Differential DNA repair pathway choice in cancer cells after proton- and photon- irradiation. *Radiother Oncol*, 116:374–380.

Fujita, M., Imadome, K., Shoji, Y., et al. (2015). Carbon-Ion irradiation suppresses migration and invasiveness of human pancreatic carcinoma cells MIAPaCa-2 via Rac1 and RhoA degradation. *Int J Radiat Oncol Biol Phys*, 93:173–180.

Furmanova-Hollenstein, P., Broggini-Tenzer, A., Eggel, M., et al. (2013). The microtubule stabilizer Patupilone counteracts ionizing radiation-induced matrix metalloproteinase activity and tumor cell invasion. *Radiat Oncol*, 8:105.

Girdhani, S., Sachs, R., and Hlatky, L. (2013). Biological effects of proton radiation: what we know and don't know. *Radiat Res*, 179:257–272.

Hofstetter, B., Vuong, V., Broggini-Tenzer, A., et al. (2005). Patupilone acts as radiosensitizing agent in multidrug-resistant cancer cells in vitro and in vivo. *Clin Canc Res*, 11:1588–1596.

http://fondazionecnao.it. Fondazione CNAO, Centro Nazionale di Adroterapia Oncologica per il trattamento dei tumori.

http://mxp.physics.umn.edu. Measurement of the energy distribution of particle showers (http://mxp.physics.umn.edu/s06/Projects/S06_ParticleShowerEnergy/theory.htm.

http://www.bioquicknews.com/node/2696. Bioquick news.

ICRU (1971). Radiation quantities and units. *ICRU report*, 19.

ICRU (2007). Prescribing, recording and reporting proton-beam therapy. *ICRU Report*, 78.

Jones, B. (2016). Why RBE must be a variable and not a constant in proton therapy. *Br J Radiol*, 89:20160116.

Kellerer, A. M. (1984). A survey of microdosimetric quantities and concepts. *Ultramicroscopy*, 14:169–174.

Kim, J., Kim, J. S., Saha, D., et al. (2003). Potential radiation-sensitizing effect of semisynthetic epothilone B in human lung cancer cells. *Radiother Oncol*, 68:305–313.

Knoll, G. (2000). *Radiation Detection and Measurements*. Jhon Wiley & Sons, 3rd edition.

Lam, G. (1989). Analysis of interaction for mixtures of agents using the linear isobole. *Bull Math Biol*, 51:293–309.

Luttjeboer, M., Lafleur, M. V. M., Kwidama, Z. J., et al. (2010). Strategies for the analysis

of in vitro radiation sensitivity and prediction of interaction with potential radiation modifyng agents. *Int J Radiat Biol*, 86:458–466.

Mirandola, A., Molinelli, S., Vilches Freixas, G., et al. (2015). Dosimetric commissioning and quality assurance of scanned ion beams at the italian National Center for Oncological Hadrontherapy. *Med Phy*, 42:5287–5300.

Mirmanoff, R., Gorlia, T., Mason, W., et al. (2006). Radiotherapy and Temozolomide for newly diagnosed glioblastoma: recursive partitioning analysis of the EORTC 26981/22981 – NCIC CE3 phase III randomized trial. *J Clin Oncol*, 24:2563–2569.

Mitteer, R. A. J., Wang, Y., Shah, J., et al. (2015). Proton beam radiation induces DNA damage and cell apoptosis in glioma stem cells through reactive oxygen species. *Sci Rep*, 5:139–161.

Moyers, M. F., Miller, D. W., Bush, D. A., et al. (2001). Methodologies and tools for proton beam design for lung tumors. *Int J Radiat Oncol Biol Phys*, 49:1429–1438.

Niemantsverdriet, M., van Goethem, M., Reinier, B., et al. (2011). High and Low LET radiation differentially induce normal tissue damage signals. *Int J Radiat Oncol Biol Phys*, 83:1291–1297.

Oehler, C., Frei, K., Rushing, E. J., et al. (2012). Patupilone (Epothilone B) for recurrent Glioblastoma: clinical outcome and translational analysis of a single-institution phase I/II trial. *Oncology*, 83:1–9.

Oehler, C., von Bueren, A., Furmanova, P., et al. (2011). The microtubule stabilizer patupilone (Epothilone B) is a potent radiosensitizer in Medulloblastoma Cells. *Neuro-Oncology*, 13:1000–1010.

O'Reilly, T., Wartmann, M., Brueggen, J., et al. (2008). Pharmacokinetic profile of the microtubule stabilizer patupilone in tumor-bearing rodents and comparison of anticancer activity with other MTS in vitro and in vivo. *Cancer Chemother Pharmacol*, 62:1045–1054.

Paganetti, H. (2014). Relative Biological Effectiveness (RBE) values for proton beam therapy. Variations as a function of biological endpoint, dose, and Linear Energy Transfer. *Phys Med Biol*, 59:R419–R472.

Paganetti, H., Niemierko, A., Ancukiewicz, M., et al. (2002). Relative biological effectiveness (RBE) values for proton beam therapy. *Int J Radiat Oncol Biol Phys*, 53:407–421.

Pagano, A., Honoré, S., Mohan, R., et al. (2012). Epothilone B inhibits migration of glioblastoma cells by inducing microtubule catastrophes and affecting EB1 accumulation at microtubule plus ends. *Biochem Pharmacol*, 84:432–443.

Podgorsak, E. B. (2005). *Radiation Oncology Physics: a handbook for teachers and students*. IAEA.

Podgorsak, E. B. (2010). *Radiation physics for medical physicists*. Springer, 2nd edition.

Puck, T. T. and Marcus, P. I. (1956). Action of X-rays on mammalian cells. *J Exp Med*, 103:653–666.

Raman, M., Lane, A., Swindell, A., and Bartram, S. (2014). *Introduction to Flow Cytometry*. AbD Serotec, A Bio-Rad Company.

Roher Bley, C., Furmanova, P., Orlowski, K., et al. (2013). Microtubule stabilising agents and ionising radiation multiple exploitable mechanisms for combined treatment. *Eur J Cancer*, 49:245–253.

Roher Bley, C., Jochum, W., Orlowski, K., et al. (2009). Role of the microenvironment for radiosensitization by Patupilone. *Clin Cancer Res*, 15:1335–1342.

Rossi, S. (2015). The National Centre for Oncological Hadrontherapy (CNAO): Status and perspectives. *Phys Med*, 31:333–51.

Schlaich, F., Brons, S., Haberer, T., et al. (2013). Comparison of the effects of photon versus carbon ion irradiation when combined to chemotherapy in vitro. *Radiat Oncol*, 8:260.

Scholz, M. (2003). *Effects of ion radiation on cells and tissues*. Advances in Polymer Science. Springer - Verlag Berlin Heidelberg .

Sinclair, W. K. and Morton, R. A. (1966). X-Ray sensitivity during the cell generation cycle of cultured Chinese Hamster cell. *Radiation Research*, 29:450–474.

Sorensen, B. S., Overgaard, J., and Bassler, N. (2011). In vitro RBE-LET dependence for multiple particle types. *Acta Oncologica*, 50:757–762.

Stalder, M., Anthony, C., and Woltering, E. (2005). Metronomic dosing enhances the antiangiogenic effect of Epothilone B. *Clin Cancer Res*, 11:247–256.

Steel, G. G. and Peckham, M. J. (1979). Exploitable mechanisms in combined radiotherapy-chemotherapy: the concept of additivity. *Int J Radiat Oncol Biol Phys*, 5:85–91.

Stupp, R., Hegi, M., Mason, W., et al. (2009). Effects of radiotherapy with concomitant and adjuvant temozolomide versus radiotherapy alone on survival in glioblastoma in a randomized phase III study: 5-year analysis of the EORTC-NCIC trial. *Lancet Oncol*, 10:459–466.

Suit, H., Goldberg, S., Niemierko, A., et al. (2003). Proton beams to replace photon beams in radical dose treatments. *Acta Oncol*, 42:800–808.

Tommasino, F. and Durante, M. (2015). Proton Radiobiology. *Cancers*, 7:353–381.

Tsuboi, K., Tsuchida, Y., Nose, T., et al. (1998). Cytotoxic effect of accelerated carbon beams on glioblastoma cell lines with p53 mutation: clonogenic survival and cell-cycle analysis. *Int J Radiat Biol*, 74:71–79.

Acknowledgments

Vorrei ringraziare tutte le persone con cui ho avuto la fortuna di lavorare durante questi anni. In particolare ringrazio il Professor Pier Francesco Bortignon e la Professoressa Daniela Bettega per avermi seguita con pazienza in questo lavoro.
Ringrazio la dottoressa Paola Calzolari per l'entusiasmo e la gentilezza con cui mi ha accolta in laboratorio.

Un ringraziamento particolare ai membri della commissione d'esame, prof. Pier Francesco Bortignon, prof.ssa Rosanna Nano e prof. Marco Durante. Ringrazio inoltre il prof. Mauro Carrara e il prof. Lorenzo Manti per il referaggio di questa tesi.

Grazie a tutte le persone che hanno reso possibili gli esperimenti e collaborato a questo studio: al Dr. Marchesini, al Dr. Pignoli (Fondazione IRCCS Istituto Nazionale dei Tumori) e a tutte le persone di CNAO che hanno collaborato agli irraggiamenti, in particolare al Dr. Ciocca, Dr.ssa Facoetti, Dott.ssa Vischioni, Dott.ssa Molinelli.
Grazie al Prof. Battistoni per la gentilezza e la disponibilità con cui mi ha aiutata.

Vorrei ringraziare i colleghi con cui ho potuto condividere questi anni di fatiche e soddisfazioni: grazie Giovanni, Alice, Simone e Simone per le belle chiacchierate, i pranzi insieme e l'aiuto che mi avete dato in momenti difficili.
Grazie ai docenti che ho avuto la fortuna di incontrare nel mio percorso di studi e che hanno saputo trasmettermi (ben al di lá di quanto insegnavano) la passione per la conoscenza. In particolare ancora una volta voglio ringraziare il Prof. Paolo Teruzzi, che mi ha fatto conoscere la bellezza del metodo scientifico.

Grazie ai miei genitori, a mio fratello Pietro, ai miei nonni, zii e cugini per la loro presenza nella mia vita, per il loro incessante sostegno e per avermi aiutata col piccolo Giacomo durante la fase finale della stesura di questa tesi.
Grazie agli amici di sempre: Stefania, Bea, Marco, Jack ed Enrico.
Grazie a Nicoletta e Lorenzo e alla loro numerosa famiglia; grazie a Magda e Luigi per il loro sostegno.

Infine, grazie a Riccardo e al piccolo Giacomo perché dove sono loro... lì c'è la mia casa!